



This is to certify that the

dissertation entitled

Synthetic Model Approach to the Active Site
Structure of Cytochrome C Oxidase

presented by

Myoung Seo Koo

has been accepted towards fulfillment
of the requirements for

Ph. D. degree in Chemistry

Chin K. Chang
Major professor

Date Nov 10, 1986



RETURNING MATERIALS:

Place in book drop to
remove this checkout from
your record. FINES will
be charged if book is
returned after the date
stamped below.

--	--	--







SYNTHETIC MODEL APPROACH TO THE ACTIVE SITE
STRUCTURE OF CYTOCHROME C OXIDASE

By

Myoung Seo Koo

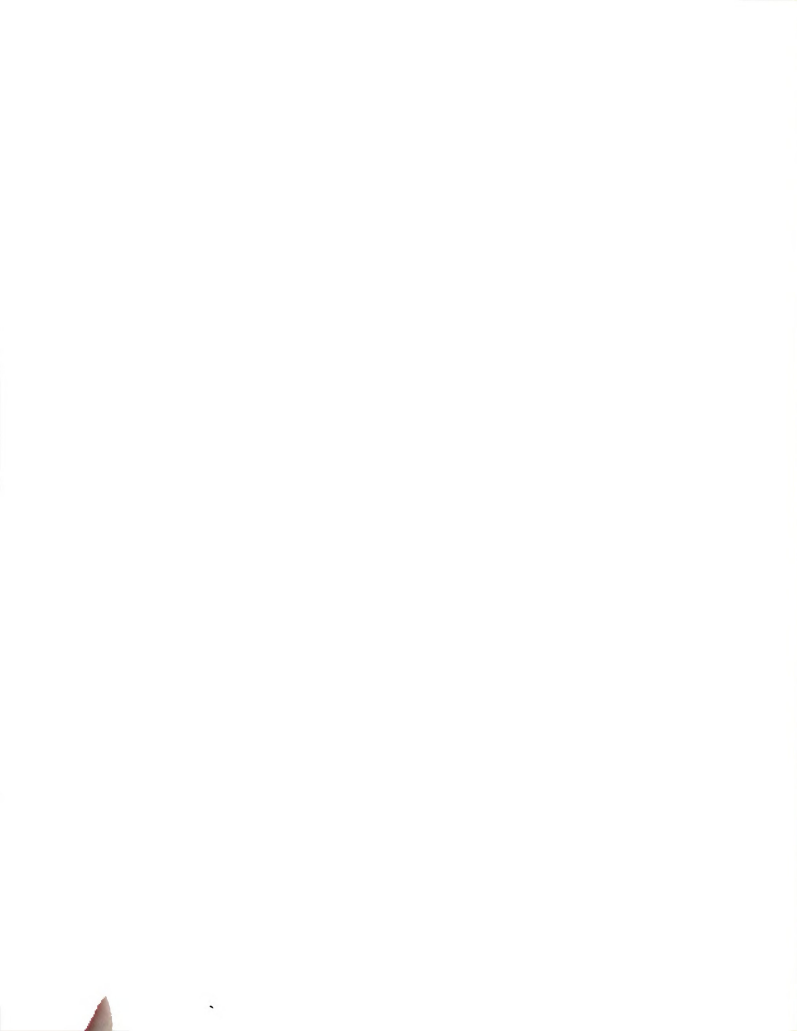
A DISSERTATION

Submitted to
Michigan State University
in partial fulfillment of the requirements
for the degree of

DOCTOR OF PHILOSOPHY

Department of Chemistry

1986



ABSTRACT

SYNTHETIC MODEL APPROACH TO THE ACTIVE SITE
STRUCTURE OF CYTOCHROME C OXIDASE

By

Myoung Seo Koo

Strong antiferromagnetic coupling ($-J \geq 200 \text{ cm}^{-1}$) between high-spin ferric heme a_3 and cupric Cu_B is a commonly accepted explanation for the EPR silent active site of the resting state cytochrome oxidase. The construction of synthetic model compounds is important for the understanding of the chemical nature of such a coupled heme-copper active site in the oxidase.

To achieve this aim, several strapped porphyrins and ligand appended, 6th coordination site blocked porphyrins were synthesized so that the Fe^{3+} and Cu^{2+} ions may be sequentially incorporated into the porphyrin and the appended ligand groups. μ -Oxo complexes of iron(III) porphyrin and copper(II) ion have been prepared; the magnetic susceptibility measurements revealed that the dithiazole strapped model compound has magnetically coupled high spin Fe(III) ($S_1=5/2$) and Cu(II) ($S_2=1/2$) ions with a resultant energy gap of $-3J = 132 \pm 5 \text{ cm}^{-1}$ between the



S = 2 and S = 3 states. This was the first example of a high spin ferric heme showing antiferromagnetic coupling with a cupric ion.

To avoid the formation of the external Fe-O-Fe dimer, the 6th site blocked model compounds were synthesized. IR (peak at 876 cm^{-1}) and magnetic susceptibility data of these model compounds demonstrated strong coupling in the μ -oxo binuclear complexes.

EPR spectra of the bis copper(II) complexes of these model compounds also showed spin interactions between two copper(II) ions.

Raman spectra of the binuclear complexes showing spin state, coordination state and ligand type were obtained.

These 6th coordination site blocked, tripyridine appended models are expected to best model the O_2 reduction site in cytochrome c oxidase.

To My Friends

ACKNOWLEDGEMENTS

I would like to express my appreciation to Professor Chi Kwong Chang for his guidance, patience, and for arranging financial support.

Appreciation is extended to Michigan State University and the National Science Foundation for financial support in the form of teaching and research assistantships.

Dr. Michail Kondylis and all of the group members are thanked for all of their help and friendship.

Robert T. Kean are also thanked for the Raman data.

The following people are acknowledged for the maintenance of friendship: Rev. Kim, Rev. Chung, Dr. Chang, Dr. Hahn, Hong, Nahm.

TABLE OF CONTENTS

Chapter	Page
LIST OF TABLES	<i>vi</i>
LIST OF FIGURES	<i>vii</i>
KEY TO ABBREVIATIONS AND SYMBOLS	<i>ix</i>
CHAPTER I - INTRODUCTION	1
Historical Perspective	1
Rationale and Outline	8
CHAPTER II - THE SYNTHESIS AND CHARACTERIZATION OF STRAPPED PORPHYRINS	17
Structural Design	17
Ligand Synthesis	18
A. Dithiazole Strapped Porphyrins	18
B. Dipyrindine Strapped Porphyrins	22
Metal Complexes	31
A. Synthesis	31
B. IR Data	31
C. Magnetic Susceptibility Data	32
D. EPR Data	34
Conclusion	36
Experimental	37
Physical Measurements	37
Materials and Synthesis	38
A. Dithiazole Strapped Porphyrins	39
B. Pyridine Strapped Porphyrins	41

c. Dipyridine Strapped Porphyrins	45
Metal and Oxygen Insertion	51
CHAPTER III - THE SYNTHESIS AND CHARACTERIZATION OF BLOCKED AND LIGAND APPENDED PORPHYRINS .	54
Introduction	54
Ligand Synthesis	56
Metal Complexes	56
A. Synthesis	59
B. IR Data	59
C. Magnetic Susceptibility Data	62
D. EPR Data	69
E. Raman Data	69
Conclusion	78
Experimental	79
Physical Measurements	79
Synthesis	80
A. Dithioether Appended Porphyrins	81
B. Tripyridine Appended Porphyrins	83
Metal and Oxygen Insertion	86
CHAPTER IV - SUMMARY AND FUTURE STUDIES	88
GLOSSARY	91
APPENDIX A	93
APPENDIX B	124
BIBLIOGRAPHY	131



LIST OF TABLE

Table	Page
Table 1. Molar magnetic susceptibility and effective magnetic moment as a function of temperature for the mononuclear Fe, binuclear Fe & Cu and μ -oxo-bridged binuclear Fe & Cu porphyrins blocked with t-butylbenzene.	63

LIST OF FIGURES

Figure	Page
Figure 1. Standard oxidation-reduction potentials for the steps involved in the conversion of oxygen to water at 25 °C and pH 7.	2
Figure 2. The structure of heme A.	4
Figure 3. Schematic representation of cytochrome c oxidase in its oxidized form. The hemes are represented as ellipses. Heme a is low-spin and heme a ₃ is high-spin.	5
Figure 4. The involvement of a μ-oxo-bridged species in the catalytic cycle of cytochrome oxidase. The ellipses represent heme a.	11
Figure 5. Previous models which failed to show coupling.	13
Figure 6. Schematic representation of the magnetic orbitals involved in the bridging of [Fe(P)-X-Cu(N ₄)] ²⁺ , where X = Cl, Br.	14
Figure 7. Schematic representation of (a) the orientation of metal atomic orbitals predicted for significant exchange interaction between a single electron in the d _{z²} orbital of high-spin Fe(III) ion in a porphyrin with an electron in the singly occupied d _{x²-y²} orbital of a Cu(II) ion in a square-planar, square-pyramidal, or tetragonal ligand field, via the p orbitals of a single bridging ligand X. The labeling of the axes around Cu as shown indicates the orthogonality of the ligand field of the Cu with respect to Fe and the singly-occupied orbital as d _{x²-y²} . Alternative labeling of the axes to match those of the Fe requires the appropriate Cu orbital to be designated d _{x²-z²} . (b) A ligand system which could maximize such orbital overlap.	15
Figure 8. Molar magnetic susceptibility and effective magnetic moment as a function of temperature for (a) solid and (b) the FeZnCl ₃ L complex and compound (3). The lines repre-	



	sent the fit of the data using $-3J = 132$ cm^{-1} . A diamagnetic correction of $-5 \times$ 10^{-4} e.m.u. mol ⁻¹ was applied to the mea- sured data.	33
Figure 9.	EPR spectrum of the bis-Cu ^{II} complex in CH ₂ Cl ₂ at 77 °K. The seven-line hyperfine pattern derived from the two copper(II) nuclei ($I = 3/2$) can be discerned on the left; only the two outermost lines are seen on the right.	35
Figure 10.	Infrared spectra of [Fe(P)-O-Cu(N ₄)(OH)] and [Fe(P)-Cl Cu(N ₄)(Cl)(OH)], blocked with t-butylbenzene.	60
Figure 11.	Infrared spectra of [Fe(P)- ¹⁶ O-Cu(N ₄)(OH)] (—) blocked with t-butylbenzene, and the ¹⁸ O labeled derivative(---).	61
Figure 12.	Molecular magnetic susceptibility and effective magnetic moment as a function of temperature for [Fe(P)-O-Cu(N ₄)(OH)], blocked with t-butylbenzene.	65
Figure 13.	Molecular magnetic susceptibility and effective magnetic moment as a function of temperature for [Fe(P)-O-Cu(N ₄)(OH)], blocked with Imidazole.	66
Figure 14.	EPR spectrum of the bis-Cu ^{II} complex, [Cu(P) Cu(N ₄)(Cl)(PF) ₆] blocked with t-butylbenzene, in CH ₂ Cl ₂ at 77 °K.	70
Figure 15.	EPR spectrum of the bis-Cu ^{II} complex, [Cu(P) Cu(N ₄)(Cl)(PF) ₆] blocked with imidazole, in CH ₂ Cl ₂ at 77 °K.	71
Figure 16.	Raman spectra of simple model complexes.	73
Figure 17.	Raman spectrum of [Fe(P)-Cl Cu(N ₄)(Cl)(OH)] blocked with t-butyl benzene.	74
Figure 18.	Raman spectrum of [Fe(P)-O-Cu(N ₄)(OH)] blocked with t-butylbenzene.	74
Figure 19.	Raman spectrum of [Fe(P)-Cl Cu(N ₄)(Cl)(OH)] blocked with imidazole.	75
Figure 20.	Raman spectrum of [Fe(P)-O-Cu(N ₄)(OH)] blocked with imidazole.	75



KEY TO ABBREVIATIONS AND SYMBOLS

ATP	Adenosine 5'-triphosphate
DMF	N,N-Dimethylformamide
DMSO	Dimethyl sulfoxide
THF	Tetrahydrofuran
c	Speed of light
g	Gyromagnetic ratio for an electron
κ	Boltzmann's constant
\mathcal{H}	Hamiltonian operator
h	Planck's constant
N	Avogadro's constant
N	Temperature independant magnetic susceptibility
β	Bohr magneton (B.M., $eh/4\pi mc$)
δ	Zero field splitting
θ	Weiss constant
μ	Magnetic moment (effective magnetic moment)
$\mu_{s.o.}$	Spin only magnetic moment
χ_m	Magnetic susceptibility per mole ($\text{cm}^3 \text{ mole}^{-1}$, c.g.s. e.m.u.)
J	Exchange integral $1.38044 \times 10^{-16} \text{ erg deg}^{-1} \text{ mole}^{-1}$
h	$6.6256 \times 10^{-27} \text{ erg s}$
β	$0.92731 \times 10^{-20} \text{ erg gauss}^{-1}$, or $4.66858 \times 10^{-5} \text{ cm}^{-1} \text{ gauss}^{-1}$



g 2.0023 (free electron)
N β^2 0.26073 cm⁻¹ erg gauss⁻² mole⁻¹
3 κ /N β^2 7.9971 mole gauss² erg⁻¹ deg⁻¹
 κ T 1.3804 x 0.5035T cm⁻¹ mole⁻¹
 (e.g. 208.4 cm⁻¹ mole⁻¹ at 300 °K)



CHAPTER I

INTRODUCTION

Historical Perspective

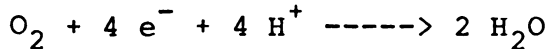
In 1886, MacMunn, a British physician, discovered the respiratory pigment, indicated by an absorption band in the spectrum of slices of various plant and animal tissues. This important observation attracted little attention at the time of its publication and became effectively lost in the literature. In 1925, Keilin rediscovered the MacMunn pigment, proved it to be a mixture of three spectroscopically identifiable components which he named cytochrome a, b, and c. Cytochrome a and c showed a special relationship to each other. Cytochrome a was the sole physiological oxidizing agent for cytochrome c, hence, the name cytochrome c oxidase. In 1939, Keilin and Hartree were able to distinguish cytochrome a and a_3 and identify cytochrome a_3 as the component that reacts with oxygen.

In general cytochrome c oxidase has been isolated from mitochondria or mitochondrial fragments by initial extraction of proteins with a surface-active agent followed by removal of contaminating detergent and protein.

Cytochrome c oxidase, the terminal oxidase in the respiratory metabolism of all aerobic organism, plants,



animals, yeasts, algae, and some bacteria, is responsible for catalyzing the reduction of dioxygen to water. The free energy developed in oxygen reduction is used to promote oxidative phosphorylation, generating ATP, to satisfy the energy requirement of the cell. It is not surprising then that this oxidase is found in high concentrations in tissues where the energy requirements are high. Especially high levels of oxidase have been observed in heart muscles, flight muscles of birds and insects, liver mitochondria, brain gray matter, and sugar cane roots. Malström suggested that 90 % of biological oxygen consumption is directed through the oxidase. The electrons are provided by reduced cytochrome oxidase in the following overall reaction:



Reduction of molecular oxygen to water, as it happens in biological systems, requires 4 electrons. From thermo-

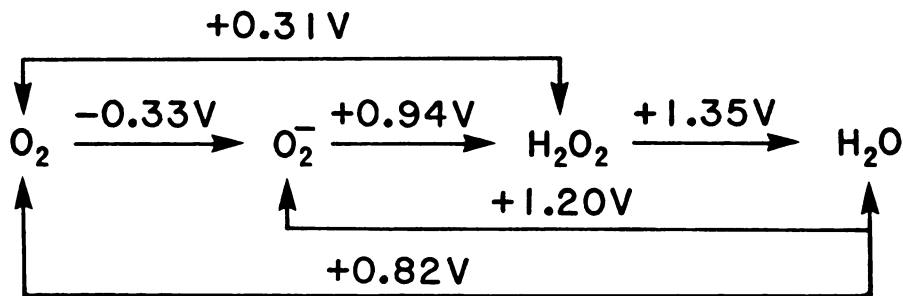


Figure 1. Standard oxidation-reduction potentials for the steps involved in the conversion of oxygen to water at 25 °C and pH 7.

dynamic as well as physiological points of view it is important to have more than one electron transferred at a time to the oxygen molecule to avoid the production of high energy and also toxic superoxide intermediate (Figure 1).¹ It is conceivable why cytochrome oxidase is especially suitable for oxygen reduction: presumably the 2 heme prosthetic groups and the 2 copper ions of cytochrome oxidase are capable of bringing about the multielectron transfer to the ligated oxygen.

The molecular weight of cytochrome oxidase appears to be approximately 140,000.² The metal content (11 n moles/mg protein) and the iron to copper ratio (1.0) are well established for the bovine enzyme, whereas in yeast, the reported metal contents are higher and more variable (5-15 n moles of iron per milligram of protein). And the copper to iron ratio is greater than unity (1.5). It is most probable that the minimal functional unit contains two hemes and two copper ions.

The structure and function of cytochrome oxidase has been the subject of much investigation and controversy over the past 40 years.³⁻⁶ The iron in the enzyme is present in the form of heme a (Figure 2). The heme a is bound to two different polypeptides, cytochrome a and cytochrome a₃.⁷ The structure of both hemes is identical (Heme a). The variation in the properties of the prosthetic groups in cytochrome a and cytochrome a₃ is undoubtedly due to differing protein environments.



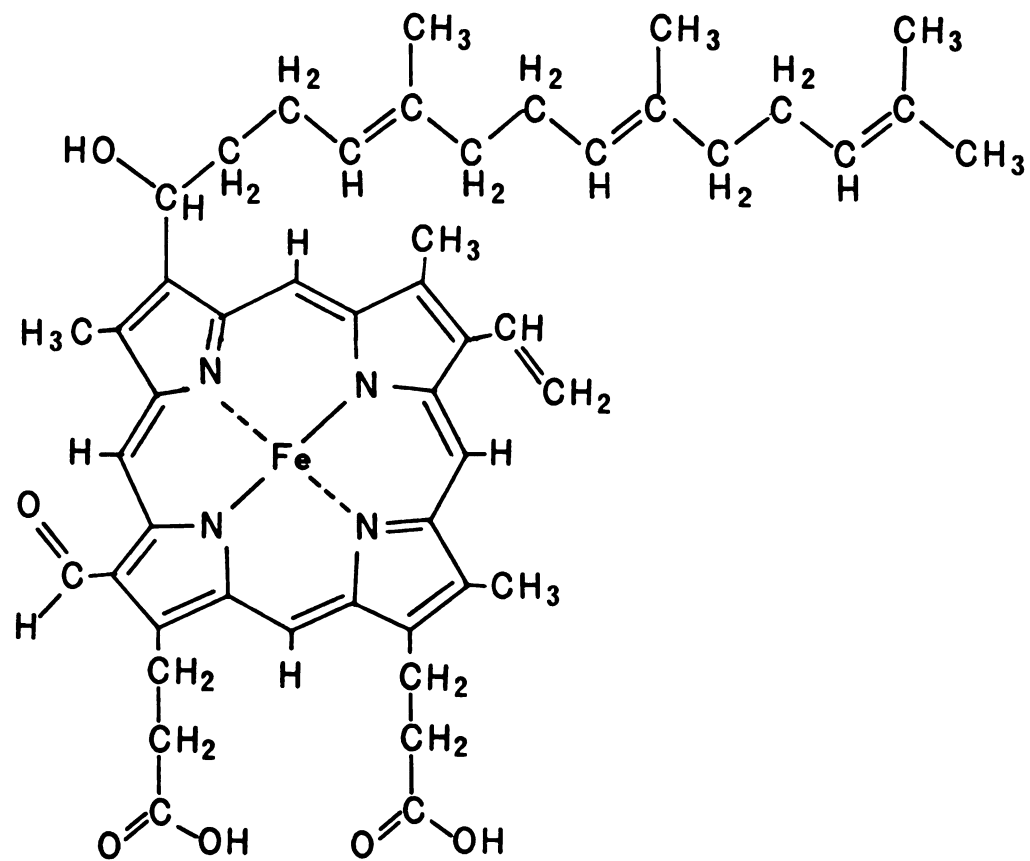


Figure 2. The structure of heme A.

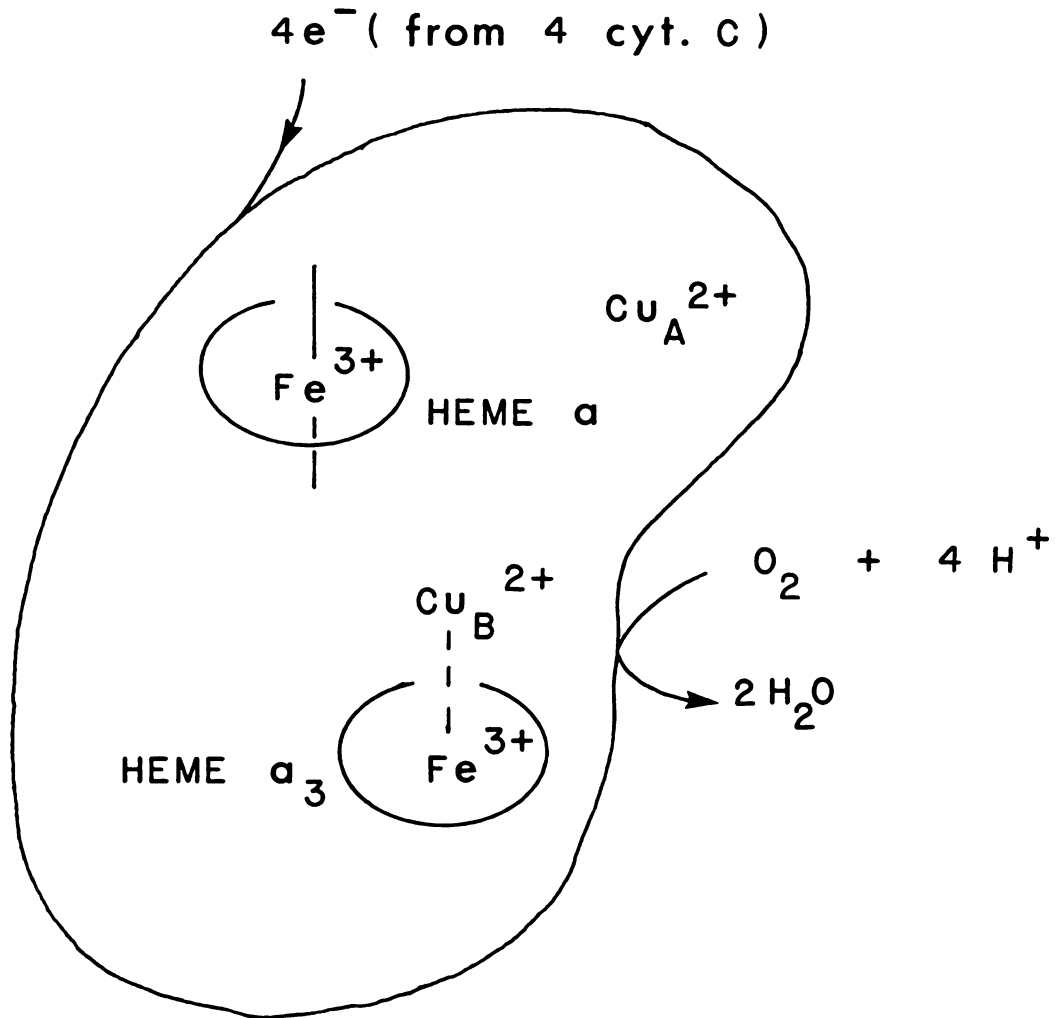


Figure 3. Schematic representation of cytochrome c oxidase in its oxidized form. The hemes are represented as ellipses. Heme a is low-spin and heme a_3 is high-spin.²¹

Current views of the oxidase generally regard cytochrome a_3 as the site of dioxygen reduction and cytochrome a as the site of cytochrome c oxidation (Figure 3).⁸

Cytochrome a_3 is associated directly with the binding (and consequent reduction) of the O_2 molecule. Cytochrome a serves as an electron shuttle, mediating the transfer of reducing equivalents from cytochrome c to the cytochrome a_3 - O_2 complex.

The coordination environment of copper is far less clear, but the easy reducibility of copper seems to require a coordination environment that stabilizes Cu(I) relative to Cu(II). The intensity of the EPR signal corresponded to only about 40 % of the total copper known to be present as copper(II) in oxidase or, as now appears likely, 80 % of one copper and none of the second copper.⁹ The EPR signal resulting from iron(III), because of its breadth and partial submission under the copper(II) signal, was proved much more difficult to study quantitatively. Nevertheless, It now seems well established that in oxidase, iron(III) is represented by signal at $g = 3, 2,$ and 1.5 with intensities that correspond to about 40 % of the heme iron present.^{10,11}

Only one iron and one copper ion are EPR detectable in the fully oxidized resting state. The signals are attributed to the cytochrome a and Cu_a pair. The lack of EPR signals is most puzzling and has been the focus of many studies.

Recent EPR,¹²⁻¹⁴ magnetic susceptibility,¹⁵⁻¹⁷ and magnetic circular dichroism (MCD)^{12-14,18} measurements have

indicated the presence of a strongly magnetically coupled Fe(III)-Cu(II) center at the cytochrome a_3 active site in the fully oxidized resting state enzymes.

An intriguing structural aspects of this active site in its oxidized form is the strong antiferromagnetic coupling between the presumed high spin $S = 5/2$ Fe(II) heme a_3 and $S = 1/2$ Cu a_3 (II) atom making these two metals EPR "invisible" and lowering their magnetic susceptibilities. The strength of this antiferromagnetic coupling, quantified by $-J$, the exchange coupling constant, is estimated to be greater than 200 cm^{-1} for the oxidase.^{15,19} The heme a_3 and Cu a_3 are assumed to be in close proximity and bridged by a ligand which can mediate very strong magnetic exchange.

Since the structure of the active site must be known in order to understand the catalytic mechanism, there have been numerous suggestions regarding its nature. Because of the problems involved in studying the natural enzyme, and the paucity of available information on simple binuclear systems containing different metal ions, there has been considerable recent interest in the synthetic analogue approach to the active site structure of cytochrome c oxidase. The important features of cytochrome c oxidase modelling studies are

- 1) Iron(III)-copper(II) complex which exhibits strong antiferromagnetic coupling.
- 2) The catalytic four electron reduction of O_2 to H_2O .
- 3) The electron transfer and spectroscopic properties

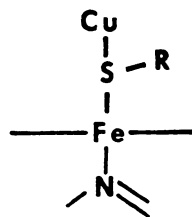
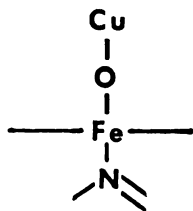
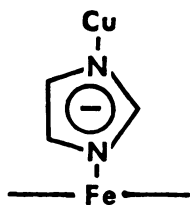
of cytochrome a.

For constructing the heme a_3 -Cu a_3 site, the minimal requirement is an Fe(III)-porphyrin and a Cu(II) group in close proximity with bridging groups which could preferably be varied in order to monitor the resulting magnetic behavior. At the same time it is hoped that the redox properties of the models would allow reduction to the Fe(II)-Cu(I) complex on which oxygen binding studies could be performed.

Rationale and outline

It has been relatively well-established that oxygen binds to only one pair of heme and copper in cytochrome c oxidase, referred to as the heme a_3 -Cu a_3 binding site, and receives electrons and protons to undergo reduction.¹ In the resting (fully oxidized) state of the enzyme, heme a_3 -Cu a_3 exhibits strong antiferromagnetic coupling with a $-J > 200 \text{ cm}^{-1}$. This large coupling phenomenon has thence inspired a number of proposals suggesting an imidazolate (from histidine),¹² oxo (from O_2 , H_2O , or tyrosine),²⁰⁻²³ or mercapto (from cysteine or methionine)^{24,25} group bridging between the heme iron and copper.

The bridging ability for histidine has recently been



demonstrated in the x-ray structure of the enzyme superoxide dimutase. Where an imidazole ring simultaneously coordinates both the cupric and zinc ions via its two nitrogen atoms. Metal substituted derivatives of superoxide dimutase of composition $(\text{Cu}^{2+})_4$ and $(\text{Cu}^{2+})_2(\text{Co}^{2+})_2$ compared to $(\text{Cu}^{2+})_2(\text{Zn}^{2+})_2$ in the native protein are magnetically abnormal with EPR and magnetic susceptibility properties diagnostic of antiferromagnetic interactions. The suggestion of histidine bridge between copper and iron would thus seem plausible.

It is further proposed that reduction is accompanied by a conformational change in the enzyme thus exposing the sixth coordination site of cytochrome a_3 to ligands.

The $S = 2$ center paramagnetism has been interpreted as arising from a cytochrome a_3^{3+} ($S=5/2$)--- Cu^{2+} ($S=1/2$) antiferromagnetically coupled iron-copper binuclear complex of total spin $S = 2$ with $-J > 200 \text{ cm}^{-1}$.

There are now several examples of synthetic complexes which contain imidazolate-bridged metal centers. Thus, there is no question of the bridging capabilities of the imidazolate anion. The controversy that has arisen is over the magnitude ($-J > 200 \text{ cm}^{-1}$) present for the $\text{Fe}^{\text{III}}\text{-Cu}^{\text{II}}$ pair of cytochrome oxidase. The construction of synthetic model compounds is important for testing the proposed structures of the oxidase active site. At present, however, there are no well defined examples of such synthetic, iron-copper binuclear complexes with imidazolate bridges.

Attempts to isolate $\text{Fe}^{\text{III}}(\text{TPP})(2\text{-methyl imidazole})\text{Cu}(\text{acac})_2$ compound was not successfully.²⁶ In fact, very few binuclear complexes containing different transition metals have been reported.

A variety of imidazolate bridged metalloporphyrins have been synthesized.²⁶⁻²⁸ All of the characterized species seem to suggest that imidazolate is not capable of mediating the strong coupling observed in cytochrome oxidase ($-J > 200 \text{ cm}^{-1}$). In view of the above inconclusive evidence for an imidazolate-bridged structure in oxidase, other alternatives must be considered (Figure 4).²³

μ -Oxo and μ -sulfido bridged alternatives seem to satisfy all the magnetic and spectroscopic data presently available for the protein, including some primary extended X-ray absorption fine structure (EXAFS) data^{24,25} which indicated an Fe---Cu separation of only $3\text{-}3.8 \text{ \AA}$ in resting oxidase, whereas imidazolate bridge requires at least 5 \AA . The μ -oxo hypothesis is particularly attractive.²⁰⁻²³ Insertion of O_2 between the two metals can then be viewed as producing, via oxidative addition, a transient μ -peroxo species which further reacts with 2 H^+ to produce H_2O and a stable mixed-metal μ -oxo center.

Exchange interactions approaching the magnitude displayed by the oxidase are known to be commonplace for synthetic $\text{Fe}^{\text{III}}\text{-O-Fe}^{\text{III}}$ centers, such as in $(\text{TPP})\text{Fe}_2\text{O}$ where $-J$ is 150 cm^{-1} . Furthermore, a transient $(\text{FeOOFe})^*$ species, reminiscent of the proposed $(\text{FeOOCu})^*$ structure for oxidase,

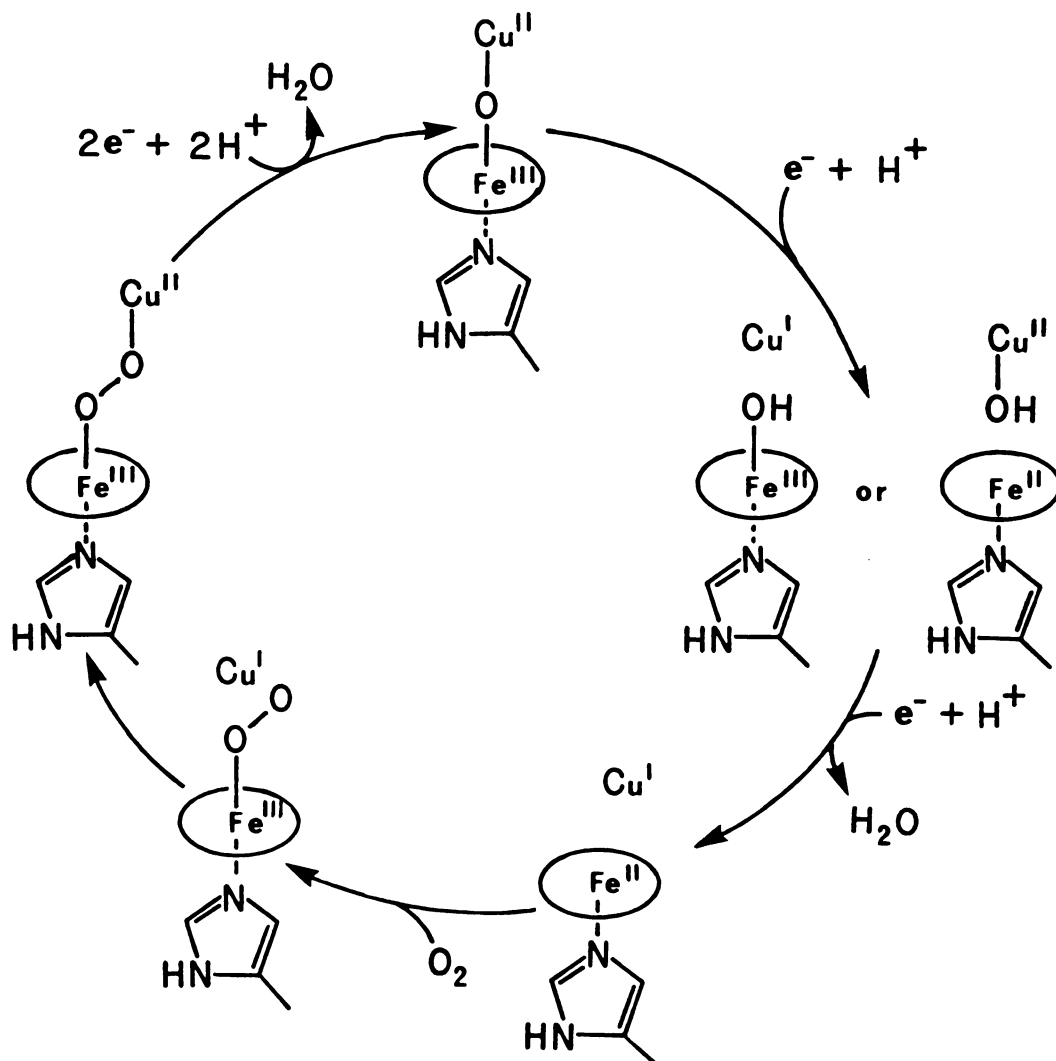


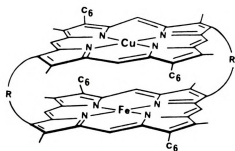
Figure 4. The involvement of a μ -oxo-bridged species in the catalytic cycle of cytochrome oxidase. The ellipses represents haem a_3 .

has been shown to be the reaction intermediates during the formation of the thermodynamically more stable $[\text{Fe}^{\text{III}}-\text{O}-\text{Fe}^{\text{III}}]$ compounds.²⁹ Similarly, oxyhemerythrin,³⁰ oxyhemocyanin,³¹ and a recently reported oxyhemocyanin model compound³² all contain μ -peroxo centers.

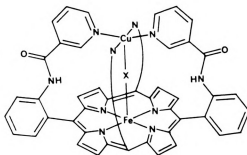
Finally, the catalytic redox cycle for the O_2 -bridging model would be completed by a 2 electron reduction of the $\text{Fe}^{\text{III}}-\text{O}-\text{Cu}^{\text{II}}$ unit and an oxide or hydroxide extrusion-protonation reaction to again generate a H_2O molecule and complete the observed overall 4 electron reduction of O_2 :
 $\text{O}_2 + 4 \text{H}^+ + 4 \text{e}^- \text{-----} \rightarrow 2 \text{H}_2\text{O}$. This final step in the proposed mechanism is supported by the fact that the 2 electron electrochemical reduction of $(\text{TPP})\text{Fe}_2\text{O}$ has been shown to result in reductive cleavage of the oxo bridge with the production of $[(\text{TPP})\text{Fe}^{\text{II}}]$ and $[(\text{TPP})\text{Fe}^{\text{II}}\text{OH}]^-$.³³

Attempts to produce single atom-bridged heme and copper complexes have met with only limited success.^{26,27,34-46} Many of the early heme-copper model systems failed to show any significant magnetic interactions between the two metal ions (Figure 5). The negative results may be attributable to several reasons:

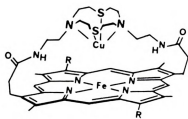
- 1) The Fe-Cu distance sometimes is too large.
- 2) The ligand framework is too rigid to allow flexibility.
- 3) The cupric ion is often held in a square planar geometry with a mismatched atomic orbitals between the metals.



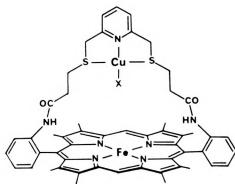
Chang (1979) "Biochemical & Clinical Aspects of Oxygen"
 Caughey, Ed. (1981)
 J. Am. Chem. Soc. 103, 5236.



Gunter, Murray, et al. (1980)
 J. Am. Chem. Soc. 102, 1470.



Chang, Lehn
 Unpublished Results



Gunter, Mander, et al. (1981)
 J. Am. Chem. Soc. 103, 6784.

Figure 5. Previous models which failed to show coupling.

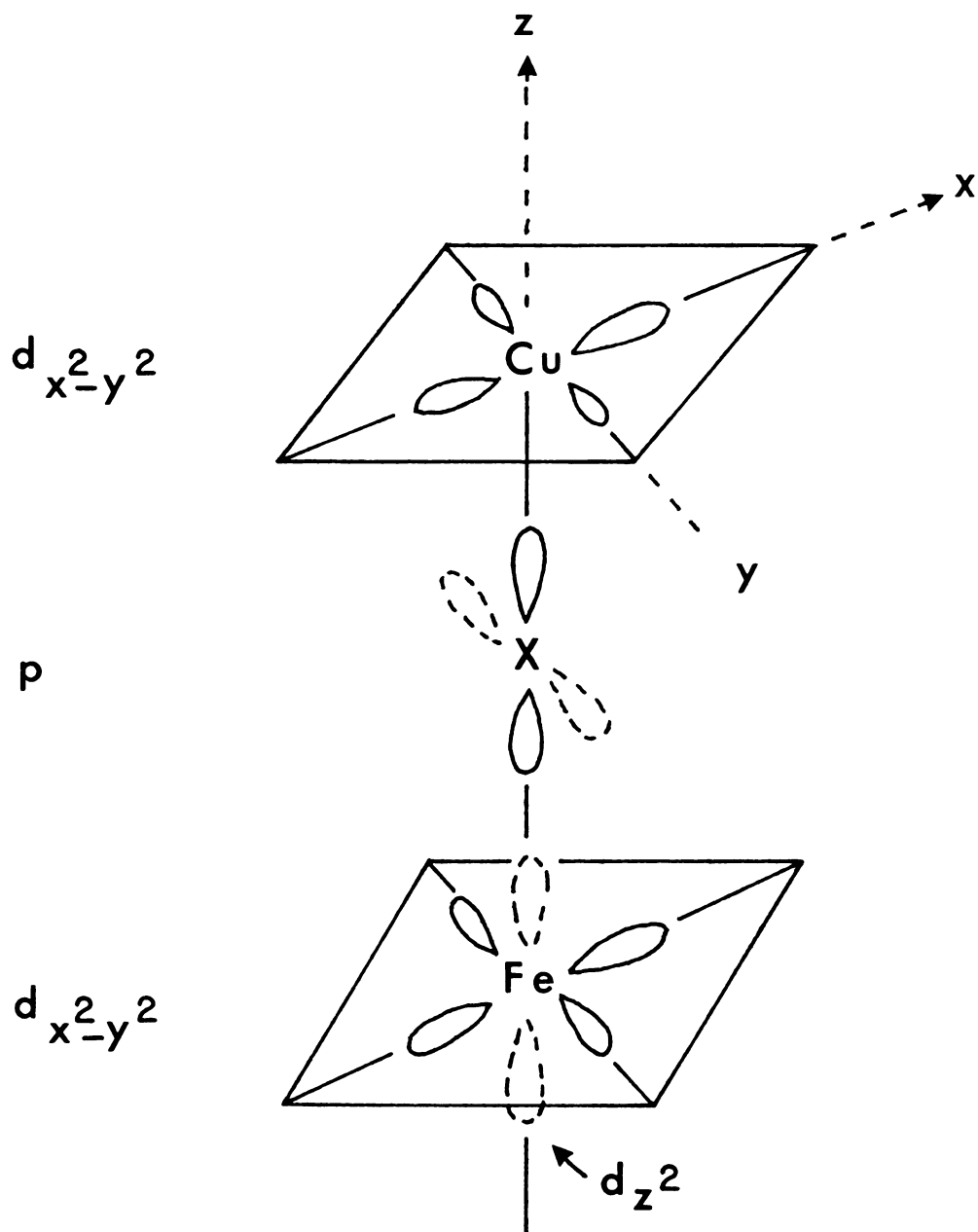


Figure 6. Schematic representation of the magnetic orbitals involved in the bridging of $[\text{Fe}(\text{P})\text{-X-Cu}(\text{N}_4)]^{2+}$, where X = Cl, Br.



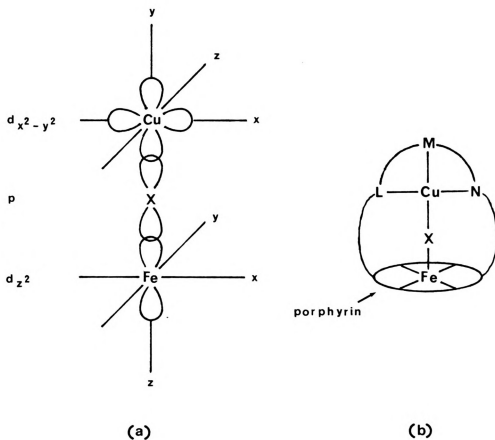


Figure 7. Schematic representation of (a) the orientation of metal atomic orbitals predicted for significant exchange interaction between a single electron in the d_{z^2} orbital of high-spin Fe(III) ion in a porphyrin with an electron in the singly occupied $d_{x^2-y^2}$ orbital of a Cu(II) ion in a square-planar, square-pyramidal, or tetragonal ligand field, via the p orbitals of a single bridging ligand X. The labeling of the axes around Cu as shown indicates the orthogonality of the ligand field of the Cu with respect to Fe and the singly-occupied orbital as $d_{x^2-y^2}$. Alternative labeling of the axes to match those of the Fe requires the appropriate Cu orbital to be designated $d_{x^2-z^2}$. (b) A ligand system which could maximize such orbital overlap.

In the case of the N_2S_2 thiaza⁴⁷ crowned porphyrin⁴⁸ the copper binding was so weak that dissociation of Cu(II) presented a serious problem.⁴⁹

Significant pathways for superexchange are therefore not possible. This is shown schematically in Figure 6: the highest occupied orbital on Cu is $d_{x^2-y^2}$, which is orthogonal to the Cl p-orbitals, while all the Fe d-orbitals are partially occupied.⁵⁰ The problem is a great lack of σ -overlap in this model.

An apparent solution would be to build a non-square planar copper ligand possessing a good affinity for Cu(II) and structurally flexible enough to assure a strain free interaction with a pendant heme group (Figure 7).³⁴

This thesis describes our effort to synthesize oxidase model compounds equipped with copper-binding ligands on top of the heme group so that interactions between the heme iron iron and copper ion may occur.

CHAPTER II

THE SYNTHESIS AND CHARACTERIZATION OF
STRAPPED PORPHYRINStructural Design

In the light of our observations on the previous model system,^{37,40,50} we expected that the most effective exchange pathway would result from σ overlap (via the p orbitals of a bridging ligand) of the singly occupied $d_{x^2-y^2}$ Cu(II) orbital with the d_z^2 orbital of the high-spin Fe(III) (Figure 7a).^{34,51} This requires a ligand system such as that represented in Figure 7b where the average ligand plane around the Cu is orthogonal to the porphyrin mean plane. These conditions (Figure 7) have been met in a heme-tridentate ligand system shown in the scheme (SCHEME I, IIA, IIB, and III).⁵²

The sulfur atoms, particularly the methionine, are thought to be necessary for the high redox potentials reported for the enzymes.⁵³ However, the binding ability of bis(pyridyl)-thioether tridentate ligand (in 24a)⁵⁴ and bis(pyridyl)-dithioether tetradentate ligands (24b, 24c),^{53,55-56} [Cu(II)Py₂S, Cu(II)Py₂S₂ complexes], was well demonstrated for the facultative linear (open-chain) quadridentate chelate groups. The central position of the

thioether donors in the chelating ligands ensures their binding to the copper ion and the variation in chelating ring size would provide some insight into the effect of stereochemistry on the spectral and redox properties.

Ligand Synthesis

A. Dithiazole Strapped Porphyrins

The requisite diamino thiazole sulphite (5) was synthesized according to scheme I where each step had a yield of at least 90 %. All compounds were characterized by ^1H NMR and mass spectrometry.

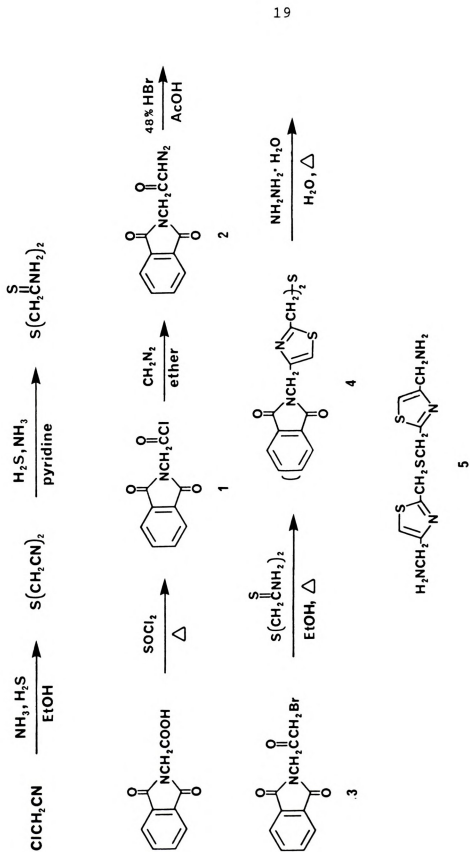
Bis(cyanomethyl) sulfide was easily generated from chloroacetonitrile by the method of Zweigbergk.⁵⁷ The sulfide was converted to bis(thiocarbamoylmethyl) sulfide by the method of Mukhina.⁵⁸ The product was found to be unstable at room temperature and slowly decomposed.

1-Bromo-3-phthalimidopropanone (3) was prepared from N-phthaloylglycine⁵⁹ by the method of Balenović.^{60,61}

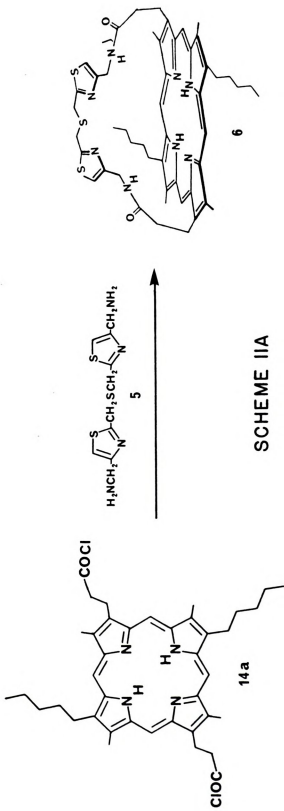
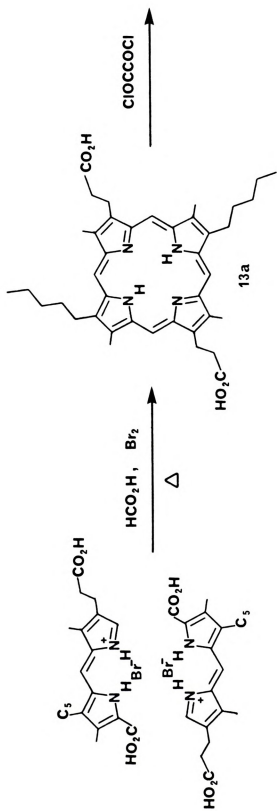
The diphtalimide 4 was synthesized by condensation of 2 equivalent amounts of 1-bromo-3-phthalimidopropanone and bis(thiocarbamoylmethyl) sulfide and hydrolyzed to the diamine (5) by the application Jones' procedure.⁶²

The diamine was treated with an equimolar quantity of the porphyrin diacid chloride (14a) in methylene chloride using a high-dilution technique.⁴⁸ Unfortunately, the space-filling plastic model of the strapped porphyrin 6 (SCHEME IIA) showed the dithiazole thioether is not on the porphyrin

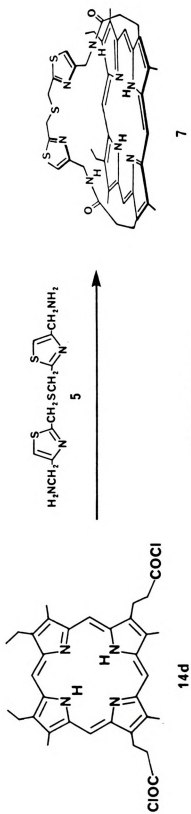
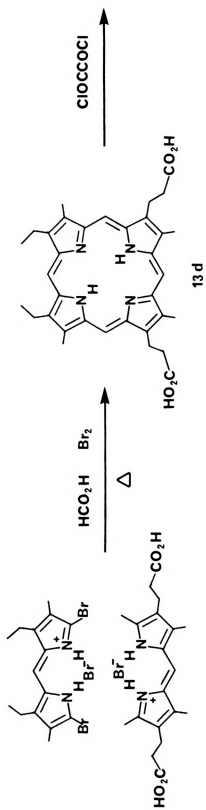




SCHEME I



SCHEME IIA



center.

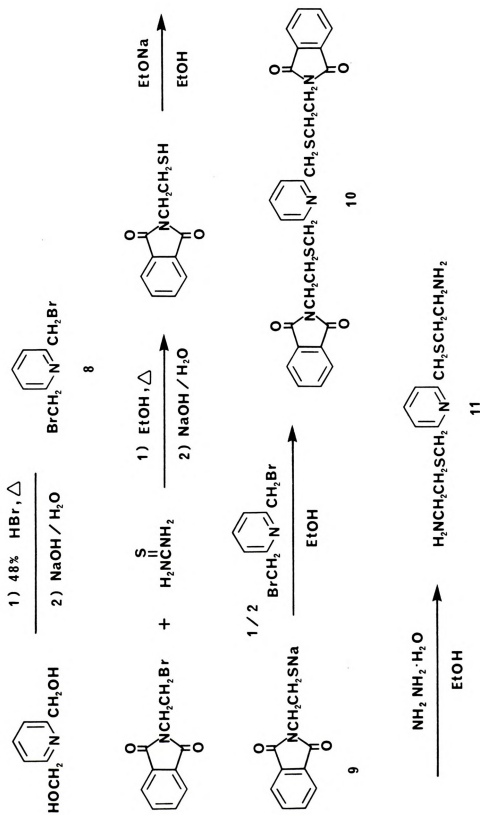
On the contrary, the dithiazole thioether of the strapped porphyrin 7 (SCHEME IIB) should be on the porphyrin center. The diamine was treated with an equimolar quantity of mesoporphyrin XII⁶³ diacid chloride in CH_2Cl_2 using a high-dilution technique. The resultant thiazole-strapped porphyrin (7) was purified by chromatography (silica gel 6 & $\text{MeOH-CH}_2\text{Cl}_2$ and crystallized from $\text{CH}_2\text{Cl}_2\text{-MeOH}$) yield 72 %.

¹H NMR spectroscopy indicated that the protons a, b, and c resonate at δ 0.86, 5.80, and 3.97, respectively: these are displaced significantly upfield from their original positions in the uncoupled amine, thereby establishing the indicated strap-on-top structure.

Porphyrins of C_{2h} symmetry were obtained by the condensation of suitable pyrroles, in the strongly acidic media, with the pyrrole aldehyde to afford the intermediate dipyrromethenes. Brominative decarboxylation and cyclization of dipyrromethenes without isolation of any of the intermediates then afforded the desired porphyrins with very good yield.⁶⁴

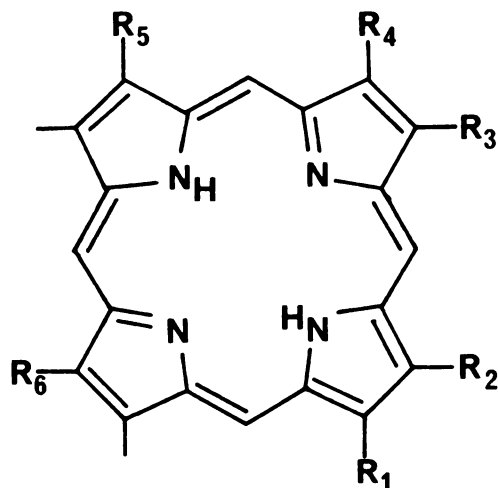
B. Dipyridine Strapped Porphyrins

Ethyl 2,5-pyridinedicarboxylate was prepared from 2,5-pyridinedicarboxylic acid. The above diester was reduced to ethyl 5-hydroxymethyl-2-pyridinecarboxylate by Matsumoto's patented method.⁶⁵ Phosphorus trichloride and dimethylformamide reagents⁶⁶ were used to convert ethyl



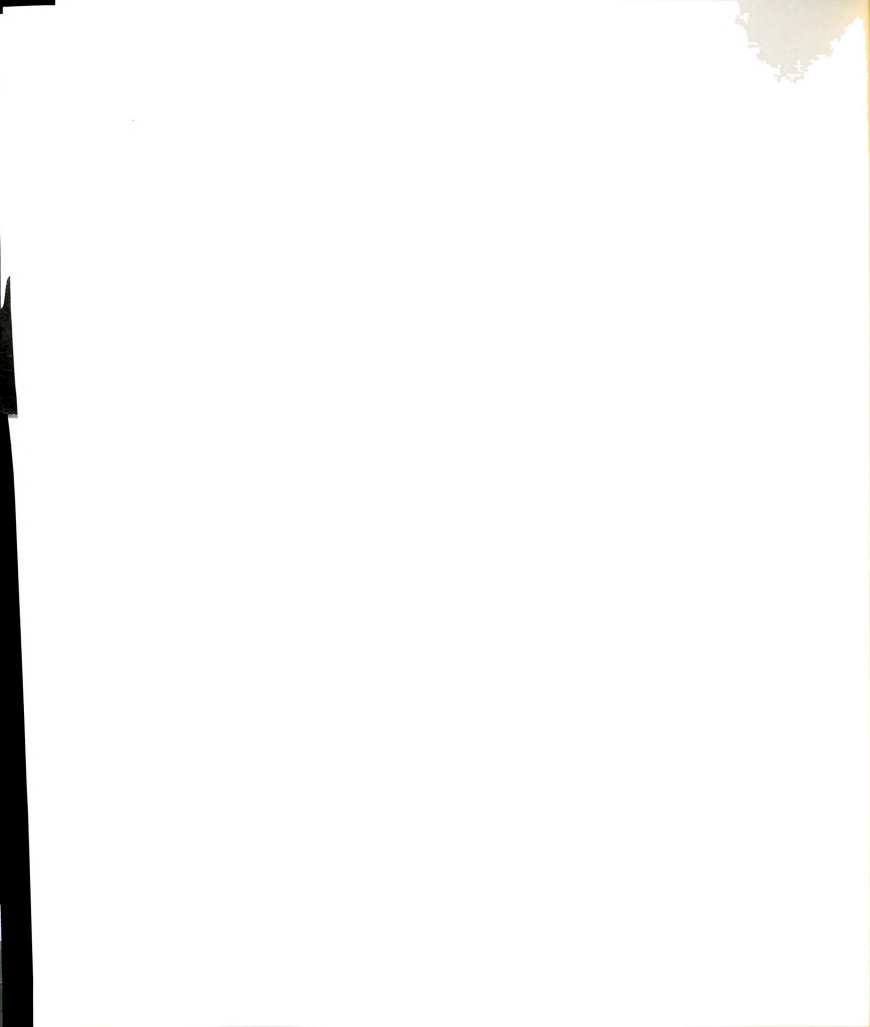
SCHEME III

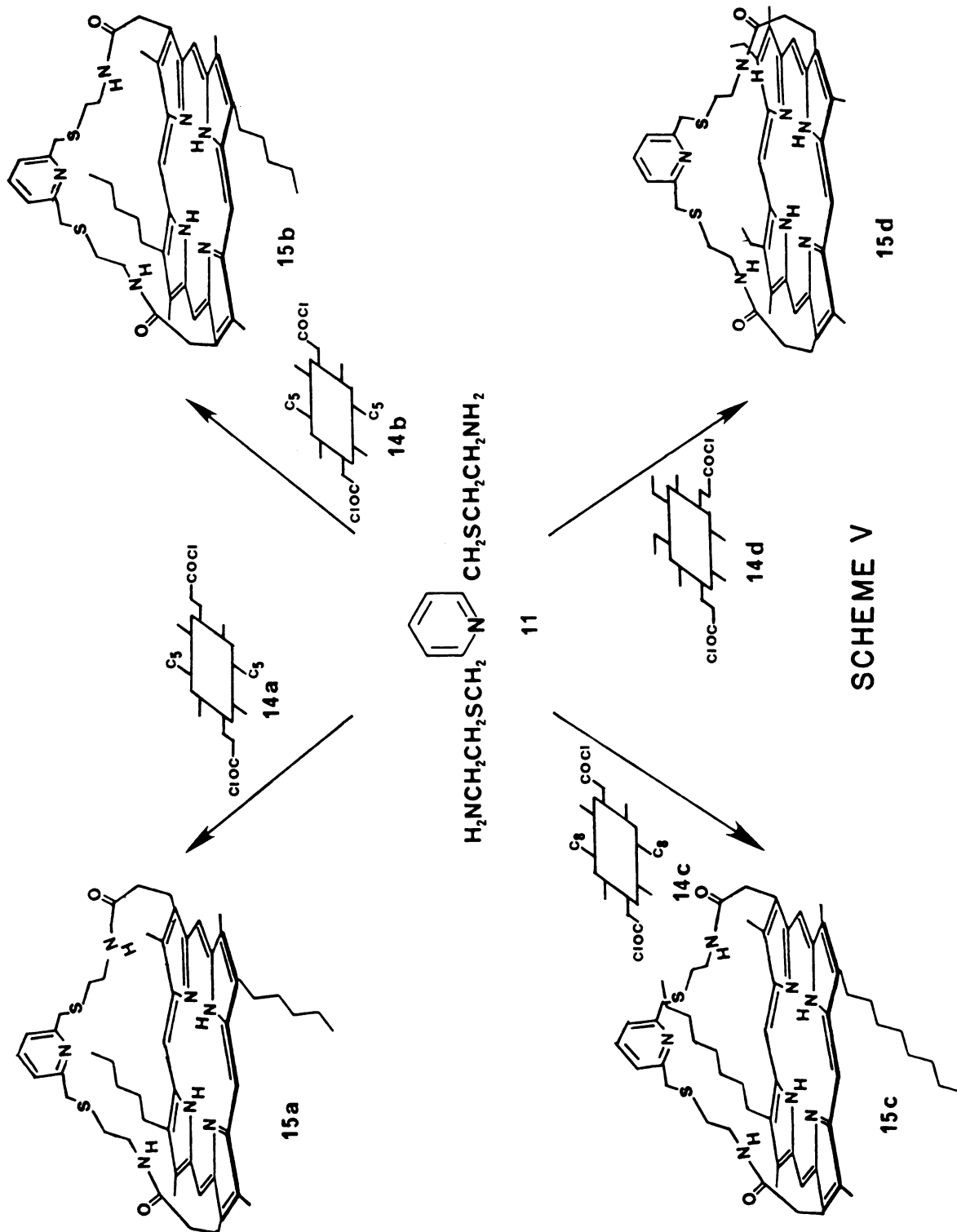




- 12 a $R_1=R_5=C_5$ $R_2=R_4=C_1$ $R_3=R_6=CH_2CH_2COOCH_3$
 b $R_1=R_5=C_5$ $R_2=R_4=C_1$ $R_3=R_6=CH_2COOCH_3$
 c $R_1=R_5=C_8$ $R_2=R_4=C_1$ $R_3=R_6=CH_2COOCH_3$
 d $R_1=R_3=C_1$ $R_4=R_5=C_2$ $R_2=R_6=CH_2CH_2COOCH_3$
- 13 a $R_1=R_5=C_5$ $R_2=R_4=C_1$ $R_3=R_6=CH_2CH_2COOH$
 b $R_1=R_5=C_5$ $R_2=R_4=C_1$ $R_3=R_6=CH_2COOH$
 c $R_1=R_5=C_8$ $R_2=R_4=C_1$ $R_3=R_6=CH_2COOH$
 d $R_1=R_3=C_1$ $R_4=R_5=C_2$ $R_2=R_6=CH_2CH_2COOH$

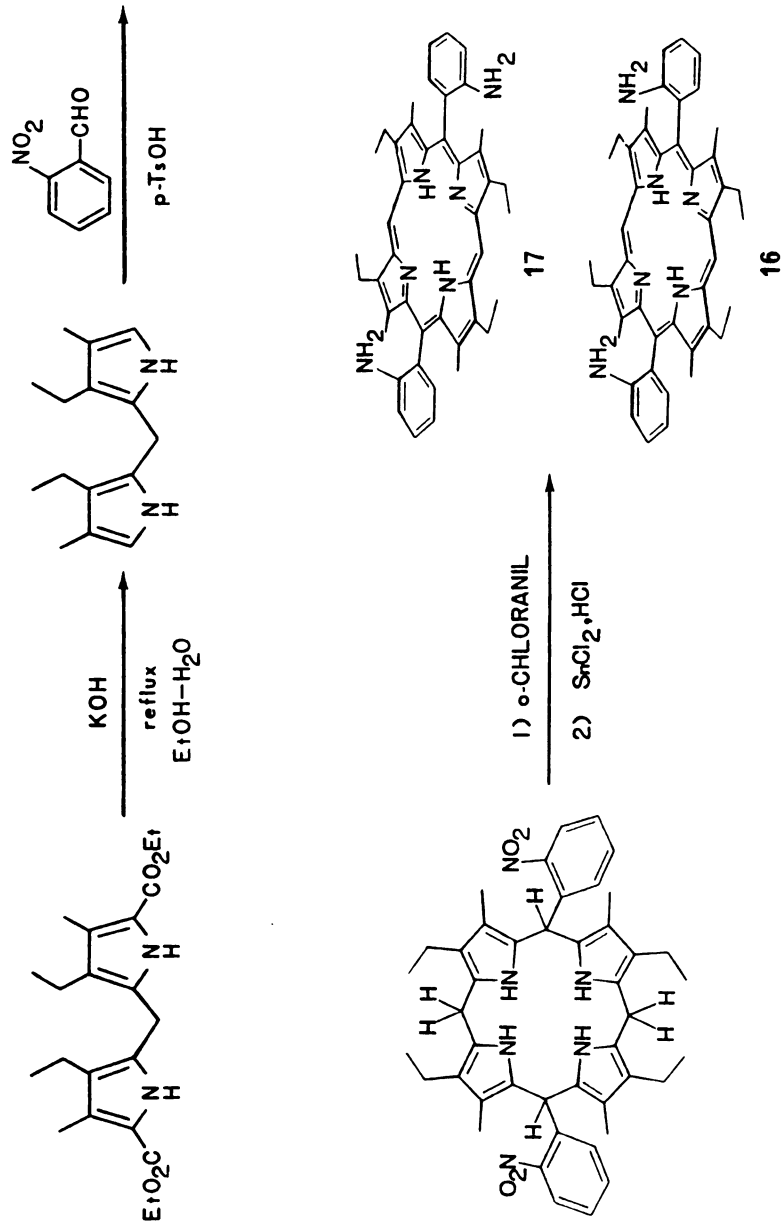
SCHEME IV





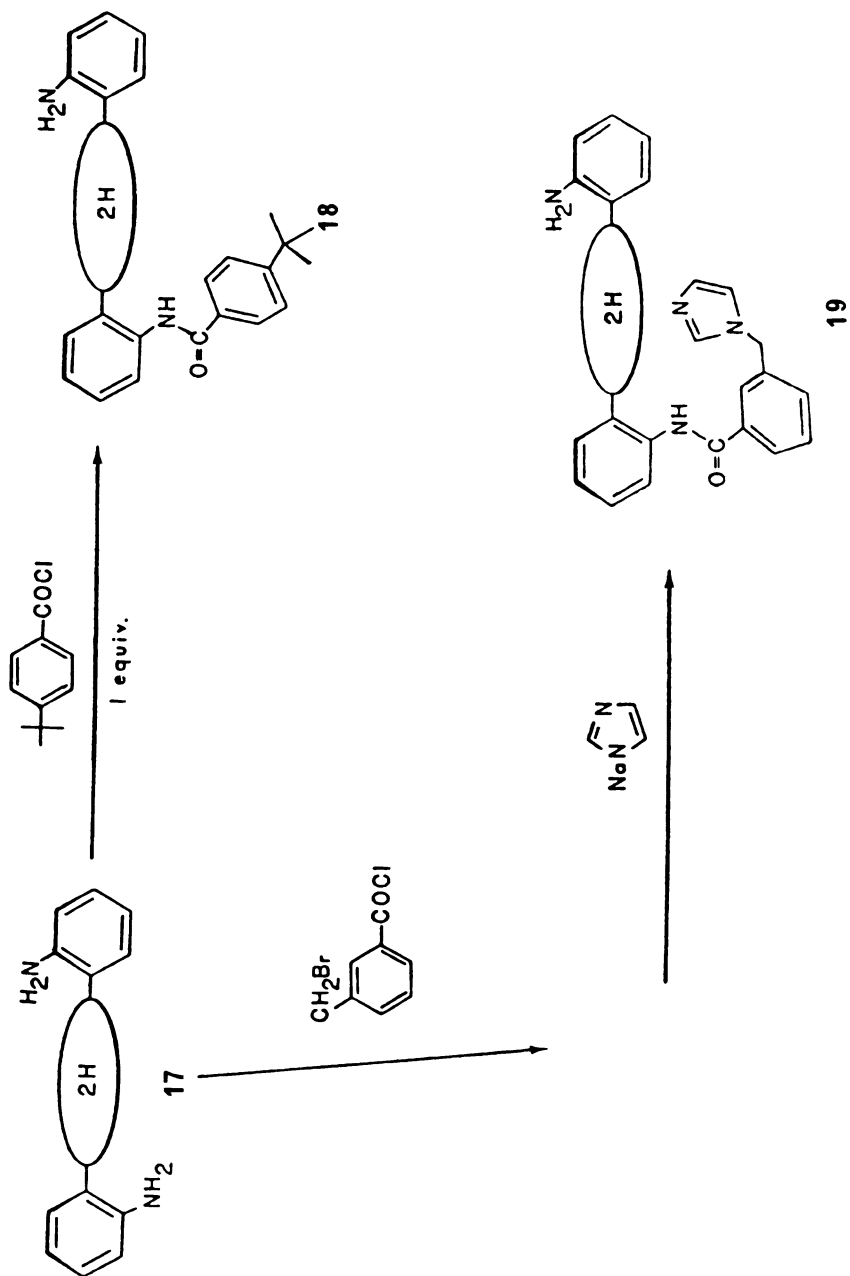
5-hydroxymethyl-2-pyridinecarboxylate to ethyl 5-chloromethyl-2-pyridinecarboxylate (SCHEME VIII). No hydrogen chloride formation was observed. Thus, the dimerization of the 2-chloromethyl can be avoided. The parent compound, 5,15-bis(o-aminophenyl)-2,8,12,18-tetramethyl-3,7,13,17-tetramethylporphyrin was prepared according to SCHEME VI by the method of Young.⁶⁷ The individual atropisomers were found to be conformationally rigid, only under prolonged heating at $>100^{\circ}$ could they be thermally equilibrated to 1:1 mixtures of cis:trans isomers. The ratio of trans/cis isomer during porphyrin synthesis was varied from 2 to 4. The cis diamino porphyrin was much more soluble in pure methylene chloride than the trans diamino porphyrin. Trans isomer can be isolated easily by using this difference in solubility. The isomer mixture was stirred in a small amount of methylene chloride; the solution was simply filtered through medium coarse funnel and washed with a small amount of methylene chloride to remove the cis isomer completely. The filtrate contains some amount of the trans isomer. The two isomers can be separated by filtering the solution through a silica gel pad, and washed with pure methylene chloride. Only the trans isomer was eluted by pure methylene chloride; the cis isomer required 1 % methanol- CH_2Cl_2 . To prepare the dipyridine strapped porphyrins, the high dilution technique at room temperature can not be used because of the low reactivity of the phenylamine. Thus, the diacid chloride was mixed with the cis





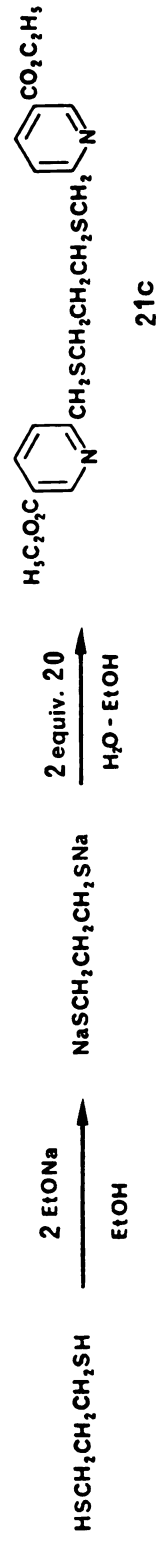
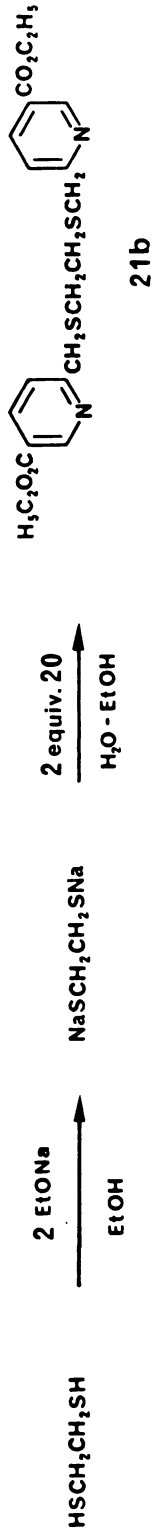
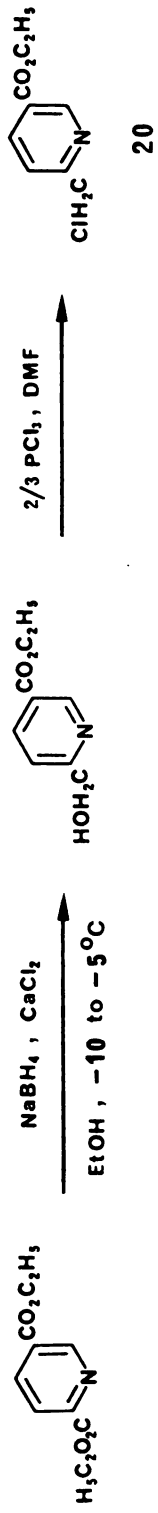
SCHEME VI





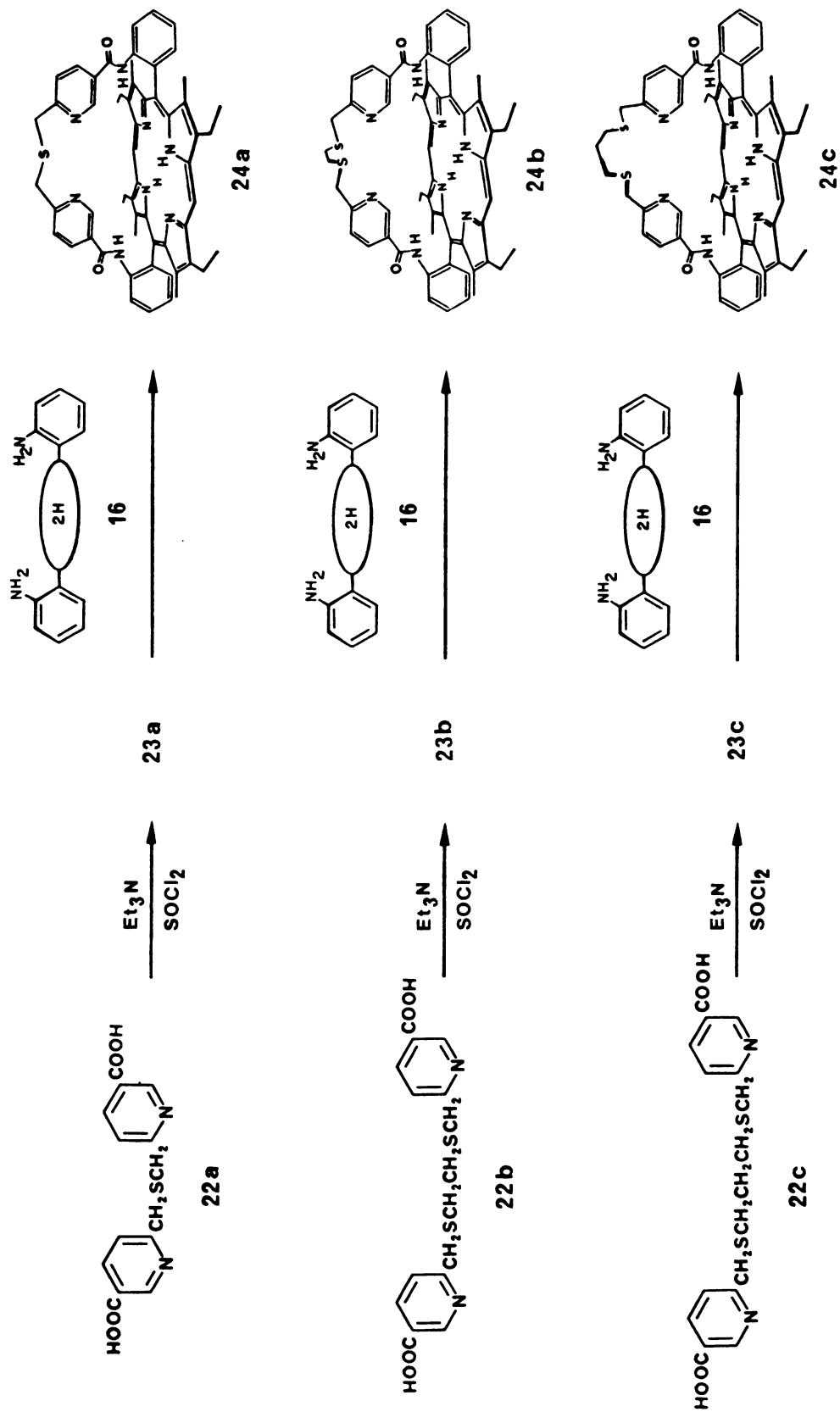
SCHEME VII





SCHEME VIII





SCHEME IX

diamino porphyrin, in the presence of triethylamine, and refluxed in methylene chloride overnight to complete the coupling reaction (SCHEME IX). The rate of coupling reaction was monitored using thin-layer chromatography. The developing rate of the dipyridine strapped porphyrins 24a, 24b and 24c was 24c > 24b > 24a on a silica gel TLC plate. The longer-chain strapped porphyrin moved faster.

Metal Complexes

A. Synthesis

Iron insertion into the porphyrin 7 was accomplished using the usual FeSO_4 -HOAc method.⁶⁸ The hemin chloride thus prepared was treated with zinc chloride or copper(II) chloride to give analytically pure FeMCl_3L , L = strapped porphyrin ligand. The hemin chloride, dissolved in CH_2Cl_2 -MeOH, was added to ammoniacal copper(II) acetate in aqueous methanol to give a solid (2), $\text{FeCu}(\text{O})(\text{H}_2\text{O})(\text{HOAc})\text{L}$.

B. IR Data

IR spectroscopy (KBr pellet) of this sample showed a peak at 880 cm^{-1} , which is absent in the spectrum of FeCuCl_3L and which is characteristic of the M-O-M anti-symmetric stretching vibration.⁶⁹ The visible spectrum of (2) appeared to be very similar to that of μ -oxo Fe^{III} porphyrin dimers (600 nm, sh; 564 nm; 386 nm). Compound (2) was reasonably stable and could be dissolved in CH_2Cl_2 and re-evaporated without undergoing any change.

To determine whether compound (2) is a Fe-O-Fe dimer, a CH_2Cl_2 solution of this compound (2) is shaken with 5 % aqueous NaOH. The resultant material, compound (3), retained the same composition and its IR (882 cm^{-1}) and absorption spectra showed no significant variations: however its magnetic susceptibilities differed drastically from solid (2).

C. Magnetic Susceptibility Data

The magnetic susceptibilities of solid (2) and the corresponding magnetic moments are shown in Figure 8 (a): μ_{eff} values of compound (3) as well as the Fe-Zn complex are shown in Figure 8 (b). The magnetic behavior of solid (2) is best understood by assuming a high-spin Fe^{III} ($S_1 = 5/2$) coupled with Cu^{II} ($S_2 = 1/2$). Such a spin coupling should result in two states: $S = 3$ and $S = 2$, with an energy gap of $3J$. The molar susceptibilities can be calculated using the simplified Van Vleck's equation (1).⁷⁰ Where N and K have their standard meaning.

$$\chi = \frac{2N\beta^2}{kT} \cdot \frac{5g_1^2 + 14g_2^2 \exp(3J/kT)}{5 + 7\exp(3J/kT)} \quad (1)$$

The experimental data can then be fitted with a non-linear least-squares KINFIT program⁷¹ to the following parameters:

$$-3J = 132 \pm 5 \text{ cm}^{-1}, \quad g_1 = 2.14 \quad g_2 = 1.82$$

The calculated best fit is also shown in Figure 8 (a). The overall features of the μ_{eff} curve are similar to those

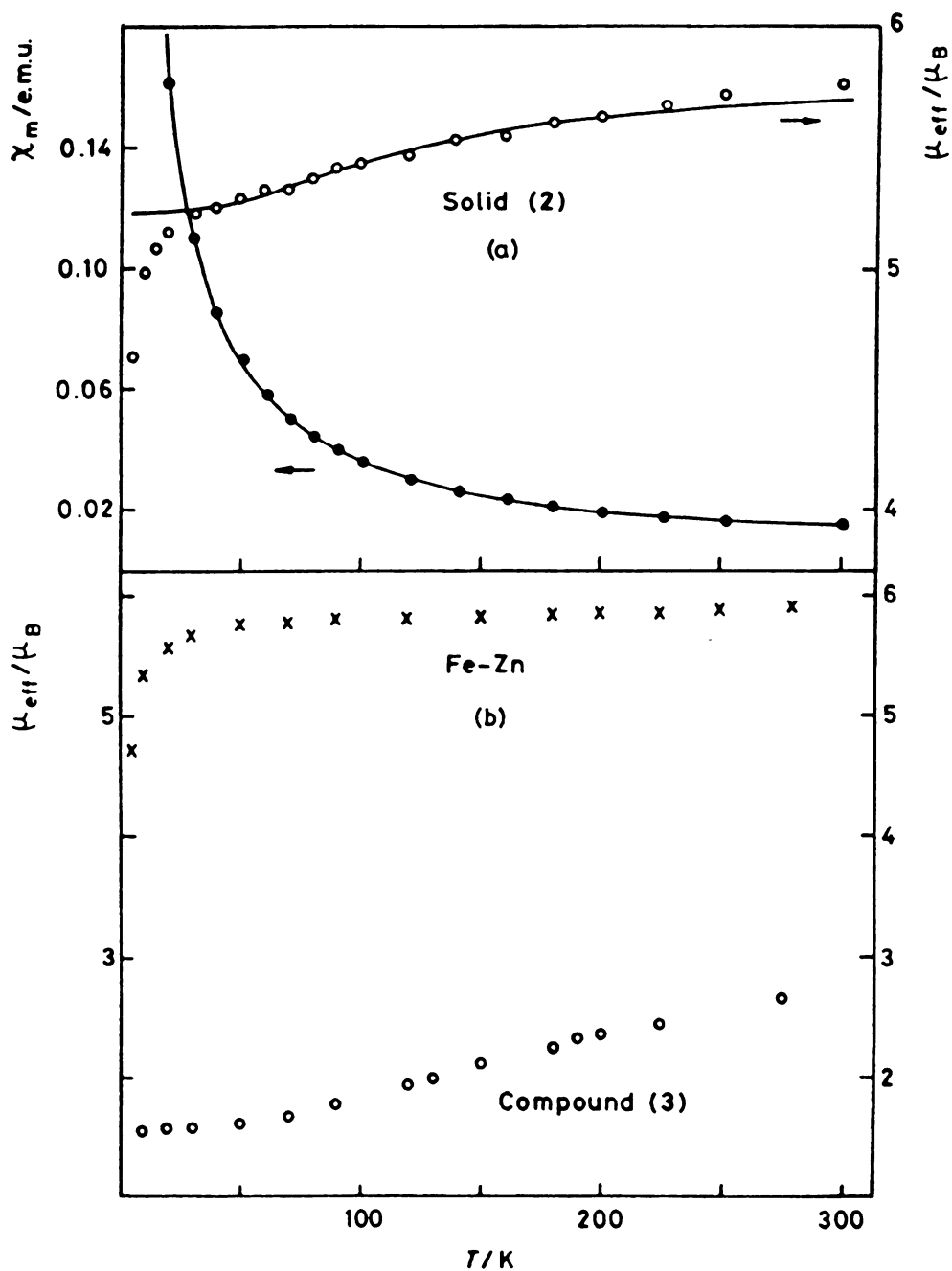


Figure 8. Molar magnetic susceptibility and effective magnetic moment as a function of temperature for (a) solid and (b) the FeZnCl_3L complex and compound (3). The lines represent the fit of the data using $-3J = 132 \text{ cm}^{-1}$. A diamagnetic correction of $-5 \times 10^{-4} \text{ e.m.u. mol}^{-1}$ was applied to the measured data.

of $\text{Cu}^{\text{II}}\text{-Mn}^{\text{II}}$ and $\text{Cu}^{\text{II}}\text{-Fe}^{\text{II}}$ complexes which have been found to exhibit energy gaps of 79.2 and 289 cm^{-1} , respectively.^{72,73}

The curve shows that below ca. 50 °K, the $S = 3$ excited state is completely depopulated. At temperatures below 20 °K, μ_{eff} drops rapidly owing to the zero-field splitting of the ground state. The susceptibility of the iron-zinc complex obeys the Curie-Weiss law and is representative of an isolated high-spin iron ($S = 5/2$).



The behavior of compound (3), however, is less straightforward. The χ^{-1} vs. T plot does not show Curie-Weiss behavior and the μ_{eff} curve cannot be fitted to any scheme involving spin pairing between iron and copper. This curve may be rationalized by considering a combination of isolated Cu^{II} ($\mu_{\text{eff}} = 1.7 \mu_{\text{B}}$) and half an intermolecular Fe-O-Fe μ -oxo-dimer.

D. EPR Data

A further proof of the configuration was provided by EPR spectroscopy. Insertion of copper using copper(II) acetate in $\text{CH}_2\text{Cl}_2\text{-MeOH}$ led to a bis- Cu^{II} complex. The dipolar interaction of the two paramagnetic copper ions resulted in the triplet EPR spectrum shown in Figure 9. The apparent zero-field splitting D value suggested a Cu-Cu distance of no greater than 4.3 Å.⁷⁴

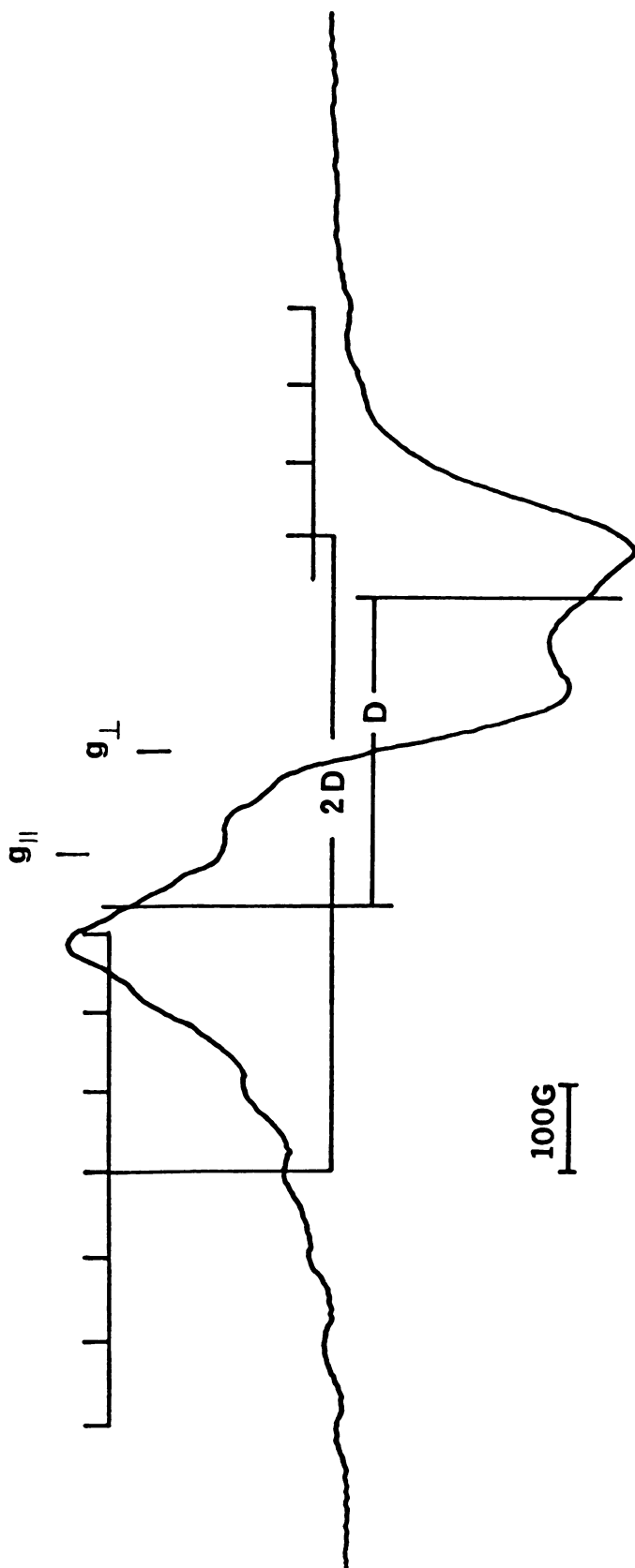


Figure 9. E.P.R. spectrum of the bis-Cu(II) complex in CH_2Cl_2 at 77°K . The seven-line hyperfine pattern derived from the two copper(II) nuclei ($I = 3/2$) can be discerned on the left; only the two outermost lines are seen on the right.

Conclusion

Combining the IR spectroscopy evidence we therefore assign solid (2) to an intramolecularly oxo-bridged Fe-O-Cu complex and compound (3) to a dimeric Fe-O-Fe complex. EPR spectra also corroborated this assignment. At 77 °K in frozen CH₂Cl₂ there was a strong $g = 2$ signal but hardly any $g = 6$ signal for compound (3) whereas for (2), both $g = 6$ and $g = 2$ signal were present but integrated spin concentration was less than the total Fe and Cu present ($< 40\%$). In the absence of definitive X-ray structures, the coordination geometry of copper is unknown although Corey-Pauling Koltun models suggest a somewhat distorted tetrahedral geometry using the two thiazole N's, the sulphide S, and the oxo group.

This oxidase model represents the first successful attempt to achieve significant spin-coupling between a copper(II) complex and a high-spin iron(III) heme. The choice of a β -substituted porphyrin instead of a mesotetra-aryl type substituted porphyrin may be important since the iron(III) complex of the latter type, especially in the presence of perchlorate or other weak-field ions, often develops spin mixing with $s = 3/2$ state.^{34,40} The magnitude of coupling present in this model is still small in comparison with the oxidase: perhaps among other things, the presence of an imidazole axial ligand is crucial. The lack of a trans-ligand also contributes to the facile formation of the external Fe-O-Fe dimer which severely limits the

chemistry that one can achieve with these compounds. The blocking of the sixth site with a ligand should eliminate this problem.

In case of the strapped porphyrin 15a, 15b, 15c, and 15d, the copper chelate with the strapped ligand was either too floppy or the distance is too large from the porphyrin center such that the EPR spectra of the bis-copper(II) complexes showed no significant interaction between the two Cu(II) ions.

For the strapped porphyrin 24a, an EPR spectrum showing coupling between the two copper ions was obtained. However, the strapped porphyrin 24b and 24c, EPR spectra showing coupling between the two copper ions were again not obtained. The lack of coupling in these two strapped systems may reflect the improper distance between the two copper(II) ions.

EXPERIMENTAL

Physical Measurements

¹H NMR spectra were recorded on a Varian T-60 or Bruker WM-250 MHz spectrometer. IR spectra were recorded in KBr pellets on a Perkin-Elmer 237B spectrophotometer. Melting points were obtained on an Electrothermal melting point apparatus uncorrected. Mass spectra were obtained with a Finnigan 4000 GC/MS system using the direct inlet mode, at 70 eV ionization energy. Elemental analyses were performed by Spang Microanalytical Laboratory, Eagle Harbor, Michigan;

C, H and N analyses were within $\pm 0.42\%$. EPR spectra were recorded by using a Bruker ER200D X-band spectrometer; Operation at low temperature was achieved by using an oxford EPR-9 liquid helium cryostat. Magnetic susceptibilities were measured with an S.H.E. computer-controlled variable temperature superconducting quantum interference device (SQUID) spectrometer capable of measurements at temperature between 1.7 and 400 $^{\circ}\text{K}$. The crystalline sample were loaded into small cylindrical containers (inside dimensions 3.5 mm by 3.8 mm diameter) made of Kel-F. Prior to loading the sample, a thread 18-21 cm long was attached to the bucket through four holes. At every temperature, the SQUID was allowed to take ten readings and an average value was printed out.

Materials

All solvents and reagents were of reagent grade quality, purchased commercially, and used without further purification except mentioned. Methylene chloride, triethylamine and collidine were distilled from calcium hydride; THF was distilled from LiAlH_4 ; Methanol and ethanol were distilled from sodium. Thionyl chloride was distilled from triethylphosphite. Silica gel for column chromatography (60-200 mesh) was from J.T. Baker (3405). Preparative silica gel plates were from Analtech, Inc. For analytical TLC, Eastman 13181 chromatography sheets were used.

Synthesis

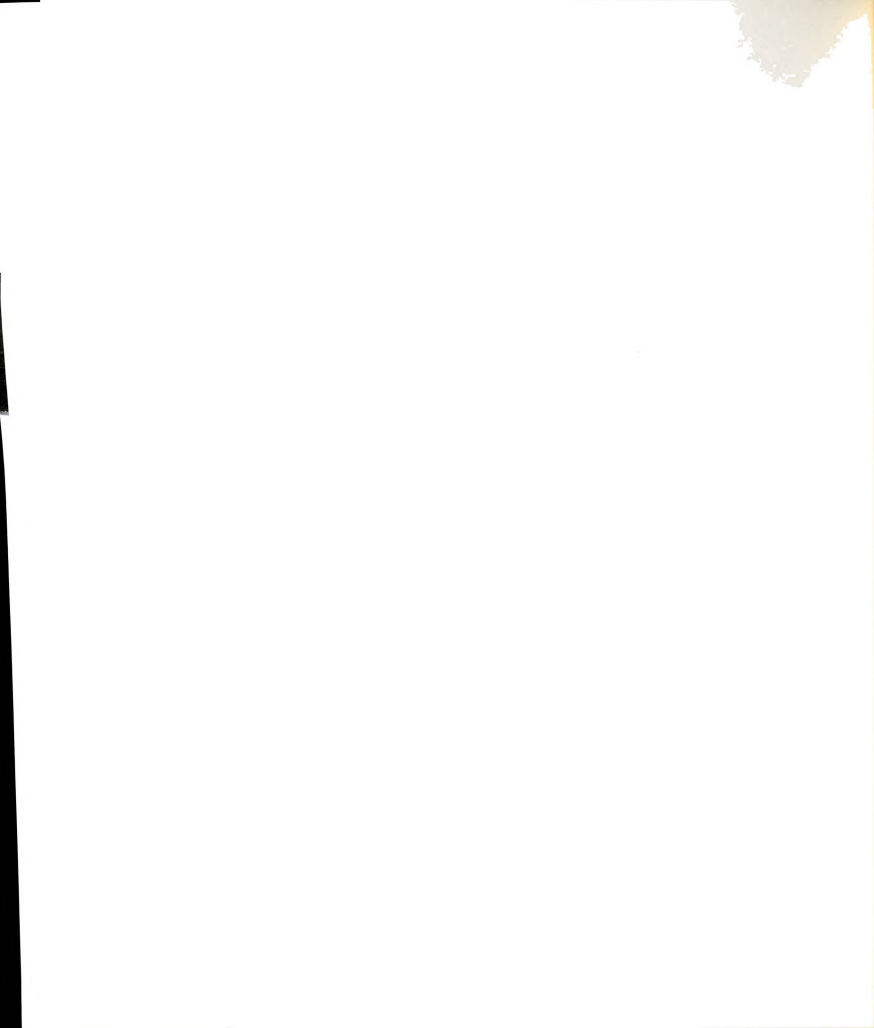
A. Dithiazole Strapped Porphyrins

Bis[4-phthalimidomethyl]thiazole-2-methyl] sulfide (4)

A suspension of 7.2 g (25.6 mmol) of 1-bromo-3-phthalimidopropanone (3) and bis(thiocarbamoylmethyl) sulfide (2.3 g, 12.8 mmol) in 20 mL of absolute alcohol was heated under reflux. After few minutes, all the solids were dissolved, and a white precipitate forms gradually. The refluxing was continued 1 h. The mixture which now contained a large quantity of white crystalline solid was cooled to room temperature, and filtered with suction. The volume of the filtrate was reduced to about 5 mL to obtain more solid. The combined solid was triturated in excess ammonium hydroxide. The yield of the sulfide was 6.7 g (97 %), mp 172-175 °C. MS, m/e (relative intensity), 290(4), 289(7), 260(6), 259(15), 258(100), 257(7), 160(17), 104(21); ¹H NMR (DMSO-d₆) δ 4.03(s, 4H, SCH₂), 4.78(s, 4H, NCH₂), 7.26(s, 2H, thiazole H), 7.77(s, 8H, Ar).

Bis[4-(aminomethyl)thiazole-2-methyl] sulfide (5)

To a solution of 3.6 g (6.6 mmol) of the above phthalimido compound in 12 mL of hot absolute alcohol was added 3 mL 100% hydrazine hydrate. The solution was heated under reflux for 30 min, and cooled to 4 °C. The resulting mixture containing a large quantity of gelatinous solid was filtered with suction and washed with cold absolute ethanol. The filtrate was evaporated in vacuo. To the residue 10 mL



chloroform was added, and the undissolved phthalhydrazide was filtered. The chloroform solution was dried over sodium sulfate and evaporated to dryness to yield a yellow oil. The yield was 1.7 g (90 %). $^1\text{H NMR}$ (CDCl_3) δ 1.69(s, 4H, NH_2), 3.90(s, 4H, NCH_2) 4.06(s, 4H, SCH_2), 6.95(s, 2H, thiazole H); IR, 3100, 3290, 3360 cm^{-1} .

7,17-[4,4'-[2,2'-(2-Thiatrimethylene)dithiazolyl]bismethyl-carbamoylethyl]-3,8,13,18-tetramethyl-2,12-dipentylporphyrin

(6)

This porphyrin was made in an analogous fashion as porphyrin 7. Yield 70 %. MS, m/e(relative intensity), 340 (65), 307(68), 200(3), 185(16), 154(15), 126(31), 11(100); $^1\text{H NMR}$ (CDCl_3) δ -4.10(br s, 2H, pyrrole NH), 1.00(t, 6H, Et), 1.22(dd, 4H, SCH_2), 1.59(six, 4H, CH_2), 1.77(quin, 4H, CH_2), 2.33(quin, 4H, CH_2), 3.05(t, 4H, COCH_2), 3.56(s, 6H, Me), 3.63(s, 6H, Me), 3.75(d, 4H, NCH_2) 4.09(t, 4H, P- CH_2), 4.63(t, 4H, P- CH_2), 5.38(s, 2H, thiazole H), 5.41(t, 2H, NH), 9.98(s, 2H, meso), 9.99(s, 2H, meso).

3,17-[4,4'-[2,2'-(2-Thiatrimethylene)dithiazolyl]bismethyl-carbamoylethyl]-2,7,13,18-tetramethyl-6,12-diethylporphyrin

(7)

The porphyrin diacid 13d (200 mg, 0.35 mmol) and an excess of oxalyl chloride (2 ml, 22.9 mmol) was refluxed in an oil bath under nitrogen gas. After the solution had become homogeneous and evolution of gas ceased (ca. 30 min)

the excess oxalyl chloride and methylene chloride were removed in vacuo to yield the porphyrin diacid chloride 14d. The porphyrin diacid chloride 19b was dissolved in dry methylene chloride (60 mL) and transferred to a 100 mL syringe under nitrogen gas. The diamino thiazole sulfide (5) (131 mg, 0.46 mmol) was dissolved in dry methylene chloride (60 mL), and 2-3 drops of dry triethylamine were added as a catalyst. The solution was transferred to a 100 mL syringe under nitrogen gas. These two syringes were mounted on a motor-driver syringe pump (Sage Instruments Co. Model 352). The solution in syringe were injected simultaneously at the same rate through stainless needles into 1000 mL dry methylene chloride in a three-necked 2-L flask equipped with rubber septa and drying tube. When the addition was complete (1 h), the solution was stirred for another hour. The mixture was evaporated in vacuo. The resultant thiazole-strapped porphyrin 7 was purified by chromatography (silica gel, 6 % MeOH-CH₂Cl₂) and crystallized from CH₂Cl₂-MeOH, yield 72 %. ¹NMR (CDCl₃) δ 0.86(s, 4H, SCH₂), 1.86(t, 6H, Et), 3.12(br s, 4H, COCH₂), 3.40(s, 6H, Me), 3.59(s, 6H, Me), 3.97(d, 4H, NCH₂), 4.07(q, 4H, Et), 4.26(br s, 4H, P-CH₂), 5.44(t, 2H, NH), 5.80(s, 2H, thiazole H), 9.61(s, 1H, meso), 9.82(s, 2H, meso), 9.97(s, 1H, meso).

B. Pyridine Strapped Porphyrins

2,6-Bis(bromomethyl)pyridine (8)

10 g (71.9 mmole) of 2,6-pyridinedimethanol mixed with

50 mL HBr (d. 1.49) was distilled through a 30 cm Widmer column until 13 mL of distillate were collected. The mixture was refluxed for 1 h. After that 17 mL were distilled off; It was refluxed again for 1 h and with 6 mL distilled off. The residue was cooled and neutralized with 5 N NaOH and suction filtered and washed with cold water. The crude product was recrystallized with 1200 mL petroleum ether to give 7.07 g product. After condensing the petroleum ether filtrate to 200 mL and cooled it in refrigerator. 3.2 g More product were obtained. Yield 80.7 %. MS, m/e(relative intensity), 263(M^+ , 6.48), 265(M^++2 , 12.96), 267(M^++4 , 6.08), 186(97), 184(100), 105(53), 77(33); 1H NMR ($CDCl_3$) δ 4.45(s, 4H, CH_2Br), 7.12-7.67(m, 3H, Py).

2,6-Bis(4-N-phthalimido-3-thiabutyl)pyridine (10)

2-N-phthalimidoethanethiol (2.07 g, 10 mmol) in ethanol (100 mL) was converted into sodium salt by the addition of sodium ethoxide prepared from sodium (0.23 g, 10 mmol) in ethanol (50 mL). To the above solution of sodium salt was added the solution of 2,6-bis(bromomethyl)pyridine (1.32 g, 5 mmol) in ethanol (30 mL). The resulting solution was evaporated and dissolved in chloroform. The chloroform solution was washed with 5 % aqueous NaOH and water, and then dried over sodium sulfate and evaporated to dryness to yield a yellow oil. Yield 85 %. 1H NMR ($CDCl_3$) δ 2.78(t, 4H, SCH_2), 3.87(s, 4H, Py- CH_2), 3.88(t, 4H, NCH_2), 7.20(m, 3H, Py), 7.68(m, 8H, Ar).

Pyridine-2,6-bis[4-(2-thiabutyl)amine] (11)

This diamine was reduced from the above compound (10) by the procedure identical with that for the diamine (5).

Yield 90 %. MS, m/e (relative intensity), 257 (M^+ , 0.46), 228 (1), 214 (4), 182 (79), 171 (50), 153 (5), 137 (100), 106 (38); 1H NMR ($CDCl_3$) δ 2.08 (br s, 4H, NH_2), 2.70 (m, 8H, CH_2CH_2), 3.78 (s, 4H, Py- CH_2), 7.07-7.70 (m, 3H, Py).

7,17-[Pyridine-2,6-bis(2-thiabutylcarbamoyl ethyl)]-2,12-dipentyl-3,8,13,18-tetramethylporphyrin (15a)

This strapped porphyrin was prepared as described for the dithiazole-strapped porphyrin 7. Yield 56.6 %. MS, m/e, 871 (M^+); 1H NMR ($CDCl_3$) δ -3.97 (s, 2H, pyrrole NH), 0.75 (m, 4H, Py- CH_2), 0.99 (t, 6H, Me), 1.18 (m, 4H, SCH_2), 1.73 (m, 4H, CH_2), 2.00 (m, 4H, CH_2), 2.32 (m, 4H, CH_2), 2.47 (m, 4H, NCH_2), 2.84 (t, 4H, $COCH_2$), 3.16 (t, 4H, CH_2), 3.57 (s, 6H, Me), 3.66 (s, 6H, Me), 4.09 (t, 4H, P- CH_2), 4.65 (t, 2H, NH), 4.79-5.30 (t, 3H, py), 9.99 (s, 2H, meso), 10.01 (s, 2H, meso).

7,17-[Pyridine-2,6-bis(2-thiabutylcarbamoylmethyl)]-2,12-dipentyl-3,8,13,18-tetramethylporphyrin (15b)

This strapped porphyrin was prepared as described for the dithiazole-strapped porphyrin 7. Yield 25 %. MS, m/e (relative intensity), 843 (M^+ , 1), 107 (23), 44 (100); 1H NMR ($CDCl_3$) δ -3.91 (s, 2H, pyrrole NH), 1.03 (m, 6H, Me), 1.40

(m, 4H, Py-CH₂), 1.61(m, 4H, CH₂), 1.74(m, 4H, CH₂), 2.10(m, 4H, CH₂), 2.30(quin, 4H, CH₂), 3.01(m, 4H, CH₂), 3.63(s, 6H, Me), 3.68(s, 6H, Me), 4.05(t, 4H, P-CH₂), 4.09(m, 3H, Py), 5.04(dd, 4H, COCH₂), 5.80(s, 2H, NH), 9.99(s, 2H, meso), 10.6(s, 2H, meso).

7,17-[Pyridine-2,6-bis(2-thiabutylcarbamoylmethyl)]-2-12-dioctyl-3,8,13,18-tetramethylporphyrin (15c)

This strapped porphyrin was prepared as described for the dithiazole-strapped porphyrin 7. Yield 10 %. ¹H NMR (CDCl₃) δ -4.40(s, 2H, pyrrole NH), 0.88(m, 6H, Me), 1.18(m, 4H, Py-CH₂), 1.33(m, 12H, CH₂CH₂CH₂), 1.53(quin, 4H, CH₂), 1.69(quin, 4H, CH₂), 1.97(m, 4H, SCH₂), 2.19(quin, 4H, CH₂), 2.91(m, 4H, NCH₂), 3.46(s, 6H, Me), 3.51(s, 6H, Me), 3.91(t, 4H, P-CH₂), 4.08(m, 3H, Py), 4.93(dd, 4H, COCH₂), 5.71(s, 2H, NH), 9.72(s, 2H, meso), 9.76(s, 2H, meso).

3,17-[Pyridine-2,6-bis(2-thiabutylcarbamoylethyl)]-8,12-diethyl-2,7,13,18-tetramethylporphyrin (15d)

This strapped porphyrin was prepared as described for the dithiazole-strapped porphyrin 7. Yield 35 %. MS, m/e (relative intensity), 843(M⁺+Fe, 3), 107(18), 44(100); ¹H NMR (CDCl₃) δ -4.39(br s, 2H, pyrrole NH), 0.36(br s, 4H, Py-CH₂), 0.96(br s, 4H, SCH₂), 1.70(t, 6H, Et), 2.23(br s, 4H, NCH₂), 2.94(br s, 4H, CH₂), 3.41(s, 6H, Me), 3.57(s, 6H, Me), 4.03(q, 4H, Et), 4.40(br s, 4H, CH₂), 4.95(t, 2H, NH), 5.15-5.45(m, 3H, Py), 9.70(s, 1H, meso), 9.87(s, 2H, meso),

9.93(s, 1H, meso).

C. Dipyridine Strapped Porphyrins

Ethyl 5-(2-hydroxymethyl)pyridinecarboxylate

In a 3-L three-necked round-bottomed flask, fitted with a calcium chloride drying tube, a thermometer, and a dropping funnel, was placed 25 g (112 mmol) of ethyl 2,5-pyridine diester in 800 mL of absolute ethanol. The flask was surrounded by an ice-salt bath, and when the temperature falls below -5°C , 2.76 g (73 mmol) of sodium borohydride was added and a suspension of 12.4 g (112 mmol) of anhydrous calcium chloride in 200 mL of absolute alcohol was added dropwise through the dropping funnel at such a rate that the temperature remains below -5°C . The mixture was stirred, and the temperature was kept below -5°C by ice and salt. Stirring was continued for 2.5 h with cooling. To the reaction mixture was then added 6.28 mL (112 mmol) of sulfuric acid to remove Ca ion. 250 g of celite was used to separate the fine particles. The mixture was filtered with suction, and the yellow filtrate was evaporated to dryness to yield a light brown solid. The crude product was recrystallized with 35 mL anhydrous ether to yield a yellow crystal.⁶⁵ Yield 15.6 g (77 %). M.P. $71-72^{\circ}$. MS, m/e (relative intensity), 181(M^+ , 62), 180(100), 153(17), 152(88), 136(44); ^1H NMR (CDCl_3) δ 1.40(t, 3H, Et), 3.93(br s, 1H, OH), 4.37(q, 2H, Et), 4.80(br s, 2H, Py- CH_2), 7.33(d, 1H, Py), 8.19(dd, 1H, Py), 9.05(br s, 1H, Py).

Ethyl 5-(2-chloromethyl)pyridinecarboxylate (20)

To dimethylformamide (15 mL) in a 50 mL flask equipped with a nitrogen inlet tube and a magnetic stirrer was added phosphorus trichloride (0.714 mL, 1.12 g, 8.2 mmol) under nitrogen. The mixture became warm and changed to a gold color on standing. Stirring was discontinued and the thick, colorless solid which had formed was allowed to stand for 40 min. The above pyridine methanol (2.85 g, 15.8 mmol) was then added. The mixture was stirred for 1 h at room temperature. The brown colored solution was decanted into a separatory funnel. The residue in the flask was washed with 10 mL of chloroform, and the chloroform solution was added to the water in the separatory funnel. The chloroform solution was washed with six 200 ml. portions of water to remove dimethylformamide completely. The yield of chloromethyl pyridine (20), yellow oil, was 2.23 g (71 %). MS, m/e (relative intensity), 199(M⁺, 33), 201(M⁺+2, 11), 173(32), 171(97), 156(34), 154(100), 136(7), 126(23), 119(5); ¹H NMR (CDCl₃) δ 1.43(t, 3H, Et), 4.41(q, 2H, Et), 4.71(s, 2H, CH₂Cl), 7.53(d, 1H, Py), 8.28(dd, 1H, Py), 9.07(d, 1H, Py).

Bis[2-(5-ethoxycarbonyl)picoly] sulfide (21a)

A mixture of 2.4 g (12 mmol) of ethyl 5-(2-chloromethyl)pyridinecarboxylate(20) and 1.44 g (6 mmol) of sodium sulfide nonahydrate in aqueous alcohol (50 mL, 70 %) was heated under reflux for 1 h. The solution was evaporated to

dryness. The residue was dissolved in methylene chloride (100 mL), washed with saturated NaHCO_3 (100 mL), and water (100 mL). After drying over anhydrous sodium sulfate, the organic layer was evaporated to dryness to yield yellow oil. Yield 87 %. MS, m/e(relative intensity), 360(M^+ , 1), 315 (2), 196(22), 165(100), 150(4); ^1H NMR (CDCl_3) δ 1.45(t, 6H, Et), 3.87(s, 4H, SCH_2), 4.42(q, 4H, Et), 7.43(d, 2H, Py), 8.21(dd, 2H, Py), 9.15(d, 2H, Py).

Bis[2-(5-carboxy)picoly] sulfide (22a)

A solution of potassium hydroxide (0.84 g, 12.7 mmol) in 10 mL of water was added to a solution of bis[2-(5-ethoxycarbonyl)picoly] sulfide(21a) (1.8 g, 5 mmol) in ethanol (20 mL). The mixture was refluxed for 2 h. The resulting dipotassium salt solution was treated with an equivalent amount of hydrochloric acid. The solvent was evaporated completely in vacuo and the white solid residue was extracted with three 30 mL portions of methylene chloride. Undissolved potassium chloride was discarded. After evaporation of solvent, the acid product was directly used to make acyl chloride without further purification. Yield 85 %. MS, m/e(relative intensity), 304(M^+ , 1); ^1H NMR (DMSO-d_6) δ 3.95(s, 4H, SCH_2), 7.53(d, 2H, Py), 8.20(dd, 2H, Py), 8.92(br s, 2H, Py).

5,15-cis-{o,o'-[6,6'-(2-Thiatriethylene)dinicotinamido] diphenyl}-2,8,12,18-tetraethyl-3,7,13,17-tetramethyl-

porphyrin (24a)

The diacid (22a) (152 mg, 0.5 mmol) was dissolved in methylene chloride (30 mL). Triethylamine (0.28 mL, 2 mmol) in methylene chloride (2 mL) was added and the reaction stirred. Thionyl chloride (0.080 mL, 1.1 mmol) was dissolved in methylene chloride (2 mL) and added dropwise to the above solution. After stirring for 1 h, the solution was evaporated to dryness in vacuo to yield the diacid chloride (23a). The crude diacid chloride (170.5 mg, 0.5 mmol) was dissolved in methylene chloride (50 mL) and added to a solution of cis-diamino porphyrin 16 (330 mg, 0.5 mmol) in methylene chloride (200 mL) containing triethylamine (1 mL, 7.2 mmol). After the addition, the mixture was refluxed for 10 h under nitrogen before being poured into water (200 mL). The organic layer was separated, washed successively with 5 % HCl (300 mL). Saturated with NaHCO₃ solution (300 mL), and water (300 mL). After drying over sodium sulfate, the mixture was evaporated to dryness and separated on a series of preparative silica gel plates (analtech 1500 micron) using 6 % MeOH-methylene chloride and crystallized from methylene chloride-MeOH, 30 % Yield. MS, m/e, 928(M⁺); ¹H NMR (CDCl₃) δ -2.31(br s, 2H, pyrrole NH), 1.74(t, 12H, Et), 2.59(s, 12H, Me), 2.84(s, 4H, CH₂), 4.02(q, 8H, Et), 6.11(d, 2H, Ar), 6.22(d, 2H, Ar), 6.98(d, 2H, Py), 7.71(t, 2H, Ar), 7.94(t, 2H, Ar), 8.37(d, 2H, Py), 8.88(d, 2H, Py), 10.30(s, 2H, meso); ¹H NMR (pyridine-d₅) δ -1.62(s, 2H, pyrrole NH), 1.55(t, 12H, Et), 2.37(s, 4H, CH₂), 2.73(s,

12H, Me), 3.85(q, 8H, Et), 4.99(br s, 2H, NH), 6.05(d, 2H, Ar), 6.44(d, 2H, Ar), 7.06(d, 2H, Ar), 7.80(t, 2H, Ar), 8.04(t, 2H, Ar), 8.51(d, 2H, Ar), 9.10(d, 2H, Py), 10.33(s, 2H, meso).

Ethyl 5,5'-[2,2'-(2,5-dithiahexamethylene)]dipyridinedicarboxylate (21b)

Ethane-1,2-dithiol (2.5 g, 26.5 mmol) in ethanol(100 mL) was converted into disodium salt by the addition of sodium ethoxide prepared from sodium (1.23 g, 53.5 mmol) in ethanol (100 mL). The above solution of disodium salt was added to the solution of ethyl 5-(2-chloromethylpyridine) carboxylate (10.57 g, 53 mmol) in ethanol (100 mL). The resulting solution was refluxed for 3 h. The solution was evaporated and dissolved in chloroform. The chloroform solution was washed with 5 % aqueous NaOH and water, and then dried over sodium sulfate and evaporated to dryness to yield a yellow oil. The crude product was purified on alumina to yield the sulfide product. The yield of the sulfide product was 10.6 g (95 %). MS, m/e(relative intensity), 420(M⁺, 1), 375(3), 256(16), 224(100), 197(47); ¹H NMR (CDCl₃) δ 1.41(t, 6H, Et), 2.70(s, 4H, SCH₂), 3.88(s, 4H, Py-CH₂), 4.41(q, 4H, Et), 7.43(d, 2H, Py), 8.23(dd, 2H, Py), 9.14(d, 2H, Py).

5,5'-[2,2'-(2,5-Dithiahexamethylene)]dipyridinedicarboxylic acid (22b)

This diacid was prepared as described for the hydrolysis of the diester 21a. Yield 89 %. MS, m/e (relative intensity), 228(9), 196(100), 169(41), 168(38), 137(31); ^1H NMR (DMSO- d_6) δ 2.69(s, 4H, SCH₂), 3.89(s, 4H, Py-CH₂), 7.49(d, 2H, Py), 8.17(dd, 2H, Py), 8.88(d, 2H, Py).

5,15-cis-[o,o'-(6,6'-(2,5-Dithiahexamethylene)dinicotin-amido]diphenyl}-2,8,12,18-tetraethyl-3,7,13,17-tetramethylporphyrin (24b)

This strapped porphyrin 24b was prepared from the dicarboxylic acid 22b as described for the strapped porphyrin 24a. Yield 58 %. MS, m/e, 988(M⁺); ^1H NMR (CDCl₃) δ -2.52 (br s, 2H, pyrrole NH), 1.69(s, 4H, SCH₂), 1.78(t, 12H, Et), 2.62(s, 12H, Me), 3.31(q, 4H, Py-CH₂), 4.05(q, 8H, Et), 6.70 (d, 2H, Ar), 7.16(d, 2H, Ar), 7.59(t, 2H, Ar), 7.73(s, 2H, Py), 7.79(s, 2H, Ar), 7.89(t, 2H, Py), 8.95(d, 2H, Py), 10.33(s, 2H, meso); (pyridine- d_5) δ -2.14(s, 2H, pyrrole NH), 0.69(s, 4H, CH₂), 1.63(t, 12H, Et), 2.78(s, 12H, Me), 3.01(s, 4H, Py-CH₂), 3.87(q, 4H, Et), 3.98(q, 4H, Et), 4.94 (br s, 2H, NH), 6.80(d, 2H, Ar), 7.05(s, 2H, Py), 7.53(d, 2H, Ar), 7.66(t, 2H, Ar), 7.85(d, 2H, Py), 8.02(br s, 2H, Ar), 9.36(d, 2H, Py), 10.32(s, 2H, meso).

Ethyl 5,5'-(2,2'-(2,6-dithiaheptamethylene)]dipyridine-dicarboxylate (21c)

This sulfide was prepared as described for the sulfide 21b except ethane-1,2-dithiol was replaced by propane-1,3-

dithiol. Yield 94 %. $^1\text{H NMR}$ (CDCl_3) δ 1.42(t, 6H, Et), 1.54-1.97(m, 2H, CH_2), 2.58(t, 4H, SCH_2), 3.91(s, 4H, Py-CH_2), 4.45(q, 4H, Et), 7.50(d, 2H, Py), 8.31(dd, 2H, Py), 9.12(d, 2H, Py).

5,5'-[2,2'-(2,6-Dithiaheptamethylene)]dipyridinedicarboxylic acid (22c)

This diacid was prepared as described for the hydrolysis of the diester 21a. Yield 90 %. $^1\text{H NMR}$ (CDCl_3) δ 1.78(m, 2H, CH_2), 2.58(t, 4H, SCH_2), 3.96(s, 4H, Py-CH_2), 7.66(d, 2H, Py), 8.38(dd, 2H, Py), 9.08(br s, 2H, Py).

5,15-cis-{o,o'-[6,6'-(2-Dithiaheptamethylene)dinicotinamido]diphenyl}-2,8,12,18-tetraethyl-3,7,13,17-tetramethylporphyrin (24c)

This strapped porphyrin 24c was prepared from the dicarboxylic acid 22c as described for the strapped porphyrin 24a. Yield 20 %. MS, m/e, 1002(M^+); $^1\text{H NMR}$ (CDCl_3) δ -2.48(br s, 2H, pyrrole NH), 1.10(q, 2H, CH_2), 1.65(t, 4H, CH_2), 1.77(t, 12H, Et), 2.61(s, 12H, Me), 3.30(s, 4H, Py-CH_2), 3.49(s, 2H, NH), 4.04(q, 8H, Et), 6.66(d, 2H, Ar), 7.08(d, 2H, Ar), 7.57(t, 2H, Py), 7.77(d, 2H, Py), 7.91(t, 2H, Ar), 8.01(s, 2H, Py), 8.97(d, 2H, Py), 10.32(s, 2H, meso).

Metal and Oxygen Insertion

The dithiazole porphyrin 7 (81.6 mg, 0.10 mmol) was



placed in a pear-shaped flask equipped with a gas-inlet tube, dissolved in pyridine (1 mL), and diluted with glacial acetic acid (20 mL). A stream of argon was passed into the solution from the tube while the mixture was placed in an oil bath preheated to 80 °C. A saturated aqueous solution of iron(II) sulfate (0.11 mmol) was syringed into the mixture, through the gas outlet side arm.⁸⁰ The temperature of the bath was raised to 90 °C and the reaction was kept at this temperature for 10 min. The flask was then removed from the heating bath, the mixture was cooled to ambient temperature. A stream of air was passed into the solution briefly to allow autooxidation of the unstable iron(II) complex. The mixture was partitioned between water (60 mL) and methylene chloride (60 mL) in a separatory funnel. The organic phase was separated and washed with 10 % HCl (60 mL) three times to ensure that no metal was bound to the thiazoles and then washed with water. The methylene chloride layer was separated and then evaporated to dryness.

The hemin chloride thus prepared was treated with zinc chloride or copper(II) chloride to obtain analytically pure FeMCl_3L , L = strapped porphyrin ligand.

If the hemin chloride, dissolved in $\text{CH}_2\text{Cl}_2\text{-CH}_3\text{OH}$, was added to ammonical copper(II) acetate in aqueous methanol, a solid (2) was obtained. Anal. Calcd: C, 53.66; H, 5.19; N, 10.88; Fe, 5.42 for $\text{C}_{46}\text{H}_{53}\text{N}_8\text{S}_3\text{O}_2\text{FeCu}$. Found: C, 53.45; H, 5.09; N, 10.52; Fe, 5.46. The composition is best described as $\text{FeCu(O)(H}_2\text{O)(OAc)L}$.

Bis Copper^{II} complex of 24a was obtained by the following procedure. To a solution of 24a (P-Py₂S) (18.6 mg, 0.02 mmol) in CH₂Cl₂ (7 mL) and CH₃OH (7 mL). A methanolic solution of CuCl₂ (excess) was added. The solution was stirred and heated at 60 °C for 20 min. The solution volume was reduced by evaporation to 1/3. The crystallized solution was cooled to room temperature and the red solid crystals were filtered off, washed well with methanol and dried in vacuo.

CHAPTER III

THE SYNTHESIS AND CHARACTERIZATION OF
BLOCKED AND LIGAND APPENDED PORPHYRINSIntroduction

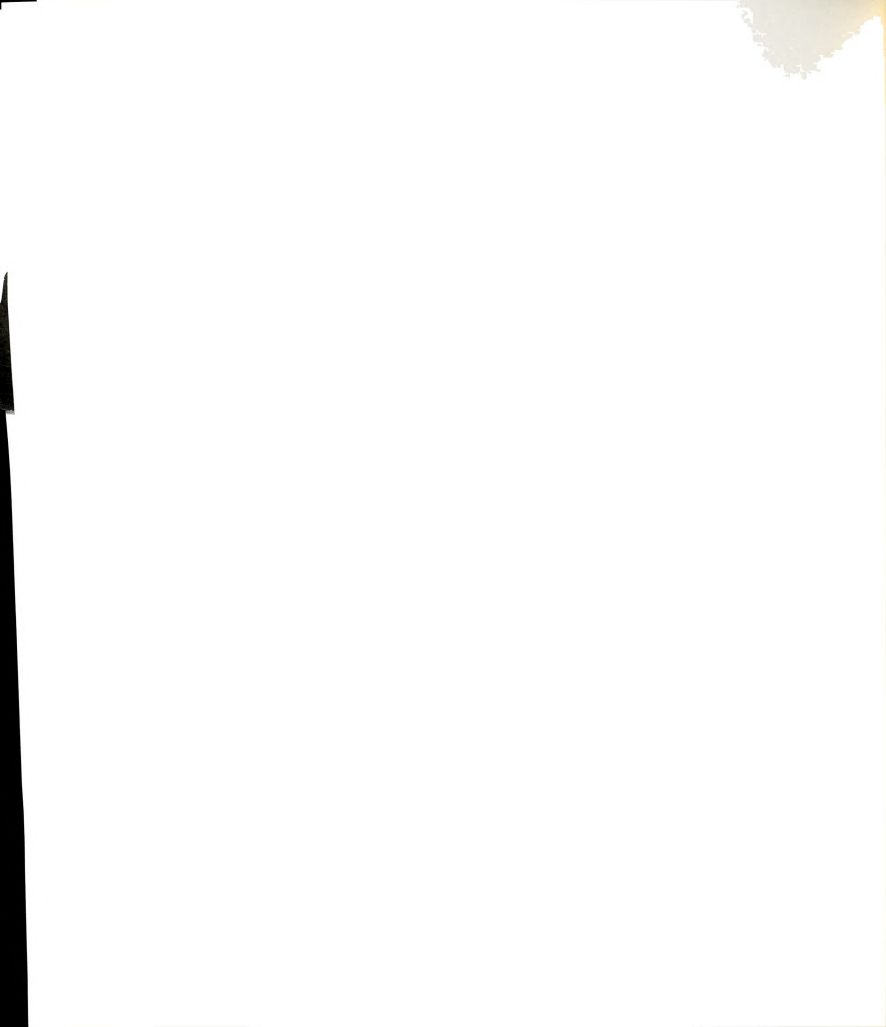
The results presented in Chapter II point to the need of designing heme-copper assemblies with the exposed face of heme group blocked or coordinated with a ligand so that intermolecular μ -oxo dimer (Fe-O-Fe) formation would be prevented. This goal has been achieved by using trans-derivatized meso-diphenyl porphyrins. This chapter describes the synthesis and preliminary studies of the Fe-Cu complexes derived from this type of super-structured porphyrin model compounds.

Young,⁶⁷ Gunter and Mander⁷⁵ have reported the synthesis of hybrid meso o-anilino octa-alkyl porphyrins. The ring methyl groups in this system hinder the rotation of the meso o-anilino rings thus allowing isolation of the atropisomers. Furthermore, the steric constraint and the conformational rigidity of the derivatized amides can be employed to enforce selective ligation and/or blocking of the porphyrin coordination site.

The effectiveness of the p-t-butyl phenyl group such as in 28a and 32a in preventing μ -oxo dimer formation has been

demonstrated.⁶⁷ The presence of an imidazole-coordinated residue in an axial position (e.g. 28b and 32b), coupled with the suggestions⁷⁶ that metal-imidazole bond rupture may play a critical role in biological process of the cytochrome c oxidase system, indicates that a detailed characterization of the structure and dynamics of the imidazole-metal bond in such porphyrin complexes could have significant biological implications.

Our experiences with the previous model systems, prompted interest in the study of copper(I) and copper(II) ions in non-planar coordination geometries with thioether and/or unsaturated nitrogen donor ligands. Four porphyrins utilizing these tripodal tetradentate chelates were constructed. Coordination complexes of Cu^{I} and Cu^{II} with nitrogen and sulfur-donating ligands continue to be of interest as models for the redox sites.⁷⁷⁻⁷⁹ Sulfur donor ligands may be important in stabilizing the configuration. In order to understand better the nature of the $\text{Cu}^{\text{I}}-\text{Cu}^{\text{II}}$ redox process, it is necessary to examine the structural and chemical consequences of this metal in various coordination environments. This has led to examination of Cu^{II} complexes with the new series of tripodal tetradentate, N_2S_2 (28a, b) and also NPY_3 (32a, b) ligands. The synthesis and X-ray structural study of the both Cu^{I} and Cu^{II} complexes of N_2S_2 ^{53,80,81} and NPY_3 ⁸²⁻⁸⁵ type have been reported. The stability of the copper(II) compounds of these ligands will enable examination of the spin coupling in the fully oxidized



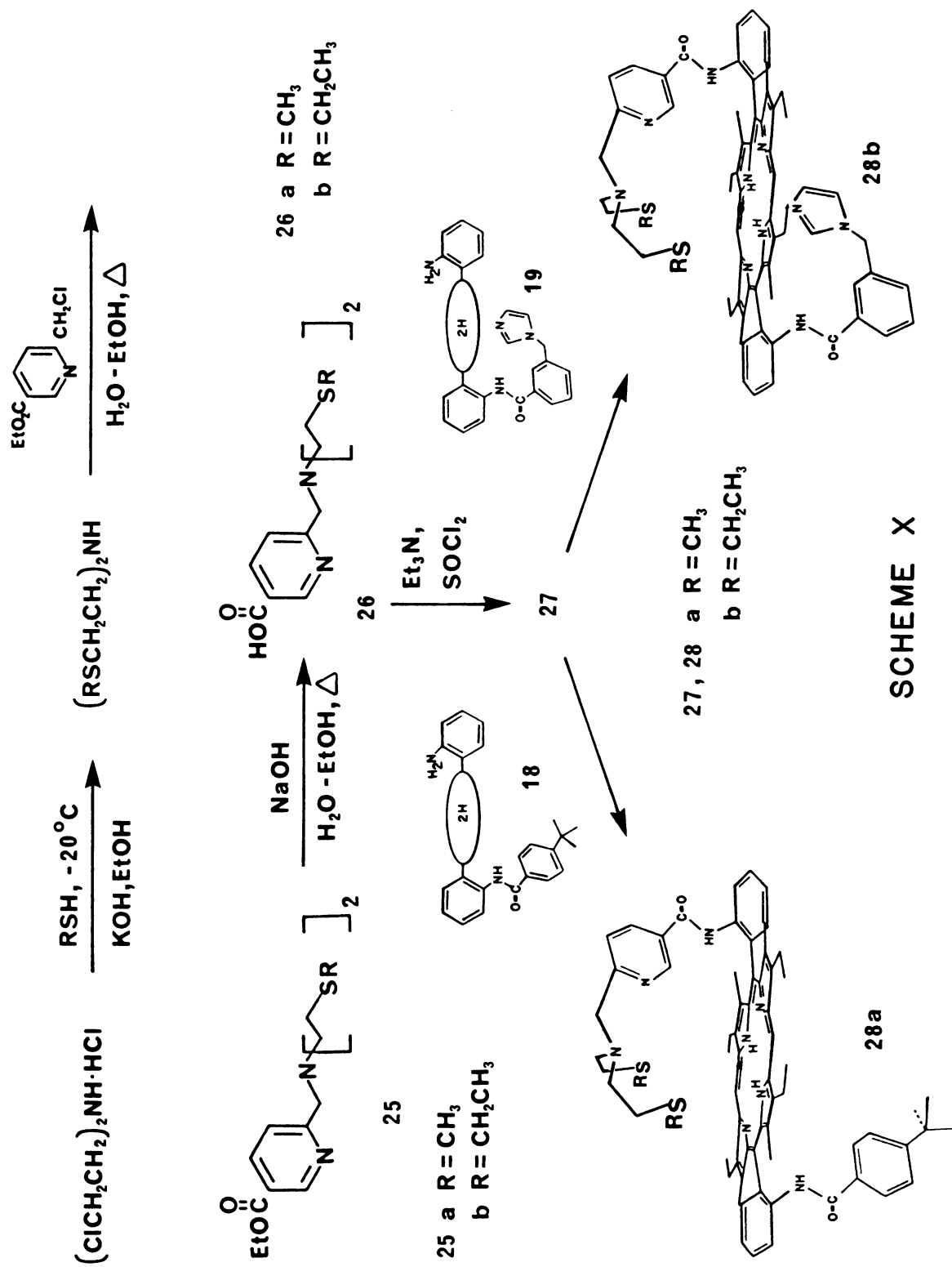
zed binuclear heme models.

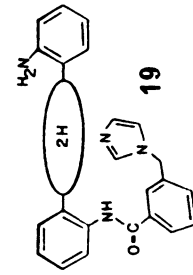
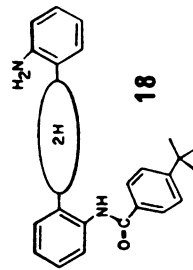
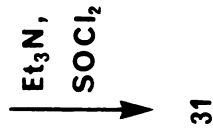
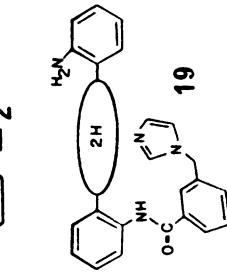
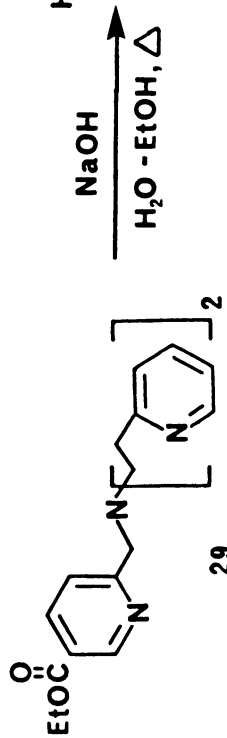
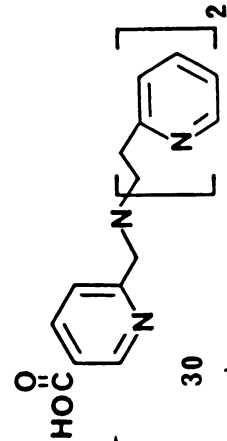
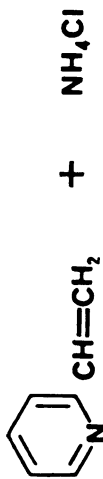
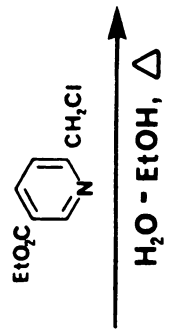
Ligand Synthesis

The hydrochloride of the sulfur-containing amines were prepared according to Razavi (SCHEME X).⁸⁶ To obtain the free base of the secondary amine, a solution of the hydrochloride in ethanol was treated with saturated sodium bicarbonate solution. Distillation of the resulting solution to dryness in vacuo left a residue, which was twice extracted with chloroform.

The tertiary amine, 25a and 25b was prepared by refluxing ethyl 2-chloromethyl pyridine 5-carboxylate with large excess amount of the secondary amine (5-7 times) in 70 % ethanol. p-tert-Butylbenzamidoporphyrin 18 and monobenzylimidazole porphyrin 19 were prepared by Young's procedure (SCHEME VII).⁶⁷ Reaction of porphyrin 17 with 1 equivalent p-tert-butyl benzoyl chloride followed by separation with silica gel column chromatography (1 % MeOH-CH₂Cl₂) yielded an almost statistical distribution of mono, di, and unsubstituted amino porphyrins. p-tert-Butylbenzoyl chloride was prepared by heating p-tert-butylbenzoic acid with large excess amount of thionyl chloride without solvent followed by evaporation in vacuo. Unsatisfactory dissolution of low-soluble trans diaminoporphyrin resulted in formation of a large amount of disubstituted aminoporphyrin.

Metal Complexes

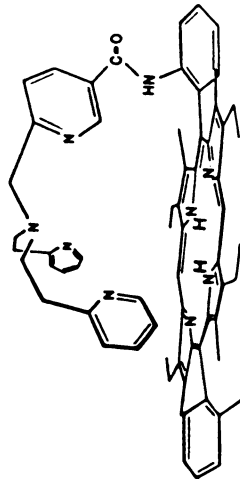




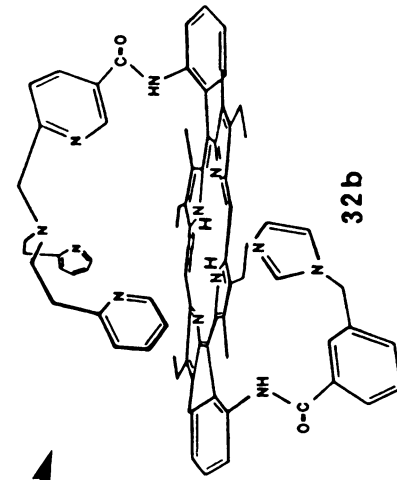
31

18

19



32 a



32 b

SCHEME XI

A. Synthesis

Insertion of Fe into the porphyrins ($\underline{32a}$, $\underline{32b}$) to give Fe(III) complexes, $[\text{Fe}(\text{P})\text{-OH}(\text{N}_4)](\underline{32a-1}$, $\underline{32b-1})$, was achieved by the ferrous bromide method⁶⁷ in THF/benzene (1:1), followed by washing with aqueous sodium bicarbonate.

Treatment of a CH_2Cl_2 -methanol(1:1) solution of these compounds ($\underline{32a-1}$, $\underline{32b-1}$) with a methanolic solution of CuCl_2 (equivalent amount), gave $[\text{Fe}(\text{P})\text{-Cl Cu}(\text{N}_4)(\text{Cl})(\text{OH})](\underline{32a-2}$, $\underline{32b-2})$.

Bis- Cu^{II} complexes, $[\text{Cu}(\text{P})\text{ Cu}(\text{N}_4)(\text{Cl})(\text{PF}_6)]$, were synthesized by addition of CuCl_2 to the porphyrins($\underline{32a}$, $\underline{32b}$), followed by precipitation using excess methanolic KPF_6 .

After treatment of a $\text{CH}_2\text{Cl}_2/\text{MeOH}(1:1)$ solution of the bimetal complexes($\underline{32a-2}$, $\underline{32b-2}$) with aqueous NaOH , μ -oxo bridged heterobinuclear metal complexes $[\text{Fe}(\text{P})\text{-O-Cu}(\text{N}_4)(\text{OH})](\underline{32a-3}$, $\underline{32b-3})$ was obtained.

B. IR Data

IR spectrum (KBr pellet)(Figure 10) of the sample $\underline{32a-3}$, $[\text{Fe}(\text{P})\text{-O-Cu}(\text{N}_4)(\text{OH})]$, showed a strong sharp peak at 876 cm^{-1} , which is absent in the spectrum of $\underline{32a-2}$, $[\text{Fe}(\text{P})\text{-Cl Cu}(\text{N}_4)(\text{Cl})(\text{OH})]$, where (P) represents the diphenyletioporphyrin moiety and (N_4) is the tripodal tetradentate ligand. Infrared absorption of μ -oxo group has been observed in the region $800\text{-}900\text{ cm}^{-1}$ for a variety of transition metal complexes, and has been attributed to the metal-oxygen-metal antisymmetric stretching vibration.⁶⁹

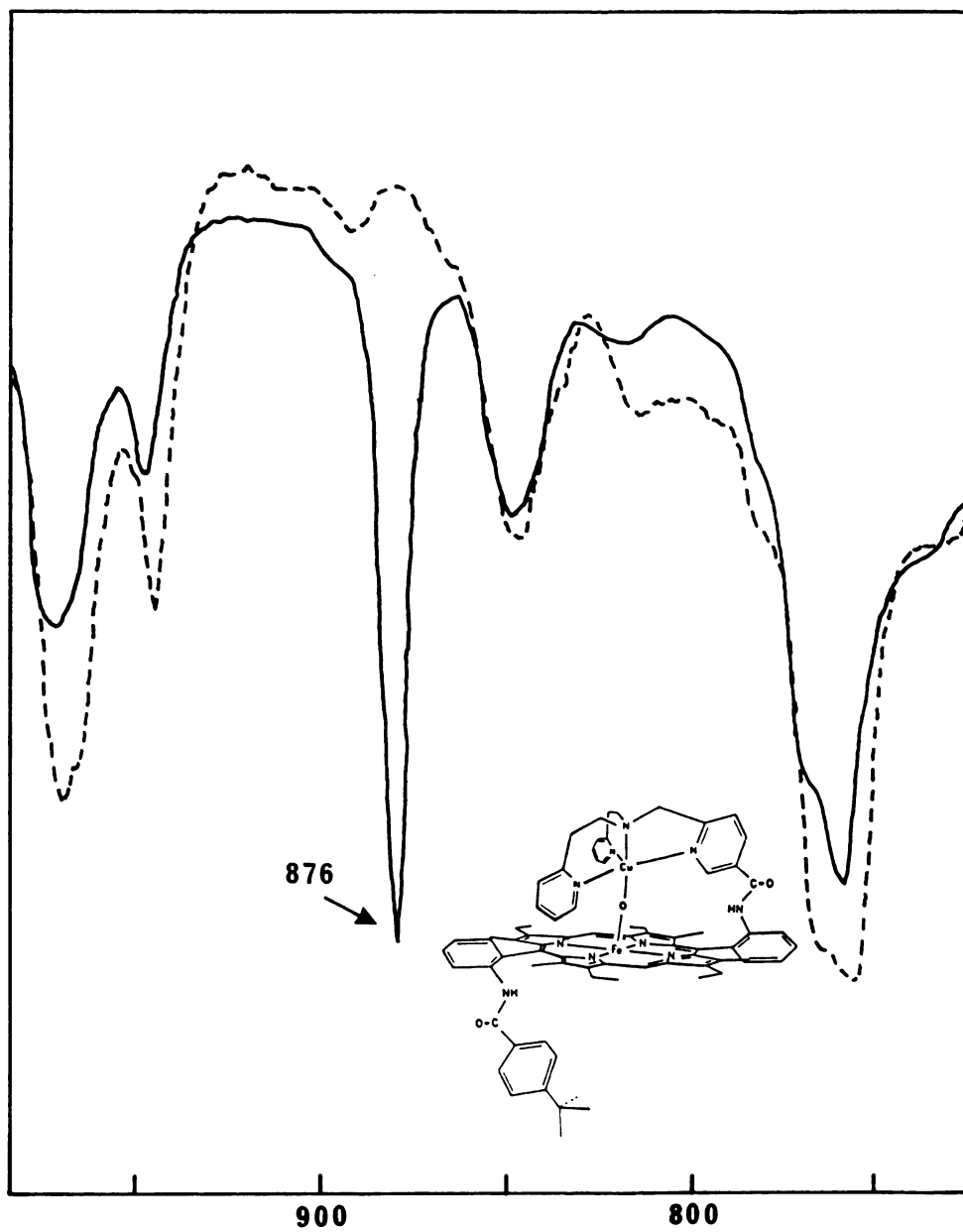


Figure 10. Infrared spectra of $[\text{Fe}(\text{P})-\text{O}-\text{Cu}(\text{N}_4)(\text{OH})]$ and $[\text{Fe}(\text{P})-\text{Cl}-\text{Cu}(\text{N}_4)(\text{Cl})(\text{OH})]$, blocked with *t*-butylbenzene.

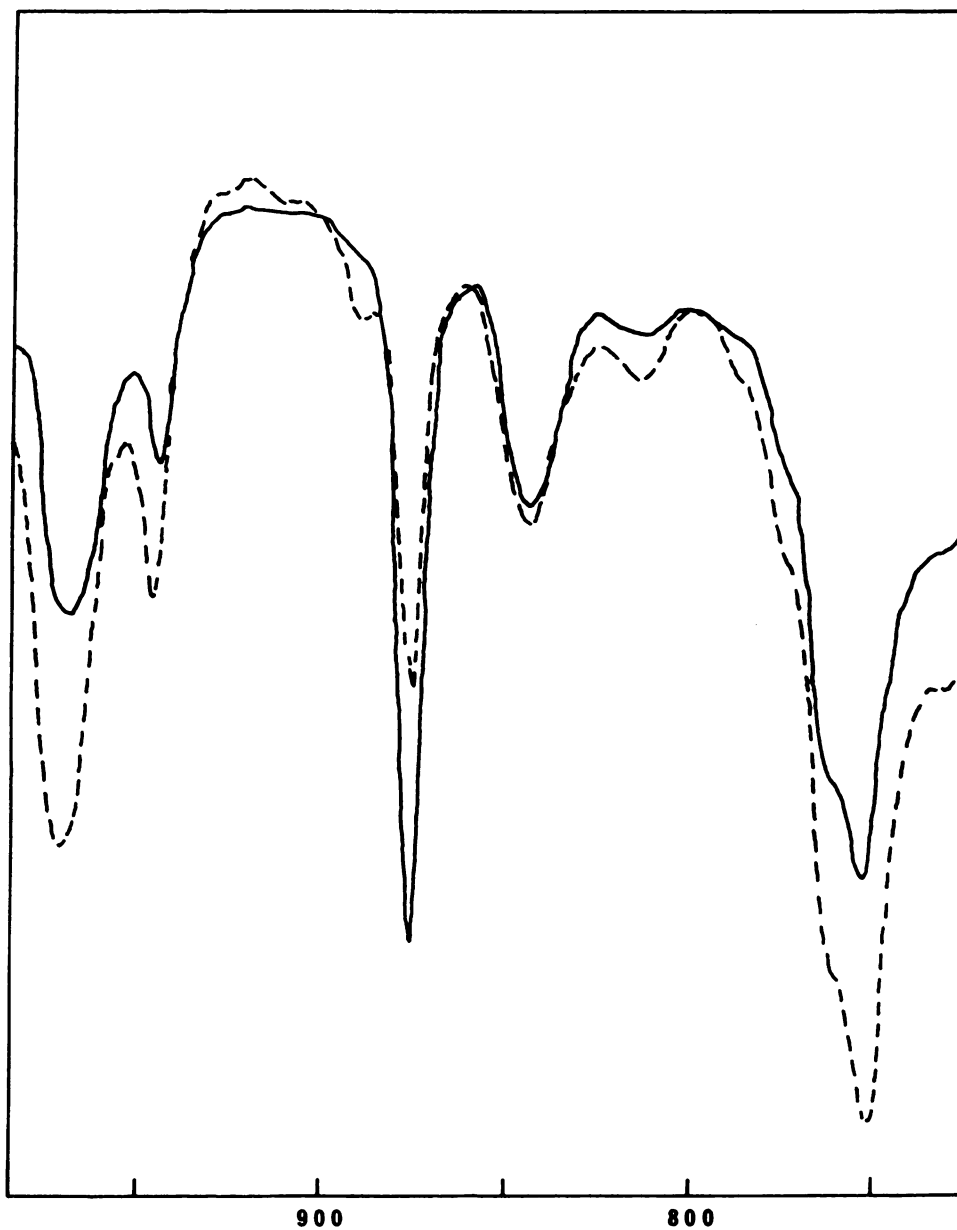


Figure 11. Infrared spectra of $[\text{Fe}(\text{P})-^{16}\text{O}-\text{Cu}(\text{N}_4)(\text{OH})]$ (—), blocked with *t*-butylbenzene, and the ^{18}O labeled derivative(---).



To determine whether a peak at 876 cm^{-1} is a M-O-M' peak, a methanol-methylene chloride solution of the iron only complex (32a-1), was treated with 35 % aqueous NaOH. The IR spectra of resultant material showed no peak at 876 cm^{-1} .

^{18}O labeling of the complex resulted in a spectrum (Figure 11) that showed considerable decrease in the intensity of the peak at 876 cm^{-1} . Due to the presence of strong absorptions in the region of $750\text{--}850 \text{ cm}^{-1}$, it was difficult to observe the expected shift to lower energy.⁸⁷ Occasionally a peak at 862 cm^{-1} was observed due to the presence of NaOH.

C. Magnetic Susceptibility Data

For large J ($> -200 \text{ cm}^{-1}$) and assuming only the $S' = 2$ level is populated, a temperature-independent μ_{eff} value of $4.90 \mu_{\text{B}}$ is predicted. Intermediate value of J (negative) would lead to a reduction in μ_{eff} at $300 \text{ }^{\circ}\text{K}$ from $6.16 \mu_{\text{B}}$, which then should further decrease and level out at $4.9 \mu_{\text{B}}$ as the temperature is decreased. In the case of $J = 0$ an uncoupled $S_{\text{Fe}} = 5/2$ and $S_{\text{Cu}} = 1/2$ pair would give $\mu_{\text{eff}} = 6.16 \text{ B.M.}$ which should be independent of temperature unless zero-field splitting causes a decrease at very low temperatures. For high-spin Fe(III) ($S = 5/2$), μ_{eff} is typically $5.9\text{--}6.1 \mu_{\text{B}}$.

Magnetic susceptibilities were measured in the temperature range $5\text{--}300 \text{ }^{\circ}\text{K}$ by the variable temperature susceptome-

Table 1. Molar magnetic susceptibility and effective magnetic moment as a function of temperature for the mononuclear Fe, binuclear Fe & Cu and μ -oxo-bridged binuclear Fe & Cu porphyrins blocked with t-butylbenzene.

No	[Fe(P)-OH (N_4)]		[Fe(P)-Cl Cu(N_4)(Cl)(OH)]		[Fe(P)-O-Cu(N_4)(OH)]				
	Temp.	Suscept.	B.M.	Temp.	Suscept.	B.M.	Temp.	Suscept.	B.M.
1	5.044	0.5613	4.76	4.999	0.5496	4.69	5.003	0.4613	4.30
2	9.998	0.3175	5.04	10.002	0.3400	5.22	9.999	0.2482	4.46
3	20.001	0.1681	5.19	20.001	0.1718	5.24	19.997	0.1261	4.49
4	29.994	0.1135	5.22	30.009	0.1247	5.47	29.973	0.0856	4.53
5	39.981	0.0863	5.25	39.980	0.0950	5.51	39.982	0.0652	4.57
6	50.036	0.0694	5.27	50.026	0.0765	5.53	50.033	0.0528	4.60
7	59.934	0.0582	5.28	59.941	0.0641	5.54	59.941	0.0444	4.61
8	80.010	0.0436	5.28	80.000	0.0480	5.54	80.110	0.0336	4.64
9	124.760	0.0280	5.29	124.760	0.0308	5.54	124.570	0.0222	4.70
10	172.020	0.0208	5.35	171.260	0.0218	5.46	171.140	0.0173	4.87
11	217.360	0.0156	5.21	218.050	0.0169	5.43	217.940	0.0141	4.96
12	275.740	0.0132	5.40	270.300	0.0139	5.48	269.240	0.0117	5.02
13	296.420	0.0124	5.42	300.790	0.0128	5.55	299.770	0.0106	5.04

14	249.200	0.0147	5.41	249.070	0.0157	5.59	248.370	0.0125	5.00
15	198.160	0.0183	5.39	198.020	0.0199	5.61	201.170	0.0150	4.91
16	152.570	0.0237	5.38	152.550	0.0261	5.64	154.740	0.0190	4.85
17	100.240	0.0353	5.32	100.220	0.0390	5.59	99.630	0.0273	4.66
18	70.018	0.0502	5.30	70.005	0.0552	5.56	70.020	0.0382	4.63
19	55.012	0.0634	5.28	54.997	0.0699	5.54	55.012	0.0480	4.60
20	44.998	0.0772	5.27	45.005	0.0850	5.53	44.998	0.0581	4.57
21	34.993	0.0982	5.24	34.968	0.1081	5.50	34.988	0.0735	4.54
22	24.995	0.1360	5.21	24.997	0.1487	5.45	24.999	0.1016	4.51
23	14.996	0.2212	5.15	15.000	0.2396	5.36	14.996	0.1673	4.48
24	7.502	0.4159	5.00	7.500	0.4441	5.16	7.498	0.3381	4.50

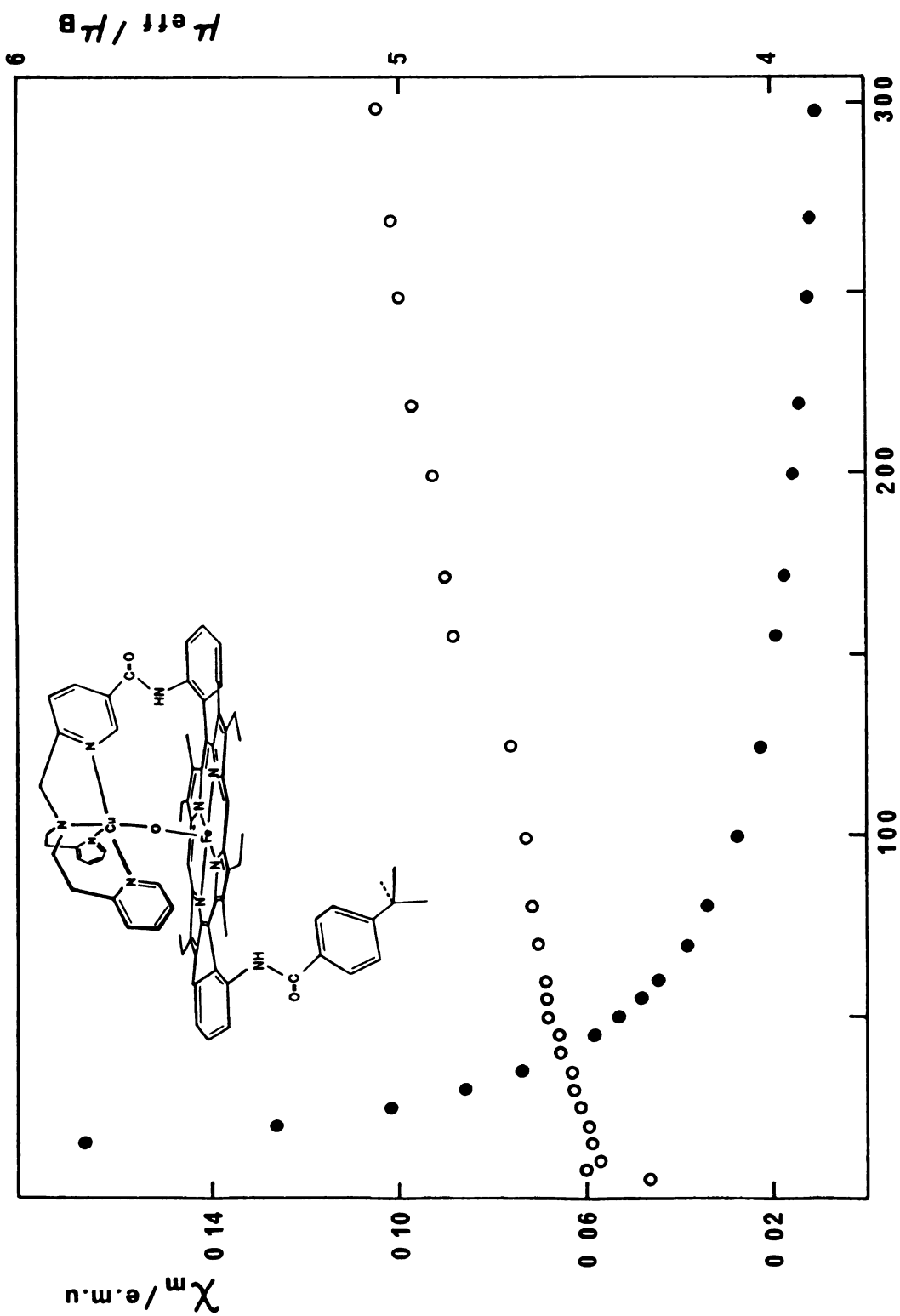


Figure 12. Molar magnetic susceptibility and effective magnetic moment as a function of temperature for $[\text{Fe}(\text{P})\text{-O-Cu}(\text{N}_4)(\text{OH})]$, blocked with *t*-butylbenzene.

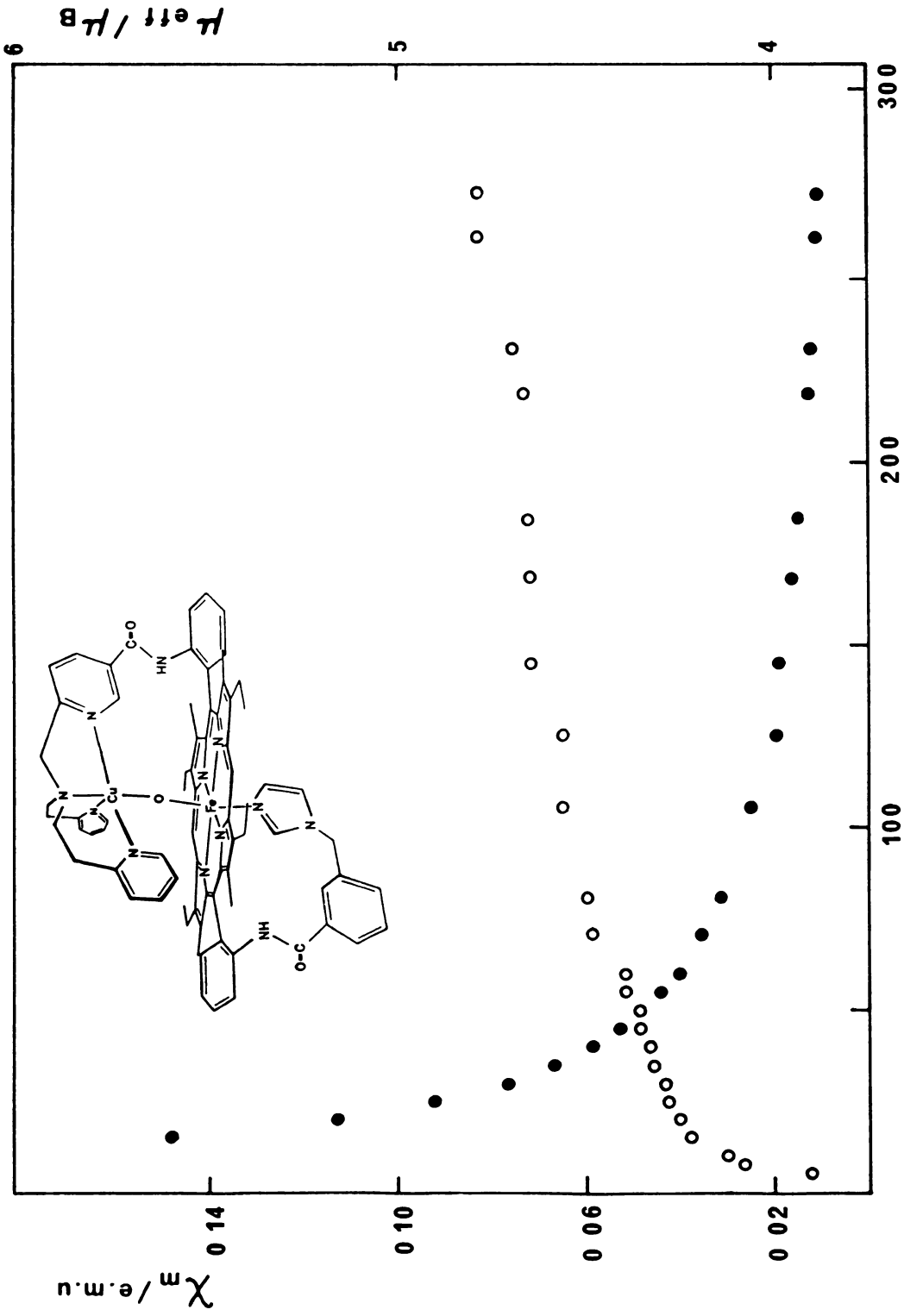


Figure 13. Molar magnetic susceptibility and effective magnetic moment as a function of temperature for [Fe(P)-O-Cu(N₄)(OH)]₂, blocked with imidazole.



ter (Table 1). Magnetic moments were calculated by the equation, $\mu_{\text{eff}} = 2.828(\mu_{\text{M}} \times T)^{1/2}$, where μ_{M} is the molar susceptibility. The hydroxide compound, copper-free mononuclear Fe complex (32a-1), $[\text{Fe}(\text{P})-\text{OH}(\text{N}_4)]$ (APPENDIX, A24), does not behave like typical high-spin heme molecules of the type $\text{Fe}(\text{porphyrin})\text{X}$ (APPENDIX B, B6). Thus, in case of 32a-1, $[\text{Fe}(\text{P})-\text{OH}(\text{N}_4)]$, μ_{eff} at 300 °K is 5.42 B.M., falling slowly to 5.29 B.M. at 125 °K and were rapidly to 4.76 B.M. at 5 °K. These are low for high-spin Fe(III) ($S = 5/2$) which has typically μ_{eff} of 5.9-6.1 μ_{B} and indicate a situation involving quantum mixing or equilibrium of $S = 3/2$ and $S = 5/2$ spin states. The chemical or structural reason for the presence of two spin-state on iron is difficult to determine with certainty but may well be due to small alternations in Fe-N and Fe-Cl distances as the temperature is altered. It has been shown recently that changes in the axial Fe-X bond in various iron(III) porphyrin can give rise to the intermediate spin state.^{88,89}

But we note that, in Figure 16, the 5 coordinate ferric heme complex with a hydroxide coordinating anion is high spin. Thus, it seems clear that the Fe complex 32a-1 is not pure 5 coordinate high complex. The Raman spectrum of Fe complex 32a-1 shows that some amount of 6 coordinate (possibly from intra- or intermolecular tripyridine ligand) Fe complex is present.

In an attempt to check the spin coupling possibility via Cl^- bridge (32a-2), we added a Curie component (1.90 μ_{B})

of Cu(II) to the observed susceptibility of the Fe(III) only complex $\underline{32a-1}$. μ_B can be calculated for an $[\text{Fe}^{\text{III}}-\text{Cl Cu}^{\text{II}}]$ centre in $\underline{32a-2}$, assuming magnetically non-interacting Fe^{III} and Cu^{II} ion centres. The resulting curve can be compared with the experimentally determined curve (APPENDIX A, A24). The magnetic behavior of $\underline{32a-2}$ could possibly arise from an uncoupled pair of Fe(III) (mixed spin $S = 3/2, 5/2$) and Cu(II) ($S = 1/2$). But we should consider that, in Figure 17, the 5 coordinate heme complex with a chloride coordinating anion is high spin. Thus, there is a little exchange coupling between Fe and Cu. But it is not strong enough to mimic the magnetic features of the Fe-Cu couple in the fully oxidized (resting) form of cytochrome oxidase.

The μ_{eff} of and Fe-O-Cu complex are plotted in Figure 12 in the temperature range 5-300 °K. The susceptibility displayed a linear Curie-Weiss temperature dependence, except for a small deviation at temperature above ca. 200 °K. They revealed a strong antiferromagnetic coupling between the copper(II) and the high-spin iron(III). The magnetic behavior of $\underline{32a-3}$ could arise from an coupled pair of Fe(III) ($S = 5/2$; $\mu_{\text{eff}} = 5.9 \mu_B$) and Cu(II) ($S = 1/2$; $\mu_{\text{eff}} = 1.9 \mu_B$). The magnetic moment of $\underline{32a-3}$ (Fe-O-Cu) is 5.04 B.M. at room temperature, which is lower than that of $\underline{32a-1}$ (Fe-OH, 5.42 B.M.). Since IR spectrum of $\underline{32a-3}$ (Figure 10) shows a peak at 876 cm^{-1} typical of a metal-oxygen-metal bond, it strongly suggests that $\underline{32a-3}$ is a heterobinuclear complex, bridged by a oxygen atoms between the two metal

centers. The magnetic moment of the complex (5.04 B.M.) is much lower than the calculated value for the high-spin iron(III)-copper(II) system at room temperature. Further, the moment decreased to 4.56 B.M. when the temperature was lowered to the liquid nitrogen temperature. All these findings suggest the operation of a strong intramolecular spin exchange interaction with a $-J$ greater than 100 cm^{-1} .

D. EPR Data

EPR-Blocked Binuclear System

Electron paramagnetic resonance was used to probe the ability of the chelating ligands to bind Cu(II) and investigate possible interaction between the two metal centers. The spectra (Figure 14, 15) measured in frozen solution (CH_2Cl_2) at 77°K , exhibited features indicative of interactions between the two metal centers. The close proximity of the metal centers in these binuclear systems allows spin coupling to occur, producing for the bis copper complex a triplet spectrum. The seven hyperfine lines were discernable in the spectrum owing to interactions between the two centers.

E. Raman Data (studied in collaboration with Robert T. Kean and Prof. G. T. Babcock)

It was necessary to study the simpler structures as a guide for the interpretation of the Fe-Cu systems. The high frequency Raman spectra of several of the simple models are

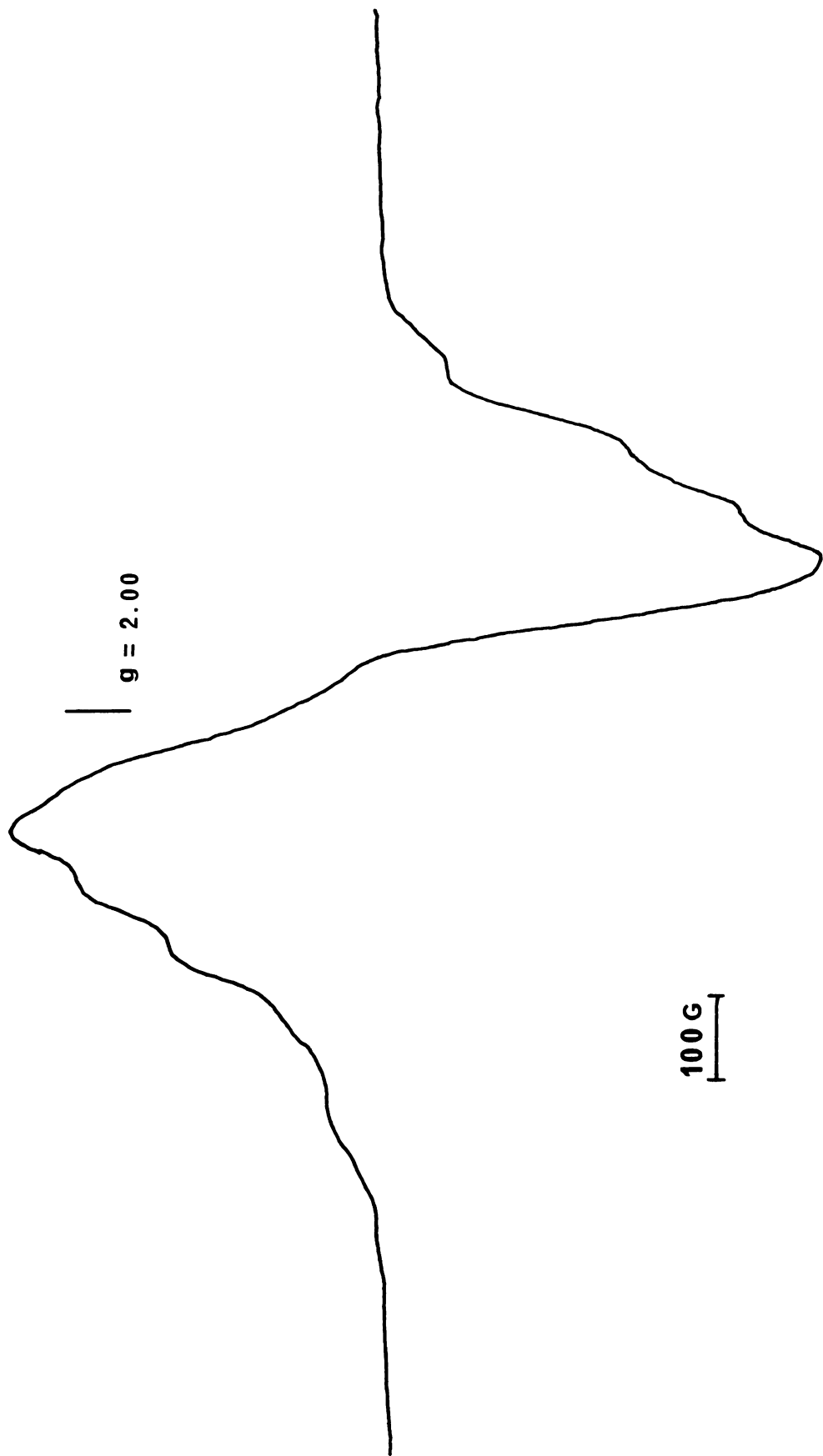


Figure 14. EPR spectrum of the bis-Cu^{II} complex, [Cu(P) Cu(N₄)(Cl)(PF₆)] blocked with t-butylbenzene, in CH₂Cl₂ at 77 °K.

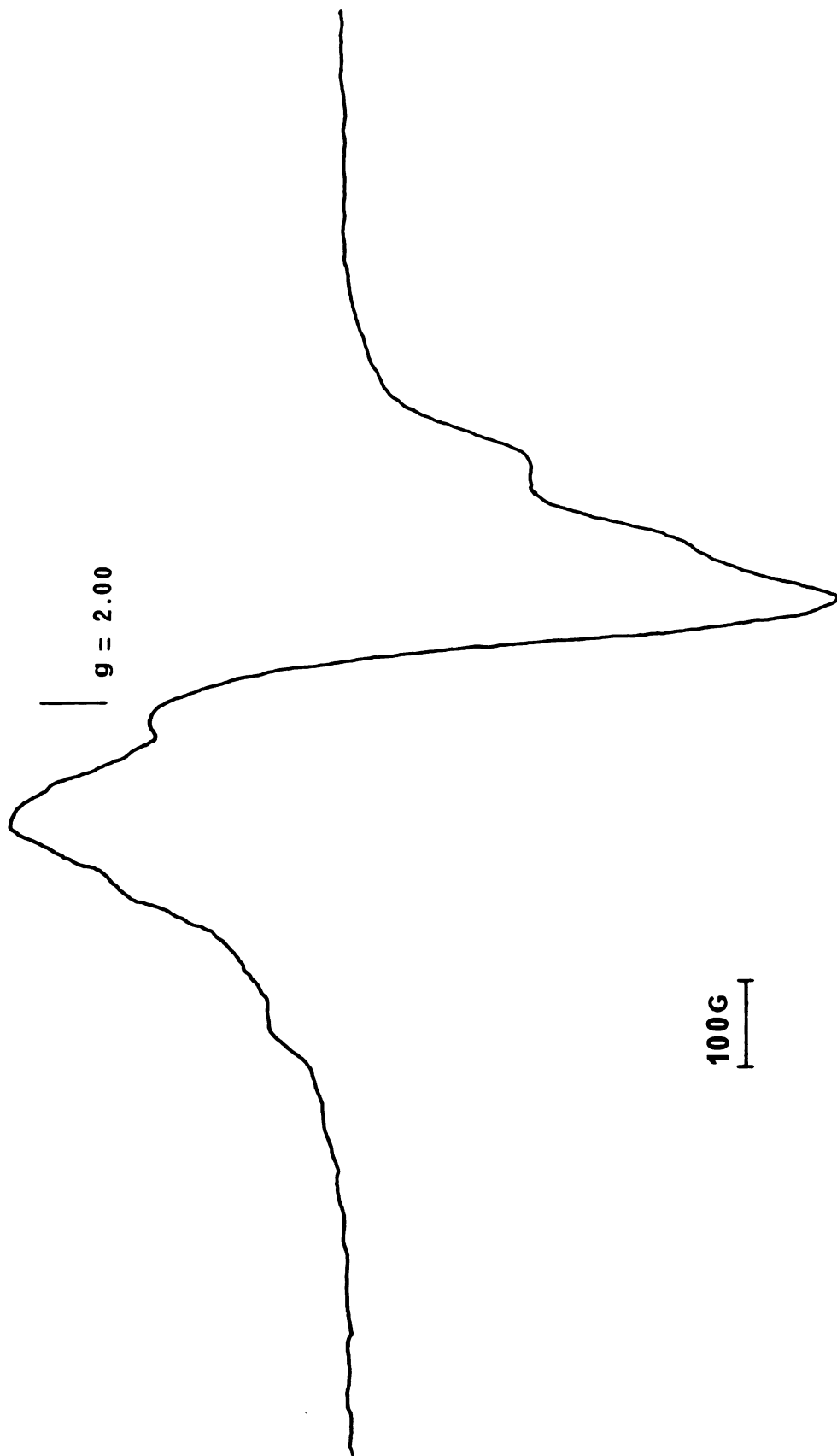
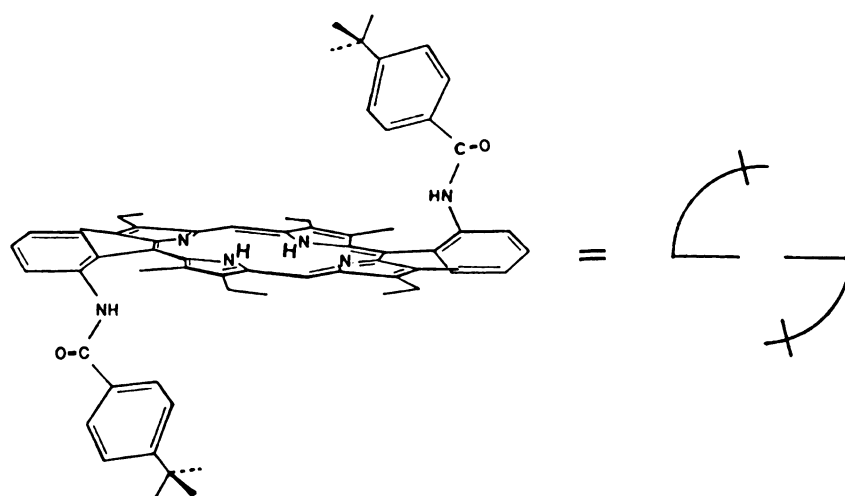


Figure 15. EPR spectrum of the bis-Cu^{II} complex, [Cu(P) Cu(N₄)(Cl)(PF₆)] blocked with imidazole, in CH₂Cl₂ at 77 °K.



Trans-5,15-bis[o-(p-t-butylbenzamido)phenyl]-2,8,12,18-tetraethyl-3,7,13,17-tetramethylporphyrin.

C = Coordination

H.S. = High Spin

L.S. = Low Spin

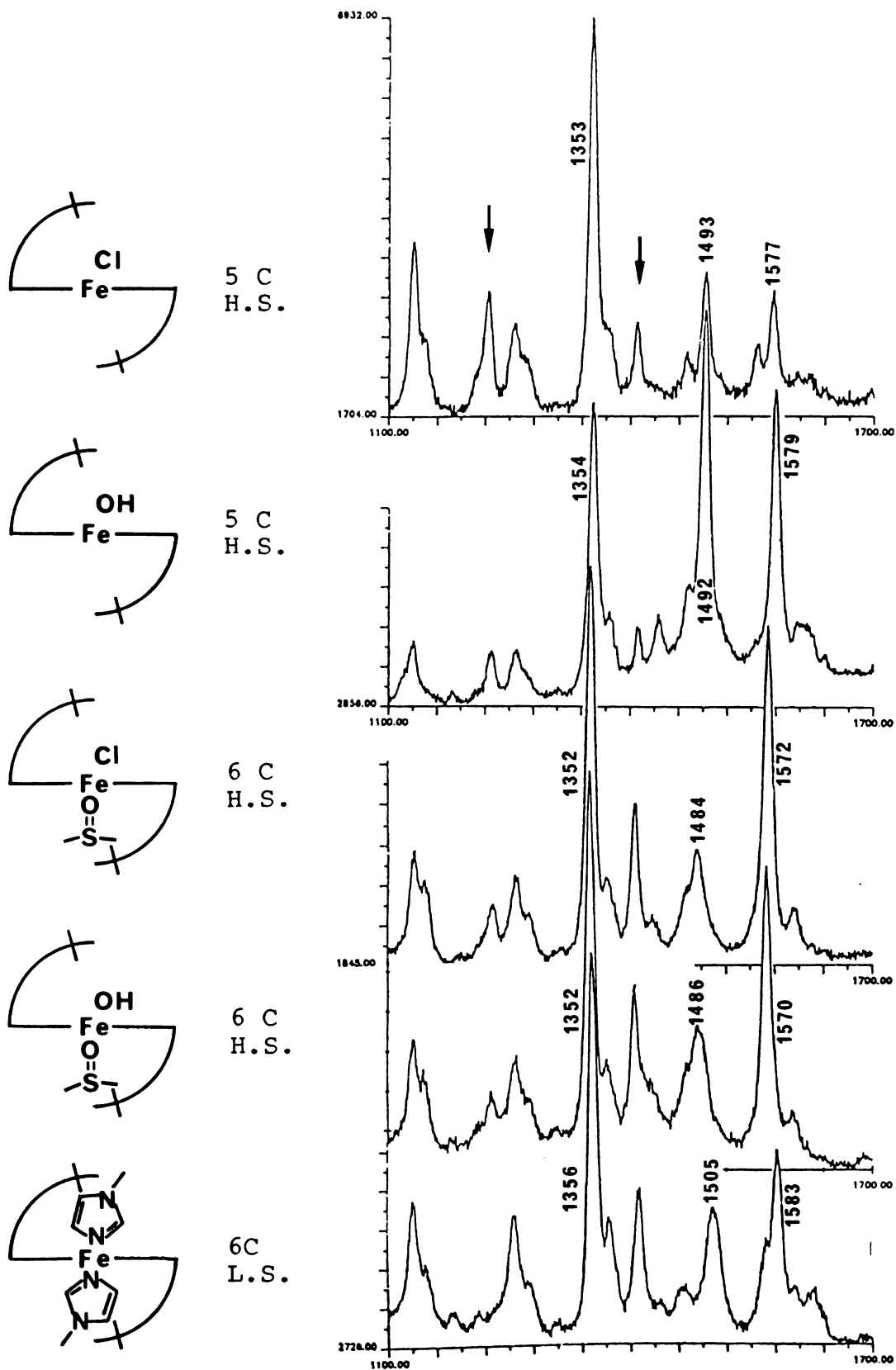


Figure 16. Raman spectra of simple model complexes.

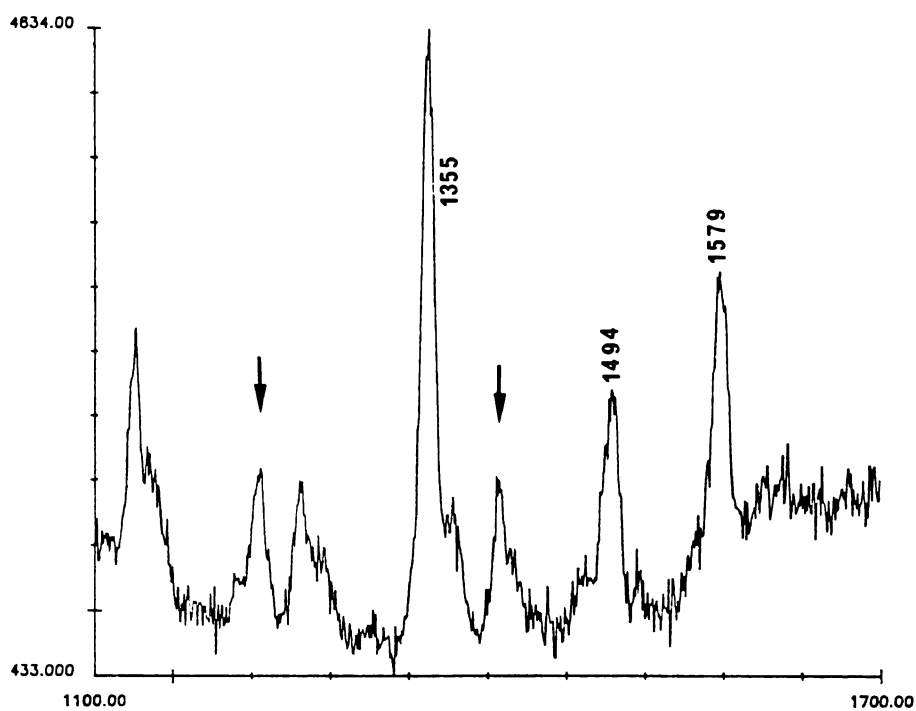


Figure 17. Raman spectrum of $[\text{Fe}(\text{P})\text{-Cl Cu}(\text{N}_4)(\text{Cl})(\text{OH})]$ blocked with *t*-butyl benzene.

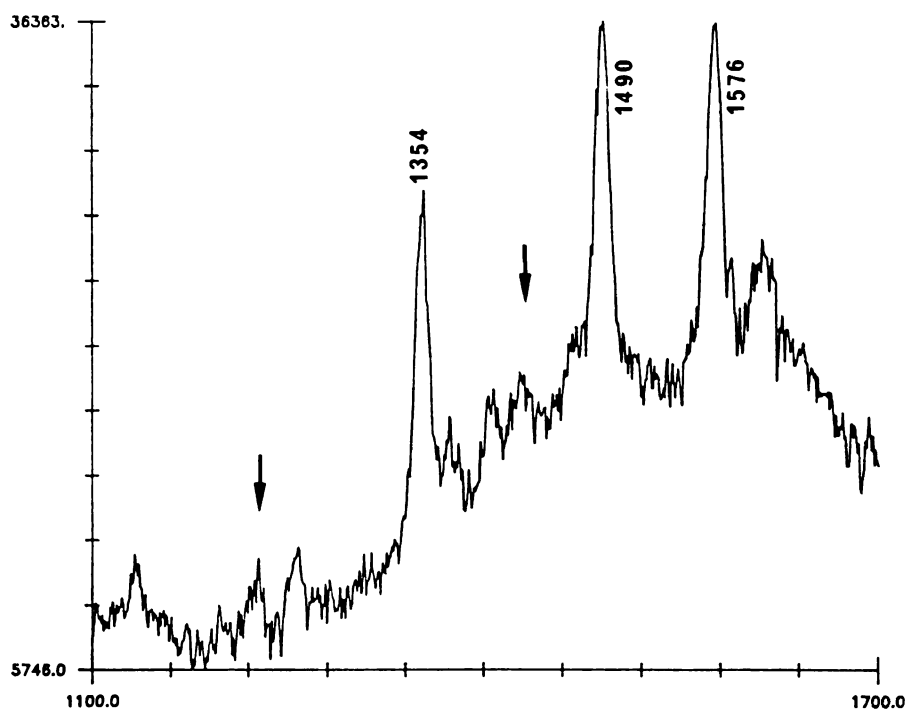


Figure 18. Raman spectrum of $[\text{Fe}(\text{P})\text{-O-Cu}(\text{N}_4)(\text{OH})]$ blocked with *t*-butyl benzene.

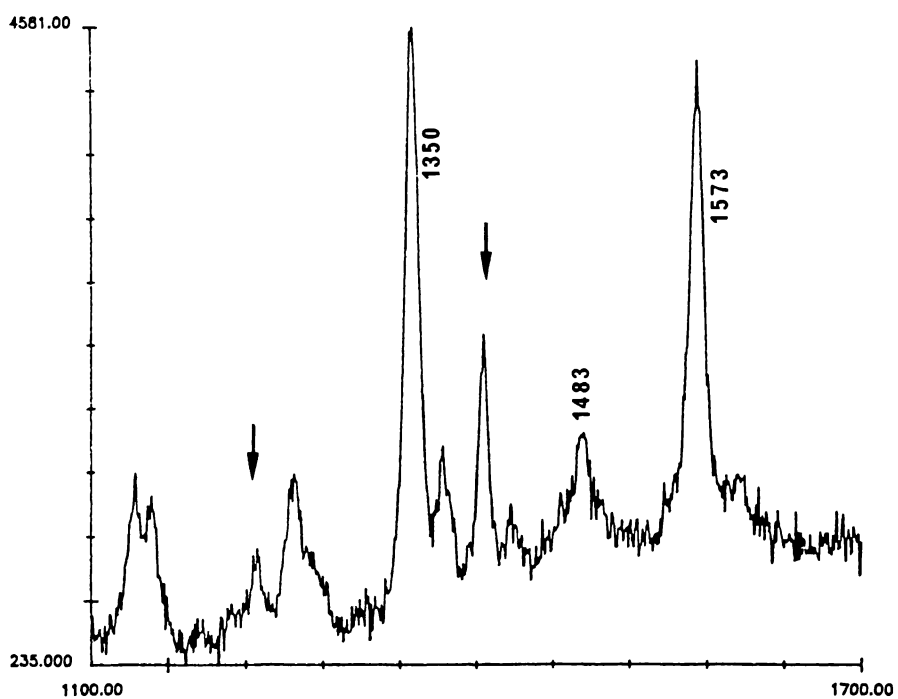


Figure 19. Raman spectrum of $[\text{Fe}(\text{P})-\text{Cl Cu}(\text{N}_4)(\text{Cl})(\text{OH})]$ blocked with imidazole.

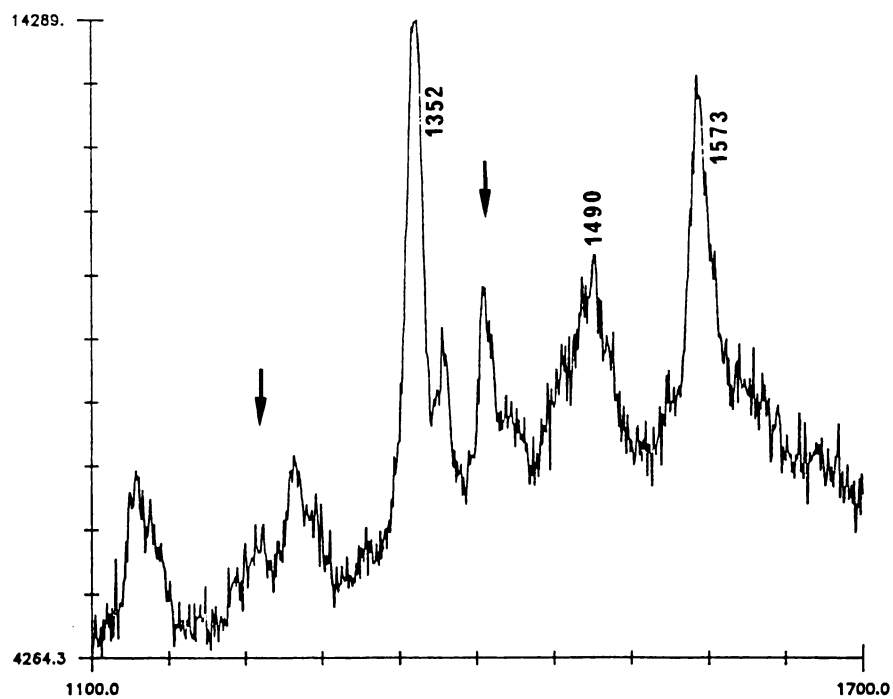


Figure 20. Raman spectrum of $[\text{Fe}(\text{P})-\text{O}-\text{Cu}(\text{N}_4)(\text{OH})]$ blocked with imidazole.

seen in Figure 16. The two peaks marked with arrows and the three labeled peaks (ν_2 , ν_3 , and ν_4) are clearly sensitive to spin state (high or low), coordination state (5 or 6), and even ligand type (Cl^- or OH^-). The assigned peaks are based on the labeling scheme of Abe and Kitagawa.^{90,91} The high frequency Raman spectra of complexes $\underline{32a-2}$, $\underline{32a-3}$, $\underline{32b-2}$ and $\underline{32b-3}$ are presented in Figure 17-20.

In the work of Abe and Kitagawa^{90,91}, a normal coordinate calculation was done on Ni octaethylporphyrin(OEP). Experimentally observed vibrational peaks were assigned by matching the observed frequencies with the calculated values. The vibrational modes of porphyrins with different ring substituents or different metals have been assigned by comparison with the Ni OEP results. Hemes are a more complicated case since the frequency of certain modes is very sensitive to the oxidation state and spin state of the Fe. This turns out to be a useful effect since the position of certain peaks can be used to determine the state of the Fe in unknown samples

An additional difficulty we encounter with these samples is the perturbation of the porphyrin pi system by the aromatic meso substituents. This effect can dramatically shift the positions of peaks relative to the OEP case.⁹² Despite this problem, the three peaks in the high frequency region are assigned as ν_4 , known as the oxidation state marker, typically shifts to lower frequency upon reduction of Fe(III) to Fe(II). The peak seen at $\sim 1354 \text{ cm}^{-1}$

in all these samples has been shown to shift to ~ 1345 upon Fe reduction.⁹³ On that basis this peak is assigned as ν_4 . Two other peaks ν_2 and ν_3 are typically very sensitive to the spin state and shift to higher frequency upon transition from high to low spin. The peaks at ~ 1571 cm^{-1} , and ~ 1485 cm^{-1} (6 coordinated high spin) are in the approximate correct locations and do demonstrate the correct behavior. Therefore the two peaks are assigned as ν_2 and ν_3 respectively. Other peaks in these spectra are also sensitive to the changes in the Fe environment but their assignments have been less obvious and they are only indicated with arrows.

It is clear from the spectra in Figure 17-20 that, based on the model compounds, none of the species are low spin. The values of ν_2 and ν_3 are too low to be low spin and the characteristic high spin peak between 1224 cm^{-1} and 1231 cm^{-1} is present in all cases. Compound 32a-2 is very clearly a 5 coordinate Cl^- species as indicated by the peak at 1225 cm^{-1} and the peak positions and relative intensities of ν_2 and ν_3 . With compound 32a-3, we see that ν_2 and ν_3 have the much greater intensities and the characteristic frequencies of a 5 coordinate OH^- species. In this case, rather than on OH^- , we have an oxygen bridging to the Cu. Compound 32b-2 has a Raman spectrum strongly indicative of 6 coordinate, high spin Cl^- as demonstrated by both peak positions and relative intensities. With compound 32b-3, the broadness of the peaks indicated some inhomogeneity in the samples; probably some Cl^- sample or some 5 coordinate

species. However it is clearly dominated by 6 coordinate high spin species and the shape and position of ν_3 indicates a fair amount of OH^- type ligation. Again this compound has an oxygen bridge to the Cu rather than a free OH^- .

Conclusion

The compound $\underline{32a-3}$ is the first well defined [Fe-Cu] binuclear blocked heme model species and, in general, represents one of the few studies involving a binuclear heme system containing two different metal ions. Taken together, these results indicate strong antiferromagnetic coupling through the oxo bridge between iron(III) and copper(II) to give a ground state with $S = 2$ characteristics.

The μ -oxo complex $\underline{32a-3}$ appear to be stable to air or moisture in the solid state and are reasonably thermally stable, but extremely sensitive to acid.

To date, relatively few studies have concerned with the lability of the coordinated imidazole moiety. The paucity of experimental data precludes any generalizations of the factors which come from metal-imidazole bond. For compound $\underline{32b-3}$, μ_{eff} varies between $4.25 \mu_{\text{B}}$ (20°K) and $4.81 \mu_{\text{B}}$ (273°K) (APPENDIX B, B3). It is possible that the spin state of Fe(III) porphyrin can be influenced by the nature of the axial groups. Using values of μ_{eff} for the Fe^{III} center (4.47 B.M. at 20°K , 4.56 B.M. at 80°K , 4.86 B.M. at 284°K), as found for $\underline{32b-1}$ (APPENDIX B, B1), and assuming $\mu_{\text{eff}} = 1.90 \mu_{\text{B}}$ for Cu^{II} , μ_{eff} values can be calculated for

an Fe-Cl-Cu centre in 32b-2, assuming magnetically non-interacting Fe^{III} and Cu^{II} ion centers. These values compared well with the experimentally determined values (APPENDIX B, B2) (4.61 B.M. at 20 °K, 4.74 B.M. at 80 °K, 4.94 B.M. at 280 °K). The magnetic moment of the Fe-O-Cu complex (32b-3) is lower than the value for the iron(III)-copper(II) system. Moreover, the IR spectrum of 32b-3 in a KBr pellet shows spectral characteristics, a peak at 876 cm⁻¹, consistent with the presence of Fe-O-Cu bond. These facts suggest the operation of the intramolecular spin exchange interaction.

Experimental

Physical Measurements

Metal chelation studies on compounds 28a and 28b has not yet been completed. The stability of the copper complexes of these ligands should enable them to serve as viable models for the O₂ binding and reduction process.

NMR spectra (CDCl₃, Me₄Si internal standard) were obtained with a Bruker WM-250 instrument. High resolution mass spectra were obtained with a JEOL HX110-HF instrument equipped with a fast atom bombardment gun. A matrix of thioglyceroldithioerythritol-dithiothreitol (2:1:1) containing 1.1 % trifluoroacetic acid was used. Visible absorption spectra (in CH₂Cl₂) were measured with a Cary 219 spectrophotometer. Preparative TLC plates were from Analtech (Silica gel G, 1500 um).

Resonance Raman spectra were obtained with a spex 1401 Ramalog scanning double monochromator using a cooled RCA photomultiplier tube. Data collection and instrument operation was achieved from a DEC LSI 11-2 computer through a house built interface. All spectra were recorded using 20 mW of power at 406.7 nm excitation (Spectra-Physics model 164 Kr ion). Samples were contained in a spinning EPR tube (at room temperature or lower) and the signal was collected utilizing a ~ 170 degree scattering geometry. The Raman spectrometer was calibrated to the 1004 cm^{-1} line of toluene for all scans.

Synthesis

A. Dithioether Appended Porphyrins

Ethyl 6-[N,N-bis(3-thiabutyl)amino]methylnicotinate (25a)

A mixture of ethyl 5-(2-chloromethyl)pyridinecarboxylate(20) (2.5 g, 12.5 mmol) and bis(3-thiabutyl) amine⁸⁶ (20.6 g, 125 mmol) in aqueous ethanol (70 %, 30 mL) was refluxed for 6 h. The solution was evaporated to dryness. The crude product was dissolved in chloroform (200 mL) and successively washed with 5 % HCl (5 x 100 mL), 5 % aqueous NaOH (100 mL), water (100 mL), dried over anhydrous sodium sulfate and evaporated to dryness to yield a red oil. Yield 70 %. MS, m/e(relative intensity), 390(M⁺, 1); ¹H NMR (CDCl₃) δ 1.41(t, 3H, Et), 2.09(s, 6H, Me), 2.72(m, 8H, CH₂CH₂), 3.89(s, 2H, Py-CH₂), 4.41(q, 2H, Et), 7.67(d, 1H, Py), 8.27(dd, 1H, Py), 9.13(d, 1H, Py).

6-[N,N-Bis(3-thiabutyl)amino]methylnicotinic acid (26a)

The ester 25a (2.5 g, 7.62 mmol) was dissolved in hot ethanol (10 mL, 95%). To this solution, a solution of KOH (0.75 g/5 mL water) was added. Refluxing was continued for 2 h. The solution was allowed to cool to room temperature and neutralized with an equivalent amount of hydrochloric acid, and then evaporated in vacuo to yield a yellow white solid. The solid residue was extracted with three 30 mL portions of chloroform. After drying over sodium sulfate, the solution was filtered and evaporated in vacuo to yield a yellow solid. The crude acid product was directly used to make acyl chloride without further purification. Yield 90 %. ¹H NMR (CDCl₃) δ 2.11(s, 6H, Me), 2.84(m, 8H, CH₂CH₂), 4.12(s, 2H, Py-CH₂), 7.77(d, 1H, Py), 7.42(dd, 1H, Py), 9.28(d, 1H, Py).

trans-5-[o-(p-tert-Butylbenzamido)phenyl]-15-(o-{6-[N,N-bis(3-thiabutyl)amino]methylnicotinamido}phenyl)-2,8,12,18-tetraethyl-3,7,13,17-tetramethylporphyrin (28a)

A solution of thionyl chloride (0.08 mL, 1.1 mmol) in 4 mL of methylene chloride under nitrogen was added to a well-stirred solution of the acid 26a (300 mg, 1 mmol) and triethylamine (0.28 mL, 2 mmol) in 20 mL of methylene chloride. The mixture was stirred at room temperature for 1 h and pumped dry. The crude acid chloride was added to a 200 mL of methylene chloride solution of porphyrin 18 containing

triethylamine. After refluxing for 10 h, the mixture was poured into ice water. The organic layer was separated, washed with 5 % NaOH, water, and dried over sodium sulfate. After evaporation, the mixture was separated on thick layer silica gel plate, with 3 % methanol-methylene chloride. The major band was collected and crystallized from hexane-CH₂Cl₂. Yield 45 %. MS, m/e, 1103(M+H)⁺; ¹H NMR (CDCl₃) δ -2.30(br s, 2H, pyrrole NH), 0.77(s, 9H, t-butyl), 1.79(t, 12H, Et), 2.12(s, 3H, Me), 2.15(m, 4H, SCH₂), 2.16(s, 3H, Me), 2.30(m, 4H, NCH₂), 2.62(s, 12H, Me), 3.23(s, 2H, Py-CH₂), 4.05(q, 8H, Et), 6.46(s, 1H, Ar), 6.49(s, 4H, Ar), 6.67(s, 2H, Ar), 7.52-8.10(m, 8H, Ar, NH), 9.06(m, 2H, Ar), 10.31(s, 2H, meso).

Ethyl 6-[N,N-bis(3-thiapentyl)amino]methylnicotinate (25b)

This ester was made in an analogous fashion as the ester 25a. Yield 65 %. MS, m/e(relative intensity), 311 (0.25), 281(7), 89(100), 61(26); ¹H NMR (CDCl₃) δ 1.24(t, 6H, Et), 1.41(t, 3H, Et), 2.52(q, 4H, Et), 2.76(m, 8H, CH₂CH₂), 3.90(s, 2H, Py-CH₂), 4.41(q, 2H, Et), 7.66(d, 1H, Py), 8.26(dd, 1H, Py), 9.13(d, 1H, Py).

6-[N,N-Bis(3-thiapentyl)amino]methylnicotinic acid (26b)

This acid was prepared by the procedure 26a except the ester 26a is replaced by the ester 25b. Yield 88 %. MS, m/e, 329(M⁺); ¹H NMR (CDCl₃) δ 1.17(t, 6H, Et), 2.47(q, 4H, Et), 2.77(m, 8H, CH₂CH₂), 4.00(s, 2H, Py-CH₂), 7.75(d, 1H, Py),



8.38(dd, 1H, Py), 9.17(d, 1H, Py).

trans-5-{o-[m-(N-Imidazolyl)toluamido]phenyl}-15-(o-{6-[N,N-bis(3-thiapentyl)amino]methylnicotinamido}phenyl)-2,8,12,18-tetraethyl-3,7,13,17-tetramethylporphyrin (28b)

This porphyrin was made in analogous fashion as porphyrin 28a. Yield 40 %. MS, m/e, 1155(M+H)⁺; ¹H NMR (CDCl₃) δ 0.86(t, 6H, Et), 1.75(m, 12H, Et), 2.12(q, 4H, Et), 2.18(m, 4H, SCH₂), 2.30(m, 4H, NCH₂), 2.58(s, 6H, Me), 2.61(s, 6H, Me), 3.23(s, 2H, Py-CH₂), 3.41(s, 2H, ArCH₂), 4.02(q, 8H, Et), 5.14(s, 1H, Im-H), 5.75(s, 1H, Im-H), 6.18(s, 1H, Im-H), 6.3-8.1(m, 15H, Ar, NH), 8.98(t, 2H, Ar), 10.29(s, 2H, meso).

B. Tripyridine Appended Porphyrins

Ethyl 6-{N,N-bis[2-(2-pyridyl)ethyl]amino}methylnicotinate (29)

A mixture of ethyl 5-(2-chloromethyl)pyridinecarboxylate (2.5 g, 12.5 mmol) (20) and bis[2-(2-pyridyl)ethyl]amine⁹⁴ (14.2 g, 62.5 mmol) in 30 mL of ethanol (70 %) was refluxed for 6 h. The solution was evaporated to dryness to yield a yellow oil. The crude product was purified on alumina with methylene chloride. Yield 80 %. MS, m/e (relative intensity), 390(M⁺, 1), 345(2), 298(3), 284(1), 226(35), 165(13), 106(100), 93(21), 78(25); ¹H NMR (CDCl₃) δ 1.39(t, 3H, Et), 2.99(s, 8H, CH₂CH₂), 3.90(s, 2H, Py-CH₂), 4.37(q, 2H, Et), 6.87-7.70(m, 7H, Py), 7.93-8.14(dd, 1H,

Py), 8.40–8.60(m, 2H, Py), 9.08(d, 1H, Py).

6-{N,N-Bis[2-(2-pyridyl)ethyl]amino}methylnicotinic acid

(30)

The ester 29 (3.0 g, 7.69 mmol) was dissolved in hot ethanol (10 mL, 95 %). To this solution, a solution of KOH (0.75 g/5 ml H₂O) was added. Refluxing was continued for 2 h. The solution was allowed to cool to room temperature and neutralized with an equivalent amount of hydrochloric acid, and then evaporated in vacuo to yield a yellow-white solid. The solid residue was extracted with 50 mL of chloroform. After drying over sodium sulfate, the solution was filtered and evaporated to yield the acid 30, a yellow solid. The crude acid product was directly used to make acyl chloride without further purification. Yield 88 %. ¹H NMR (CDCl₃) δ 2.99(s, 8H, CH₂CH₂), 3.93(s, 2H, Py-CH₂), 6.85–7.70(m, 6H, Py), 7.97–8.43(m, 2H, Py), 8.90(d, 1H, Py), 9.23(br s, 2H, Py).

6-{N,N-Bis[2-(2-pyridyl)ethyl]amino}methylnicotinic acid chloride (31)

A solution of thionyl chloride (0.08 ml, 1.1 mmol) in 4 mL of methylene chloride under nitrogen was added to a well-stirred solution of the acid 30 (363 mg, 1 mmol) and triethylamine (0.28 mL, 2 mmol) in 20 mL of methylene chloride. The mixture was stirred at room temperature for 1 h and pumped dry. After dissolving in methylene chloride (50

mL), this acid chloride (31) was immediately used to prepare 32a and 32b.

trans-5-[o-(p-tert-Butylbenzamido)phenyl]-15-[o-(6-{N,N-bis[2-(2-pyridyl)ethyl]amino}methylnicotinamido)phenyl]-2,8,12,18-tetraethyl-3,7,13,17-tetramethylporphyrin (32a)

This porphyrin was made in an analogous fashion as porphyrin 28a. Finally, the product 32a was separated on thick layer silica gel plate, with 6 % MeOH-methylene chloride. Yield 71 %. MS, m/e, 1165(M+H)⁺; ¹H NMR (CDCl₃) δ -2.28(br s, 2H, pyrrole NH), 0.75(s, 9H, t-butyl), 1.77(m, 12H, Et), 2.49(s, 8H, CH₂CH₂), 2.61(s, 6H, Me), 2.62(s, 6H, Me), 3.28(s, 2H, Py-CH₂), 4.05(m, 8H, Et), 5.96-8.00(m, 21H, Ar, NH), 8.51(dd, 2H, Ar), 9.07(m, 2H, Ar), 10.32(s, 2H, meso).

trans-5-[o-[m-(N-Imidazolyl)toluamido]phenyl]-15-[o-(6-{N,N-bis[2-(2-pyridyl)ethyl]amino}methylnicotinamido)phenyl]-2,8,12,18-tetraethyl-3,7,13,17-tetramethylporphyrin (32b)

This porphyrin was made in an analogous fashion as porphyrin 28a. Yield 75 %. MS, m/e, 1189(M+H)⁺; ¹H NMR (CDCl₃) δ -2.32(s, 2H, pyrrole NH), 1.74(m, 12H, Et), 2.48(s, 8H, CH₂CH₂), 2.61(s, 6H, Me), 2.62(s, 6H, Me), 3.24(s, 2H, Py-CH₂), 3.29(s, 2H, ArCH₂), 4.02(m, 8H, Et), 5.11(s, 1H, Im-H), 5.74(s, 1H, Im-H), 6.16(s, 1H, Im-H), 6.01-8.06(m, 23H, Ar, NH), 8.98(m, 2H, Ar), 10.31(s, 2H, meso).

Metal and Oxygen Insertion

Two bis-Cu^{II} complexes, [Cu(P) Cu(N₄)(Cl)(PF₆)], blocked with t-butyl benzene or blocked with imidazole respectively, were prepared by the following procedure.

To a solution of (P-N₄) (32a) (23.3 mg, 0.02 mmol) in CH₂Cl₂ (7 mL) and CH₃OH (7 mL) was added a methanolic solution of CuCl₂ (excess). The solution was stirred and heat at 50 °C for 20 min. To this solution after its volume was reduced by evaporation to 1/3, excess methanolic KPF₆ was added to induce precipitation. The solution was allowed to cool to room temperature. The red crystals were filtered off, washed well with methanol, and dried in vacuo. Imidazole blocked bis copper complex, [Cu(P) Cu(N₄)(Cl)(PF₆)] was prepared by the above procedure; red crystals.

Porphyrin 32a (58.2 mg, 0.05 mmol) was dissolved in 1:1 THF : benzene (20 mL), containing collidine (2 drops). A stream of argon was bubbled into the solution for ca. 5 min to remove oxygen and FeBr₂ was then added. The solution was heated under argon for ca. 30 min and the solvent was removed in vacuo. A stream of air was then bubbled into the solution for ca. 5 min to oxidize iron completely followed by removal of solvent in vacuo. The residue was redissolved in CH₂Cl₂ (80 mL), extracted with 10 % HCl, washed with water and eluted on alumina column. To obtain the ferric hydroxide form, the solution was washed with saturated aqueous sodium bicarbonate. The hemin hydroxide (30.9 mg, 0.025 mmol) was dissolved in 1:1 methylene chloride :

ethanol (6 mL). Copper(II) chloride (33.6 mg, 0.025 mmol) was added to the above solution. The resulting solution was heated in an oil bath for 20 min and then evaporated to dryness to give $\text{FeCuCl}_2\text{OHL}$, L = Appended porphyrin ligand.

The resulting bimetal complex (13.7 mg, 0.01 mmol), $[\text{Fe}(\text{P})-\text{Cl} \text{ Cu}(\text{N}_4)(\text{Cl})(\text{OH})]$, was dissolved in 1:1 CH_2Cl_2 : CH_3OH (10 mL). After addition of 0.03 mL of 35 % aqueous NaOH, the solution was stirred for 30 min and evaporated successively in small portions (10 x 1 mL). The residue was extracted with 2 mL CH_2Cl_2 and pumped dry. μ -Oxo bridged heterobinuclear metal complex, $[\text{Fe}(\text{P})-\text{O}-\text{Cu}(\text{N}_4)(\text{OH})]$, was obtained.

CHAPTER IV

SUMMARY AND FUTURE STUDIES

The active site structure and related function of cytochrome c oxidase is one of the most controversial and enigmatic problems in metalloenzyme chemistry.

Strong antiferromagnetic coupling ($-J \geq 200 \text{ cm}^{-1}$) between high-spin ferric heme a_3 and cupric Cu_B is a commonly accepted explanation for the EPR silent active site of the resting state cytochrome oxidase. This explanation is consistent not only with EPR results but also with the bulk magnetic susceptibility which is significantly lower than what we would be expected for the same system with isolated spins.

The construction of synthetic model compounds is important for the understanding of the chemical nature of such a coupled heme-copper active site in the oxidase.

To achieve this aim, several strapped porphyrins, 6, 7, 15a, 15b, 15c, 15d, 24a, 24b, and 24c, and ligand appended, 6th coordination site blocked porphyrins, 28a, 28b, 32a, and 32b, were synthesized so that the Fe^{3+} and Cu^{2+} ions may be sequentially incorporated into the porphyrin and the appended ligand groups. μ -Oxo complexes of iron(III) porphyrin (7) and copper(II) ion have been prepared; the

magnetic susceptibility measurements revealed that the dithiazole strapped model compound has magnetically coupled high spin Fe(III) ($S_1=5/2$) and Cu(II) ($S_2=1/2$) ions with a resultant energy gap of $-3J = 132 \pm 5 \text{ cm}^{-1}$ between the $S = 2$ and $S = 3$ states. This was the first example of a high spin ferric heme showing antiferromagnetic coupling with a cupric ion.

To avoid the formation of the external Fe-O-Fe dimer, the 6th site blocked, with t-butylbenzene or imidazole, model compounds were synthesized. IR (peak at 876 cm^{-1}) and magnetic susceptibility data of these model compounds demonstrated strong coupling (ca. $-J \geq 100 \text{ cm}^{-1}$) in the μ -oxo binuclear complexes.

EPR spectra of the bis copper(II) complexes of these model compounds also showed spin coupling between two copper(II) ions.

Raman spectra of the binuclear complexes showing spin state, coordination state and ligand type were obtained.

These 6th coordination site blocked, tripyridine appended models are expected to be able to mimic the O_2 reduction site in cytochrome c oxidase. In case of 28a and 28b, the stability of the copper complexes of these ligands will enable the study of the catalytic four electron reduction of O_2 to H_2O .

This thesis describes the development of the synthesis and demonstrates the viability of the models. Future work will focus on the ligand binding and catalytic reactions

associated with these binuclear metal systems.

GLOSSARY

ANTIFERROMAGNETISM: This arises if the magnetic vectors of neighboring centers tend to couple antiparallel.

ANTIFERROMAGNETIC EXCHANGE INTERACTION MECHANISMS: It is generally accepted that the mechanism of the the exchange interaction involves the mutual pairing of electronic spins via some form of orbital overlap, analogous to the formation of a chemical bond. The following two mechanisms are usually used to account for antiferromagnetic exchange: (a) direct interaction, and (b) superexchange.

BOHR MAGNETON: $\beta = eh/4\pi mc = 0.927 \times 10^{-20}$ erg gauss⁻¹.

CURIE-WEISS LAW: $\chi_A = C/(T+\theta)$.

Where θ is a constant (The Weiss constant). If this equation is obeyed, a plot of $1/\chi_A$ vs. T will be a straight line.

CYSTEINE: HS-CH₂-CH(NH₂)-CO₂H.

EFFECTIVE MAGNETIC MOMENT:

$$= (3\kappa/N\beta^2)^{1/2} (\chi_A T)^{1/2}.$$

$$= 2.828 (\chi_A T)^{1/2} \text{ Bohr magnetons (in c.g.s. units).}$$

$$\text{spin only value, } \mu_{s.o.} = [4S(S+1)]^{1/2} \quad (1)$$

Since each electron has $S = 1/2$ it is easy to see that for n unpaired electrons, Equation (1) becomes

$$\mu_{s.o.} = [n(n+2)]^{1/2} \text{ Bohr magnetons.}$$

Thus it is possible in principle to define the number of unpaired electrons in a metal complex from its magnetic moment and vice versa.

EXAFS: The Extended X-ray Absorption Fine Structure, EXAFS, reflects the absorptivity due to the photoelectron backscattering from the atoms surrounding the absorber. This modulation depends on the atomic number of absorber and scatter, the distance between them, and the spread of this distance induced by static or thermal disorder. The possibility of identifying near-neighbor atoms and determining their distance gives the EXAFS phenomenon its special interest.

The EXAFS techniques can be applied to amorphous samples in any physical state or biological matrix.

g-VALUE: A dimensionless parameter which can be determined from the experimental EPR spectrum. It is determined solely by the spin and orbital angular momenta of the unpaired electron. In a spherically symmetric environment (S-state) the orbital angular momentum is zero, and the g has the free-spin value 2.0023. Thus, in an organic free radical, the electron is highly delocalized, leading to very little orbital angular momentum and consequently only small deviation from the free spin g-value. For transition metal ions, the molecular or electric fields arising from ligand atoms or from neighboring ions quench the orbital motion of the electrons partly or completely. One therefore observes deviations from the free spin g-value.

HISTIDINE: $\text{Im-CH}_2\text{-CH(NH}_2\text{)-CO}_2\text{H}$.

METHIONINE: $\text{H}_3\text{C-S-CH}_2\text{-CH}_2\text{-CH(NH}_2\text{)-CO}_2\text{H}$.

PROSTHETIC GROUP: A cofactor firmly bound to the enzyme protein.

SPIN HAMILTONIAN: $\mathcal{H} = -2JS_1S_2$.

Where J is an exchange integral between centers 1 and 2. J is negative for an antiferromagnetic interaction and positive for a ferromagnetic interaction.

TYROSINE: $\text{HO-CH}_2\text{-CH(NH}_2\text{)-CO}_2\text{H}$.

ZERO FIELD SPLITTING: If there are two or more unpaired electrons in systems ($S > 1$), the individual magnetic moments interact with the magnetic fields generated by other electrons. The interactions among the electrons may be of purely magnetic dipolar nature (triplet states of organic molecules) or may arise through the effect of electric or ligand fields in the molecule (transition metal ion). In both cases the spin multiplets are not degenerate even in the absence of an external magnetic field, leading to a zero-field splitting. For transition metal ions, zero-field splitting is observed whenever there is a deviation from cubic symmetry.



APPENDIX A



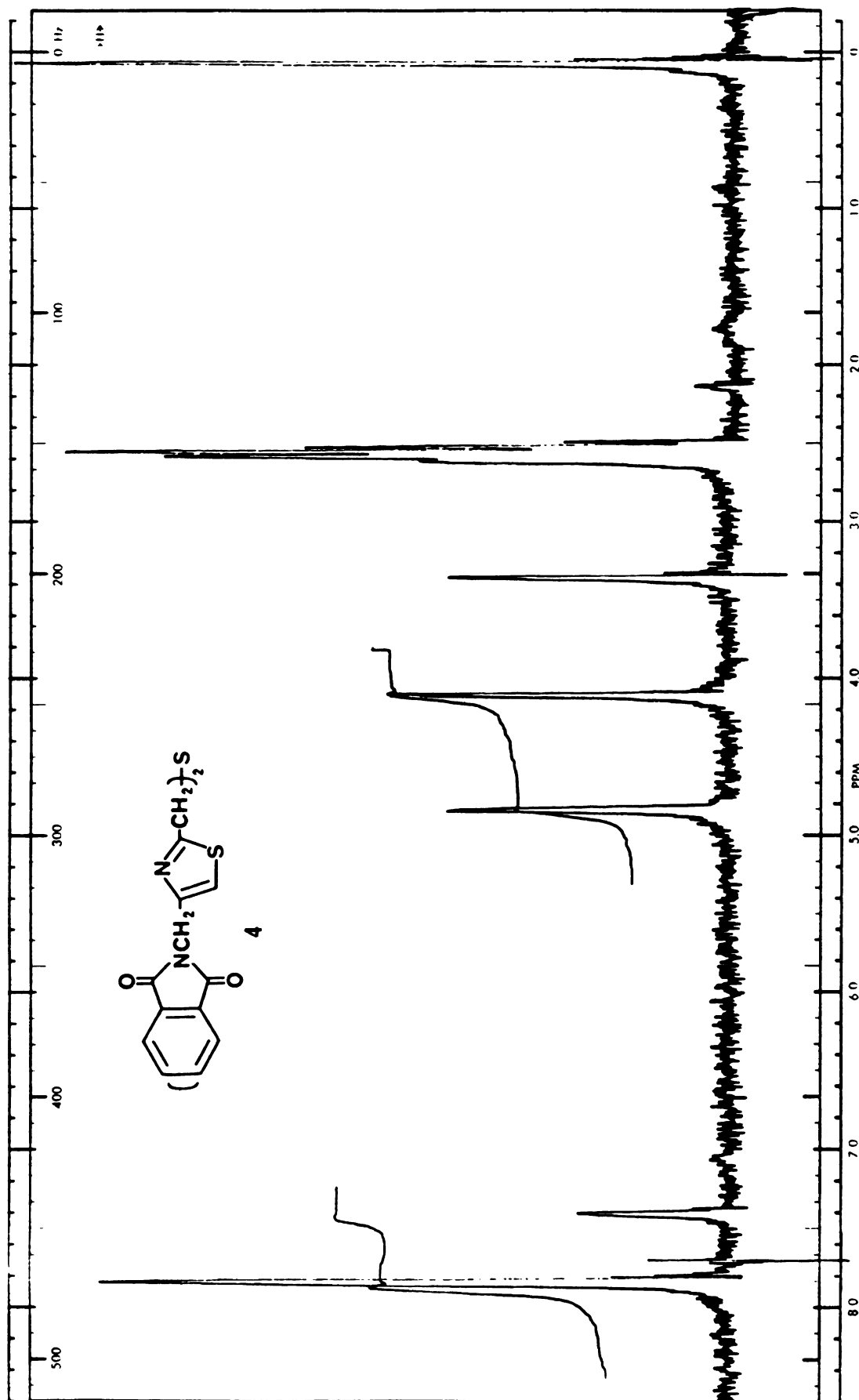
List of
Appendix Figures

Figure		Page
A1.	60 M Hz ^1H NMR spectrum of Bis[4-(phthalimidomethyl)thiazole-2-methyl] sulfide(4), DMSO-d_6 .	96
A2.	60 M Hz ^1H NMR spectrum of Bis[4-(aminomethyl)thiazole-2-methyl] sulfide(5), CDCl_3	97
A3.	250 M Hz ^1H NMR spectrum of 7,17-{4,4'-[2,2'-(2-Thiatriethylene)dithiazolyl]bismethylcarbamoylethyl}-3,8,13,18-tetramethyl-2,12-dipentylporphyrin(6), CDCl_3	98
A4.	250 M Hz ^1H NMR spectrum of 3,17-{4,4'-[2,2'-(2-Thiatriethylene)dithiazolyl]bismethylcarbamoylethyl}-2,7,13,18-tetramethyl-6,12-diethylporphyrin(7), CDCl_3	99
A5.	60 M Hz ^1H NMR spectrum of Pyridine-2,6-bis[4-(2-thiabutyl)amine(11)], CDCl_3	100
A6.	250 M Hz ^1H NMR spectrum of 7,17-[Pyridine-2,6-bis(2-thiabutylcarbamoylethyl)]-2,12-dipentyl-3,8,13,18-tetramethylporphyrin(15a), CDCl_3	101
A7.	250 M Hz ^1H NMR spectrum of 7,17-[Pyridine-2,6-bis(2-thiabutylcarbamoylmethyl)]-2,12-dipentyl-3,8,13,18-tetramethylporphyrin(15b), CDCl_3	102
A8.	250 M Hz ^1H NMR spectrum of 7,17-[Pyridine-2,6-bis(2-thiabutylcarbamoylmethyl)]-2,12-dioctyl-3,8,13,18-tetramethylporphyrin(15c), CDCl_3	103
A9a.	250 M Hz ^1H NMR spectrum of 3,17-[Pyridine-2,6-bis(2-thiabutylcarbamoylethyl)]-8,12-diethyl-2,7,13,18-tetramethylporphyrin(15d), CDCl_3	104
A9b.	250 M Hz ^1H NMR spectrum of 3,17-[Pyridine-2,6-bis(3-thiabutylcarbamoylethyl)]-8,12-diethyl-2,7,13,18-tetramethylporphyrin(15d), amide H decoupled, CDCl_3	105
A10.	60 M Hz ^1H NMR spectrum of Ethyl 5-(2-chloromethyl)pyridinecarboxylate(20), CDCl_3	106
A11.	60 M Hz ^1H NMR spectrum of Bis[2-(5-ethoxy-	

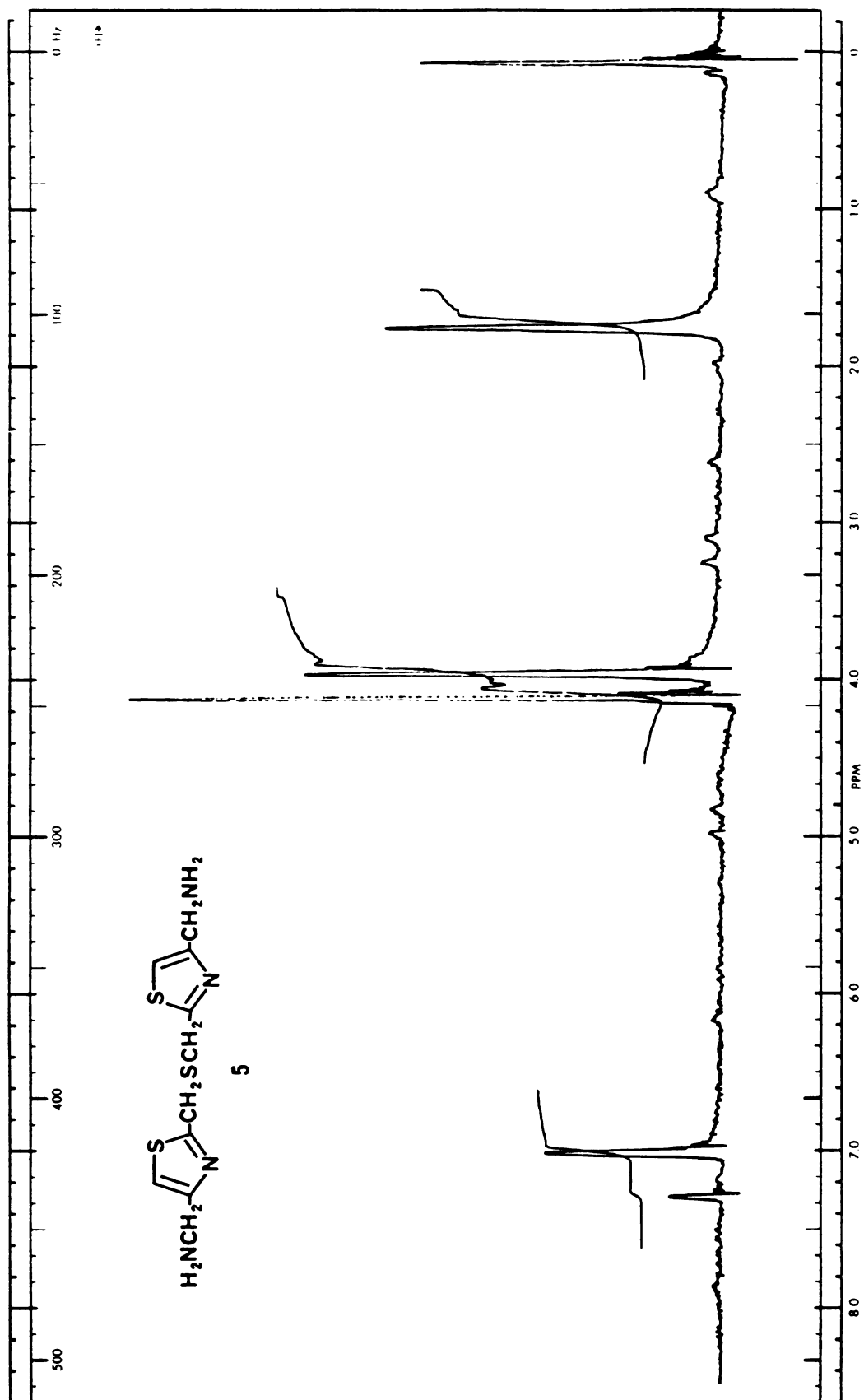


	carbonyl)picoly] sulfide(21a), CDCl ₃	107
A12a.	250 M Hz ¹ H NMR spectrum of 5,15-cis-{o,o'-[6,6'-(2-Thiatrimethylene)dinicotinamido]diphenyl}-2,8,12,18-tetraethyl-3,7,13,17-tetramethylporphyrin(24a), CDCl ₃	108
A12b.	250 M Hz ¹ H NMR spectrum of 5,15-cis-{o,o'-[6,6'-(2-Thiatrimethylene)dinicotinamido]diphenyl}-2,8,12,18-tetraethyl-3,7,13,17-tetramethylporphyrin(24a), Pyridine-d ₅	109
A13.	60 M Hz ¹ H NMR spectrum of Ethyl 5,5'-[2,2'-(2,5-dithiahexamethylene)]dipyridinedicarboxylate(21b), CDCl ₃	110
A14a.	250 M Hz ¹ H NMR spectrum of 5,15-cis-{o,o'-[6,6'-(2,5-Dithiahexamethylene)dinicotinamido]diphenyl}-2,8,12,18-tetraethyl-3,7,13,17-tetramethylporphyrin(24b), CDCl ₃	111
A14b.	250 M Hz ¹ H NMR spectrum of 5,15-cis-{o,o'-[6,6'-(2,5-Dithiahexamethylene)dinicotinamido]diphenyl}-2,8,12,18-tetraethyl-3,7,13,17-tetramethylporphyrin(24b), Pyridine-d ₅	112
A15.	60 M Hz ¹ H NMR spectrum of Ethyl 5,5'-[2,2'-(2,6-dithiaheptamethylene)]dipyridinedicarboxylate(21c), CDCl ₃	113
A16.	250 M Hz ¹ H NMR spectrum of 5,15-cis-{o,o'-[6,6'-(2,6-Dithiaheptamethylene)dinicotinamido]diphenyl}-2,8,12,18-tetraethyl-3,7,13,17-tetramethylporphyrin(24c), CDCl ₃	114
A17.	60 M Hz ¹ H NMR spectrum of Ethyl 6-[N,N-Bis(3-thiabutyl)amino]methylnicotinate(25a), CDCl ₃	115
A18.	250 M Hz ¹ H NMR spectrum of trans-5-[o-(p-tert-Butylbenzamido)phenyl]-15-(o-{6-[N,N-bis(3-thiabutyl)amino]methylnicotinamido}phenyl)-2,8,12,18-tetraethyl-3,7,13,17-tetramethylporphyrin(28a), CDCl ₃	116
A19.	60 M Hz ¹ H NMR spectrum of Ethyl 6-[N,N-bis(3-thiapentyl)amino]methylnicotinate(25b), CDCl ₃	117
A20.	250 M Hz ¹ H NMR spectrum of trans-5-{o-[m-(N-Imidazolyl)toluamido]phenyl}-15-(o-{6-[N,N-bis(3-thiapentyl)amino]methylnicotinamido}phenyl)-2,8,12,18-tetraethyl-3,7,13,17-tetramethylporphyrin(28b), CDCl ₃	118

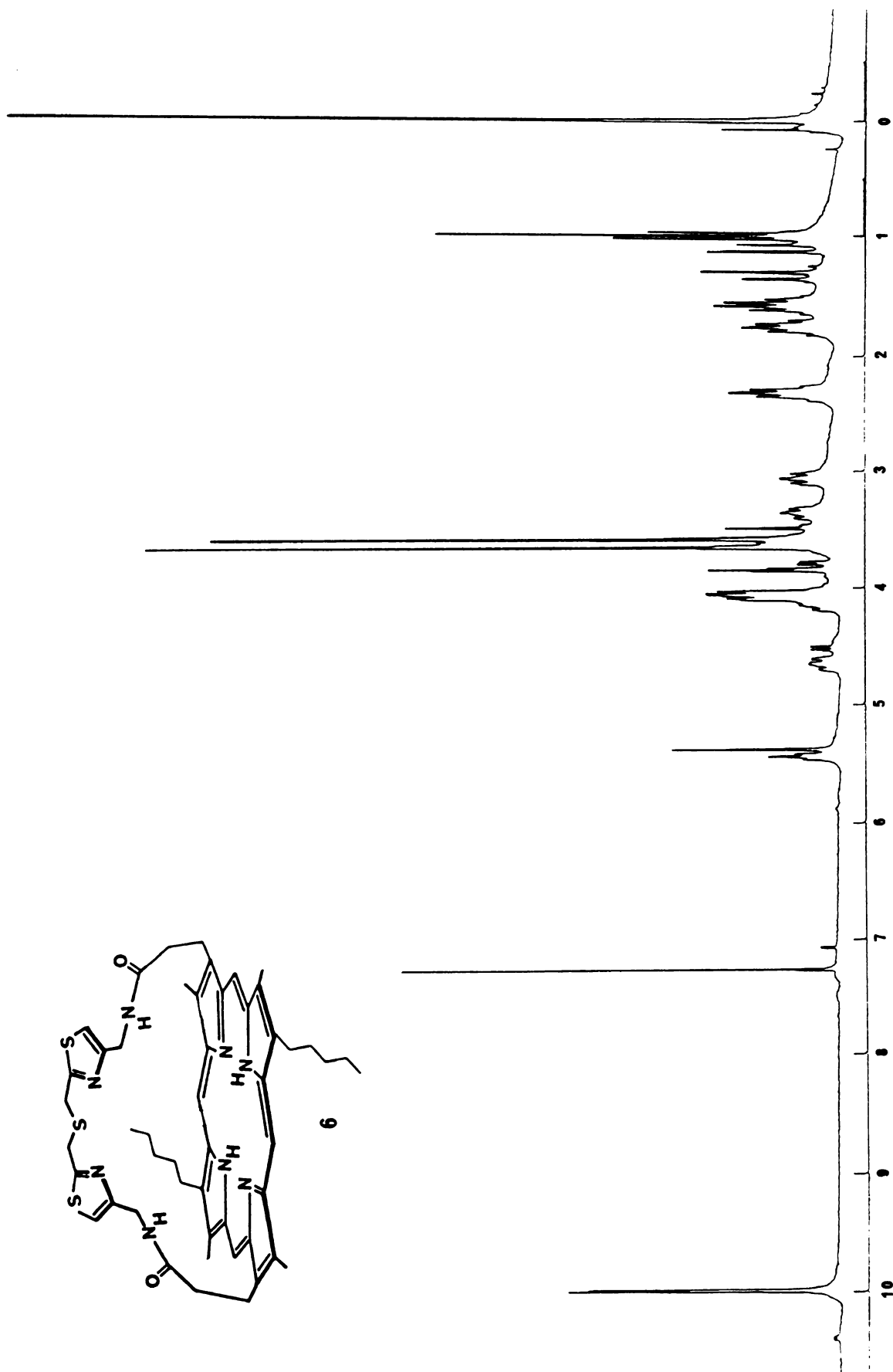
- A21. 60 M Hz ^1H NMR spectrum of Ethyl 6-{N,N-bis[2-(2-pyridyl)ethyl]amino}methylnicotinate(29), CDCl_3 119
- A22. 250 M Hz ^1H NMR spectrum of trans-5-[o-(p-tert-Butylbenzamido)phenyl]-15-[o-{6-{N,N-bis[2-(2-pyridyl)ethyl]amino}methylnicotinamido)phenyl]-2,8,12,18-tetraethyl-3,7,13,17-tetramethylporphyrin(32a), CDCl_3 120
- A23. 250 M Hz ^1H NMR spectrum of trans-5-{o-[m-(N-Imidazolyl)toluamido]phenyl}-15-[o-(6-{N,N-bis[2-(2-pyridyl)ethyl]amino}methylnicotinamido)phenyl]-2,8,12,18-tetraethyl-3,7,13,17-tetramethylporphyrin(32b), CDCl_3 121
- A24. Effective magnetic moment as a function of temperature for $[\text{Fe}(\text{P})\text{-OH}(\text{N}_4)]$ and $[\text{Fe}(\text{P})\text{-Cl Cu}(\text{N}_4)(\text{Cl})(\text{OH})]$, blocked with t-butylbenzene(32a-1 and 32a-2). 122
- A25. Effective magnetic moment as a function of temperature for $[\text{Fe}(\text{P})\text{-OH}(\text{N}_4)]$ and $[\text{Fe}(\text{P})\text{-Cl Cu}(\text{N}_4)(\text{Cl})(\text{OH})]$, blocked with imidazole (32b-1 and 32b-2). 123



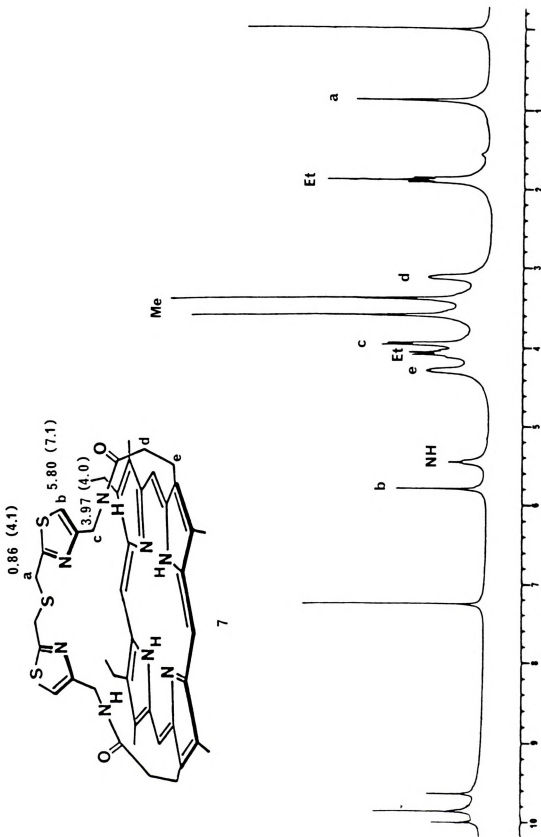
A1. 60 M Hz ^1H NMR spectrum of bis[4-(phthalimidomethyl)thiazole-2-methyl] sulfide (4), DMSO-d_6 .



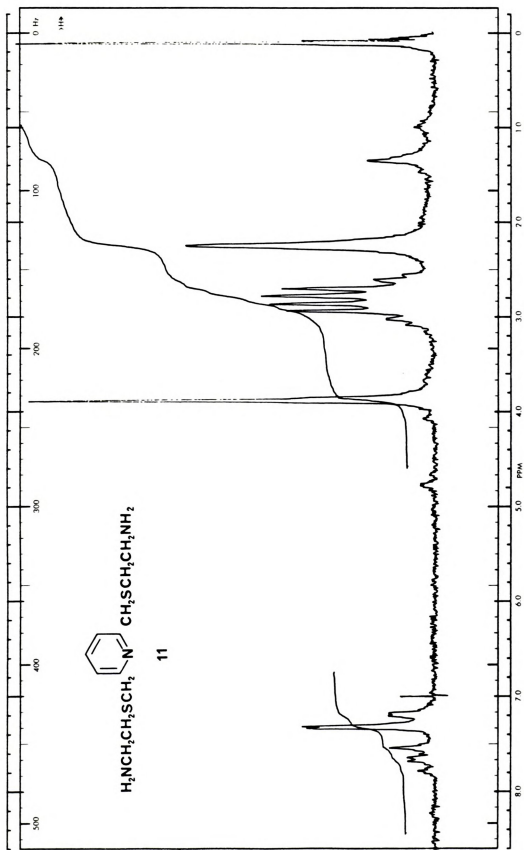
A2. 60 M Hz ^1H NMR spectrum of bis[4-(aminomethyl)thiazole-2-methyl] sulfide (5), CDCl_3 .



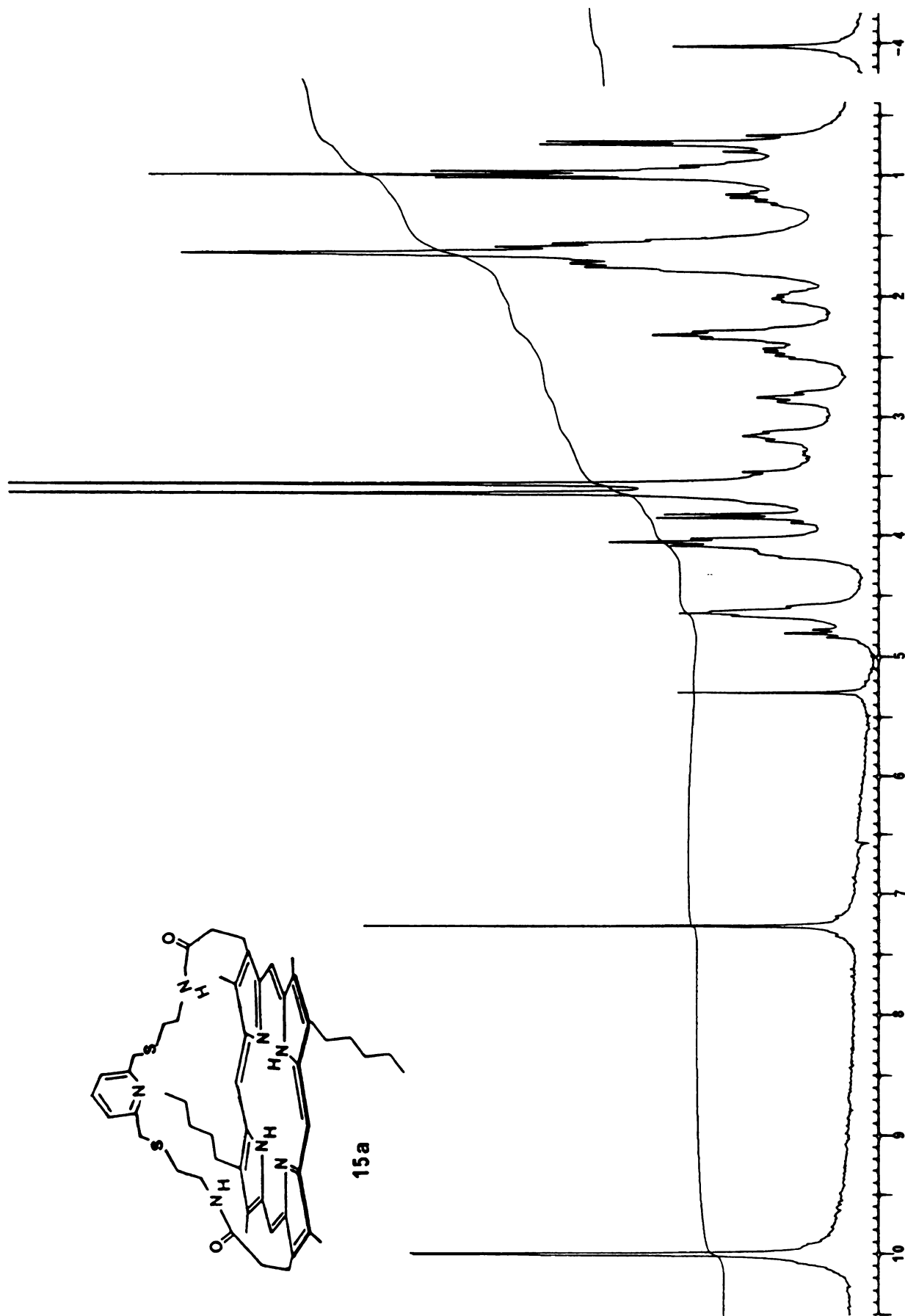
A3. 250 M Hz ^1H NMR spectrum of 7,17-[4,4'-[2,2'-(2-thiatriethylene)-dithiazolyl]bismethylcarbamoyl-3,8,13,18-tetramethyl-2,12-dipentylporphyrin(6), CDCl_3 .



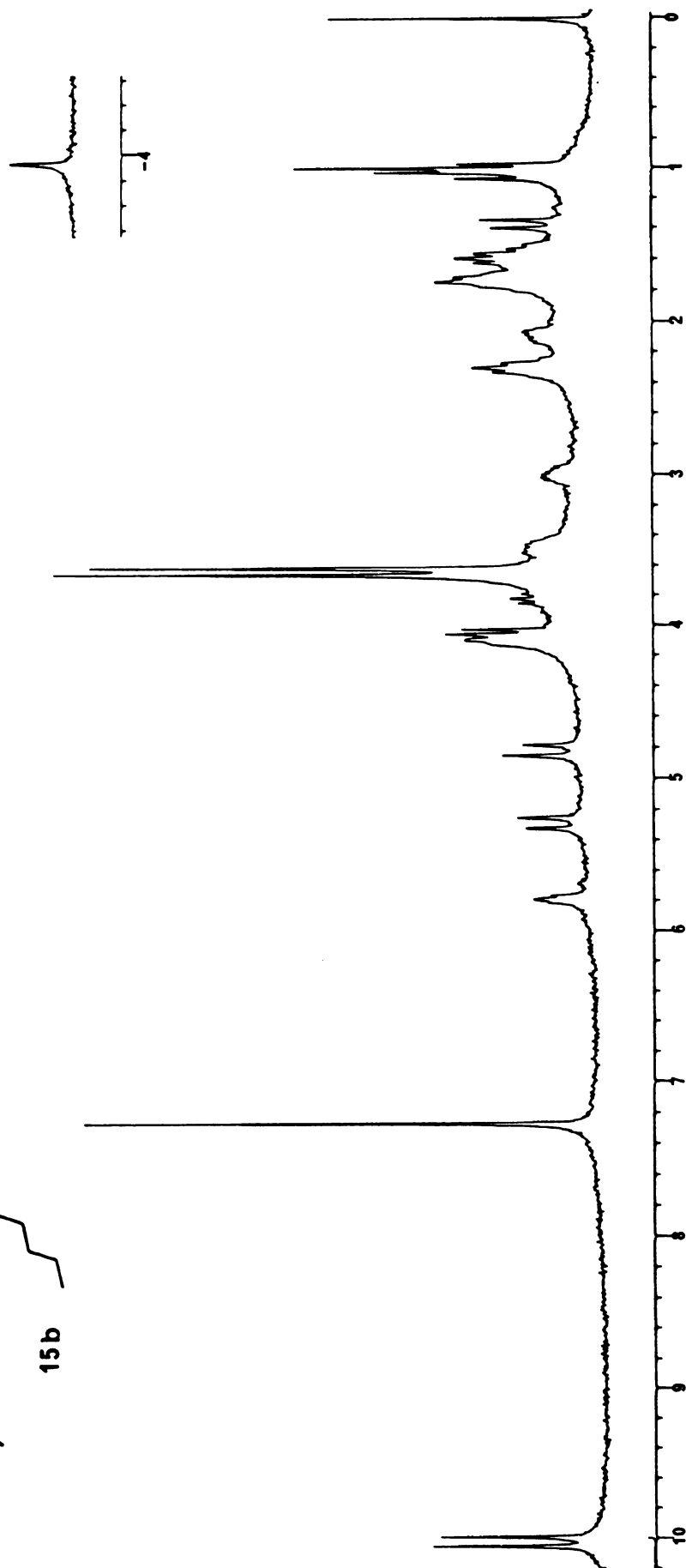
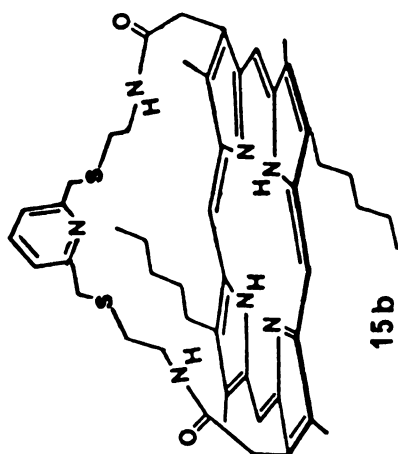
A4. 250 M Hz ^1H NMR spectrum of 3,17-[4,4'-[2,2'-(2-thiazolymethylene) dithiazolyl]bismethylcarbamoyl ethyl]-2,7,13,18-tetramethyl-6,12-diethylporphyrin (7), CDCl_3 .



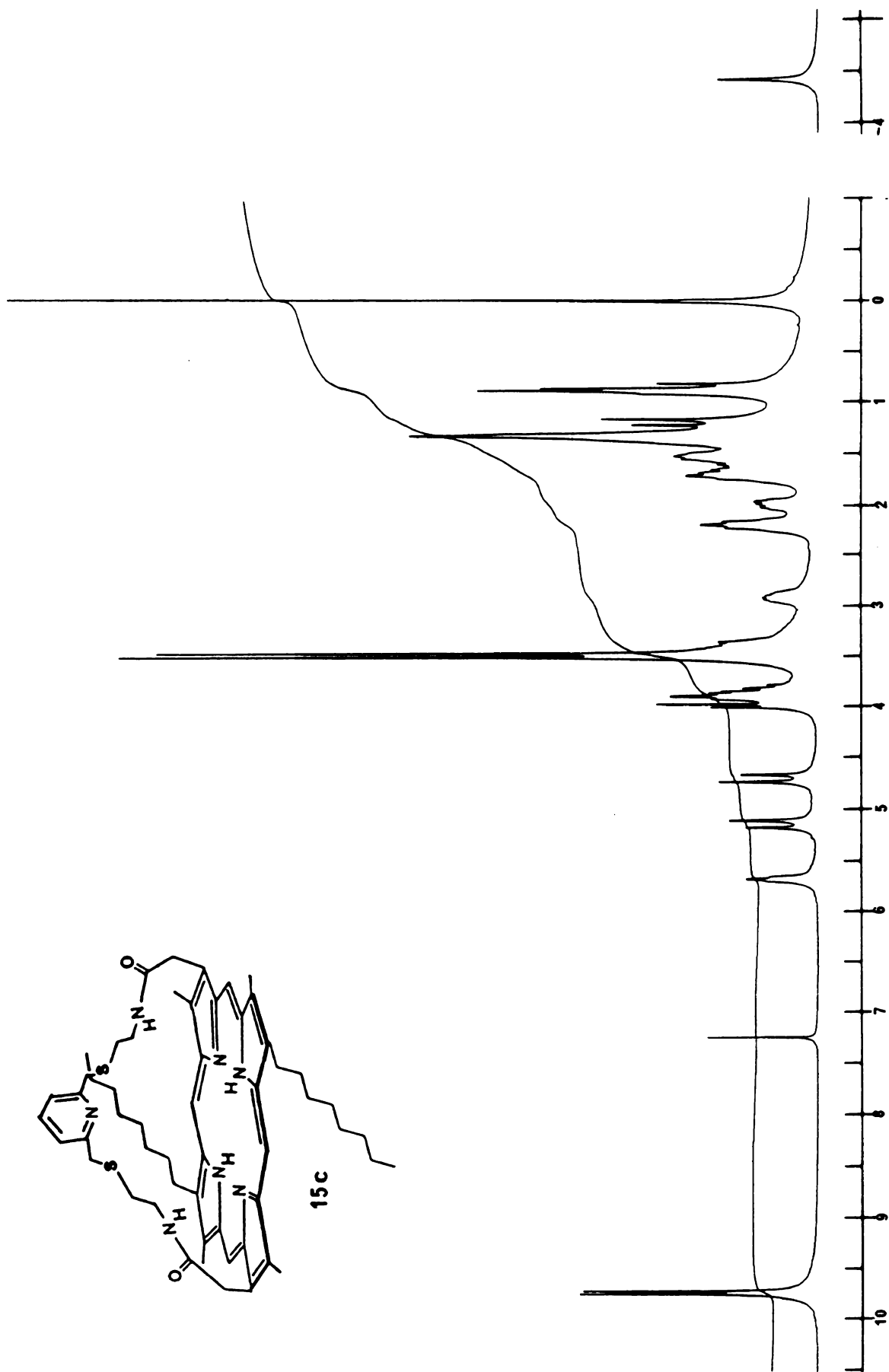
A5. 60 M Hz ^1H NMR spectrum of pyridine-2,6-bis[4-(2-thiabutyl)amine] (11), CDCl_3



A6. 250 M Hz ¹H NMR spectrum of 7,17-[pyridine-2,6-bis(2-thiabutylcarbamoyl-ethyl)]-2,12-dipentyl-3,8,13,18-tetramethylporphyrin (15a), CDCl₃.

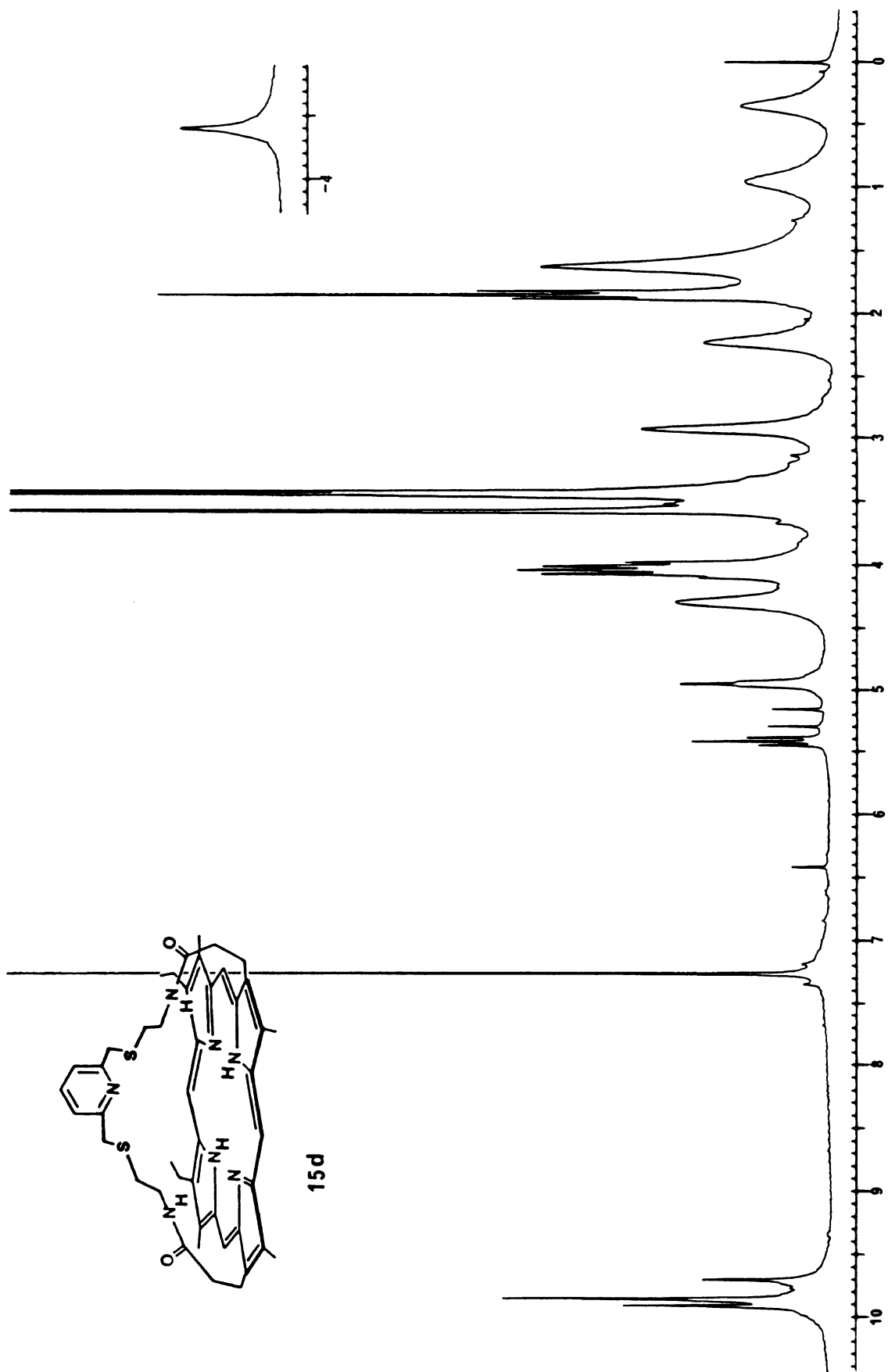


A7. 250 M Hz ^1H NMR spectrum of 7,17-[pyridine-2,6-bis(2-thiabutylcarbamoyl-methyl)]-2,12-dipentyl-3,8,13,18-tetramethylporphyrin (15b), CDCl_3 .

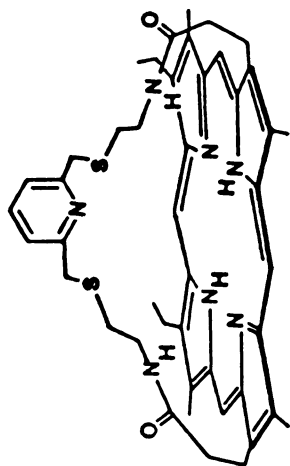


A8. 250 M Hz ¹H NMR spectrum of 7,17-[pyridine-2,6-bis(2-thiabutylcarbamoyl-methyl)]-2-12-dioctyl-3,8,13,18-tetramethylporphyrin(15c), CDCl₃.

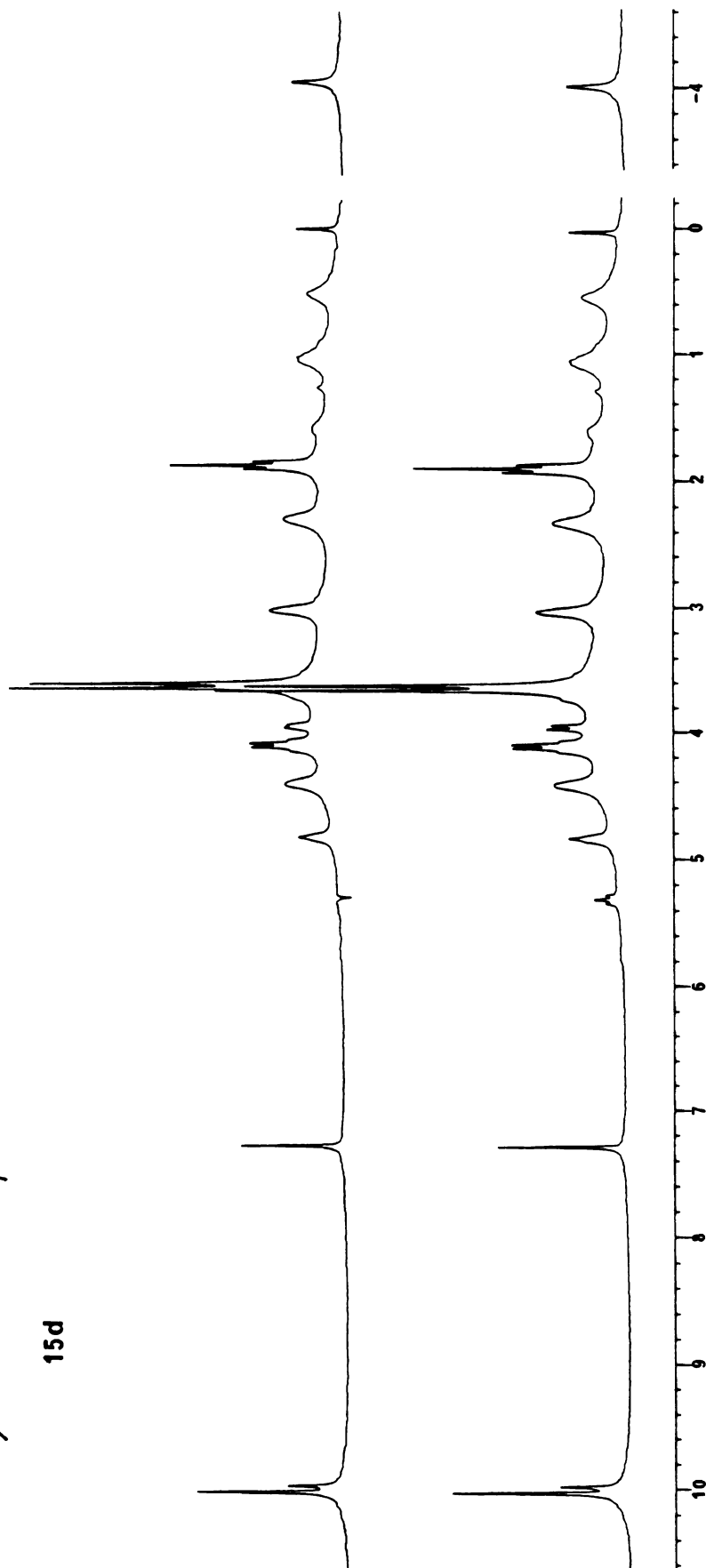




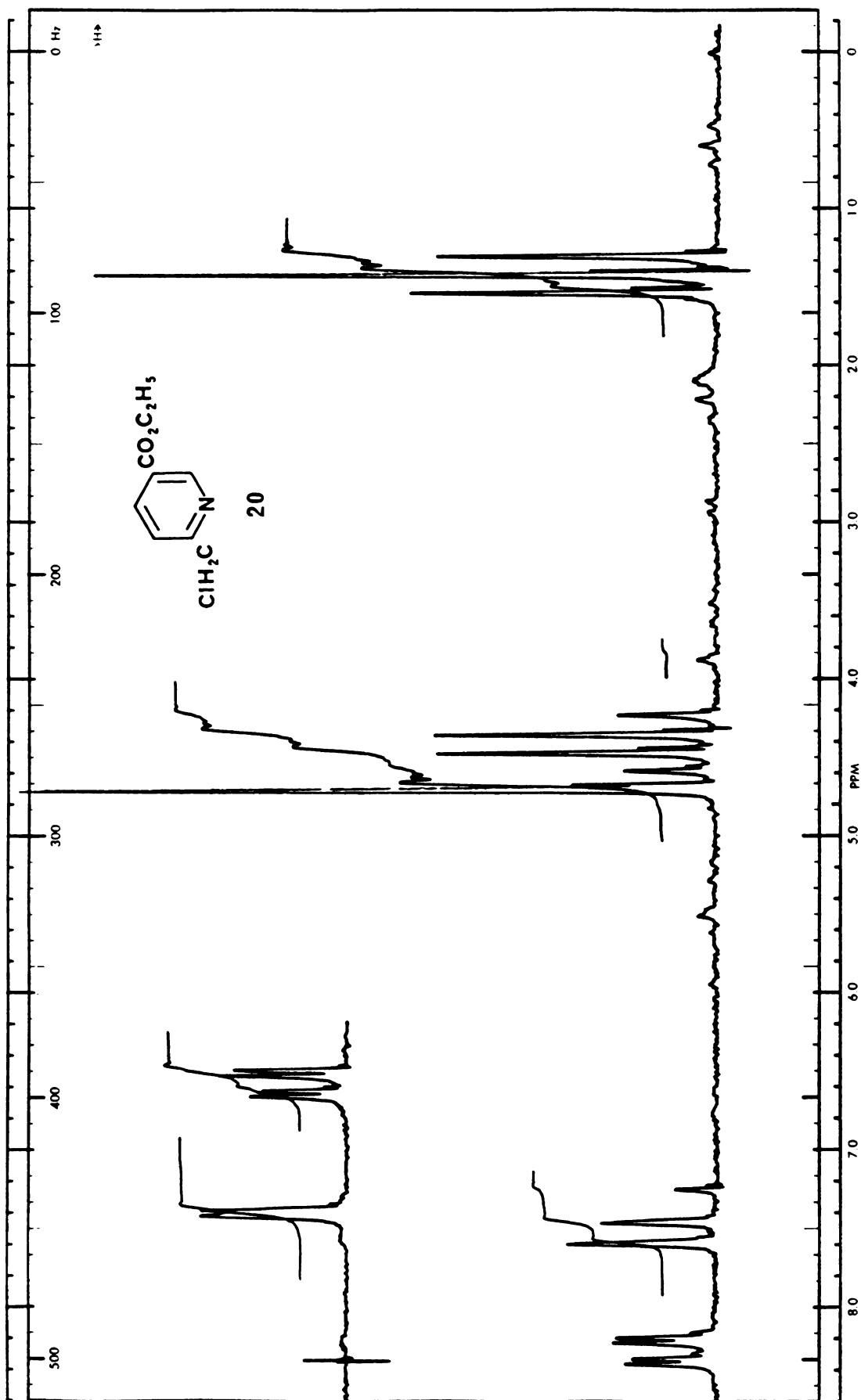
A9a. 250 M Hz ^1H NMR spectrum of 3,17-[pyridine-2,6-bis(2-thiabutylcarbamoyl-ethyl)]-8,12-diethyl-2,7,13,18-tetramethylporphyrin (15d), CDCl_3 .



15d

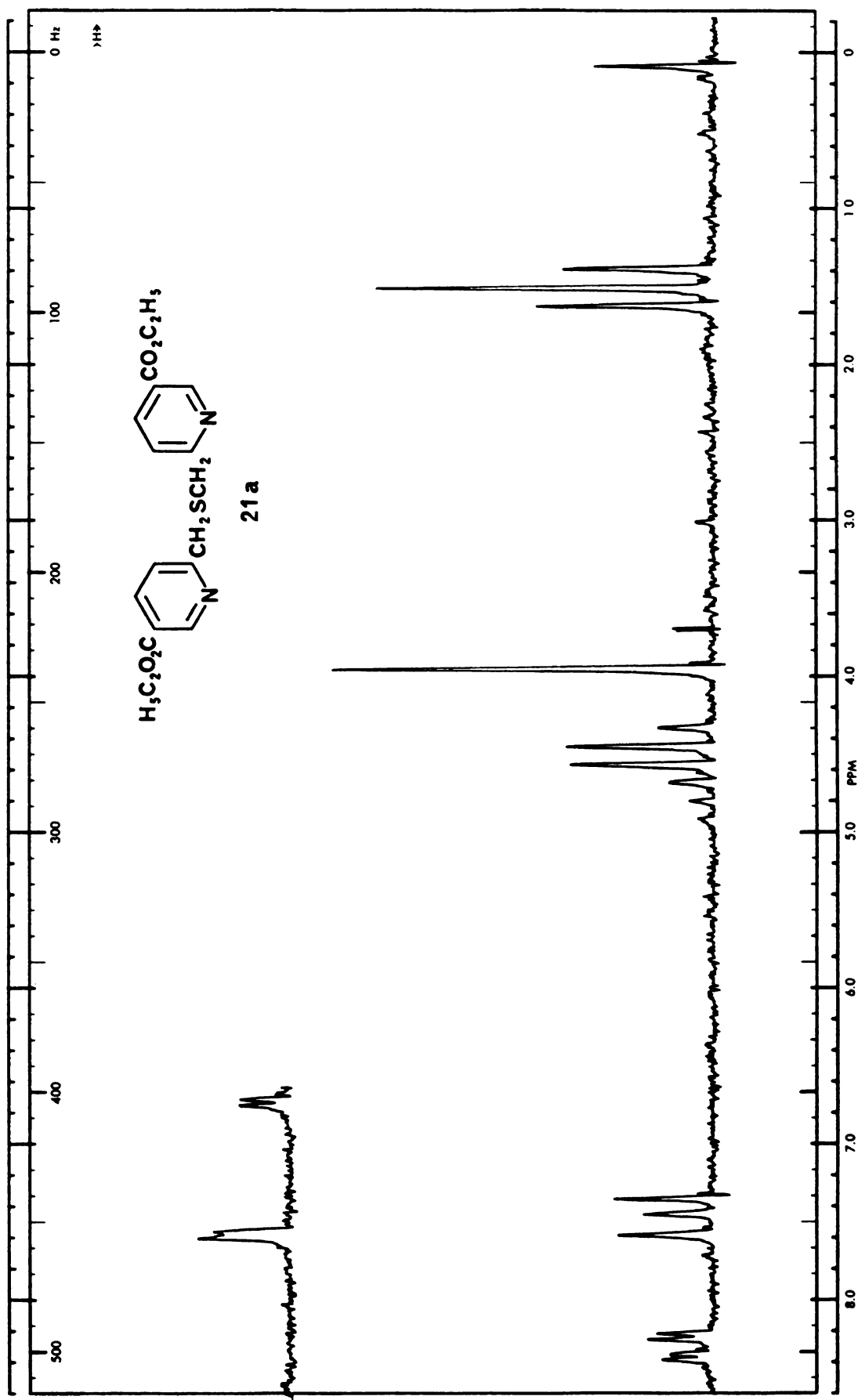


A9b. 250 M Hz ^1H NMR spectrum of 3,17-[pyridine-2,6-bis(3-thiabutylcarbamoyl-ethyl)]-8,12-diethyl-7,13,18-tetramethylporphyrin (15d), amide H decoupled, CDCl_3 .

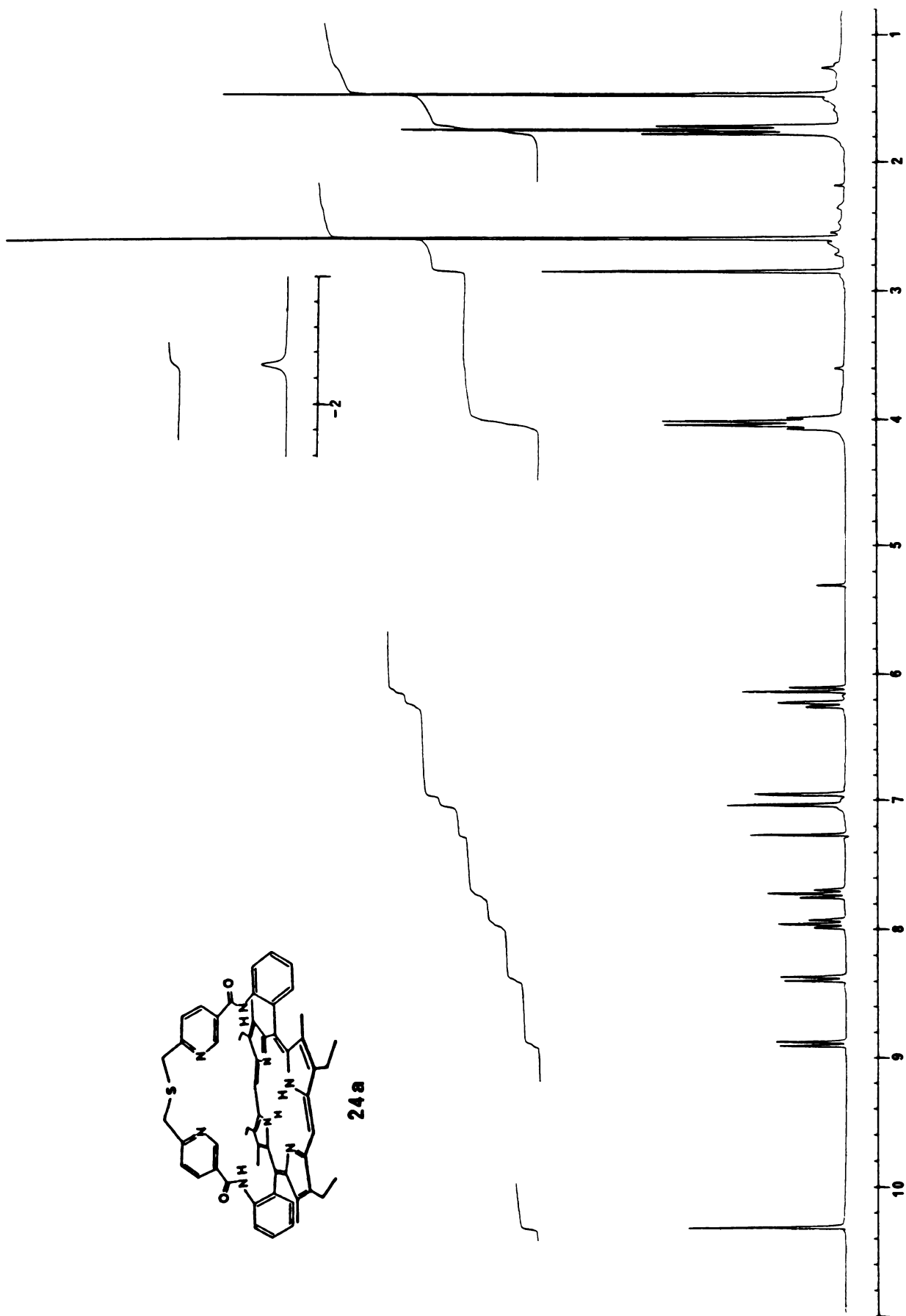
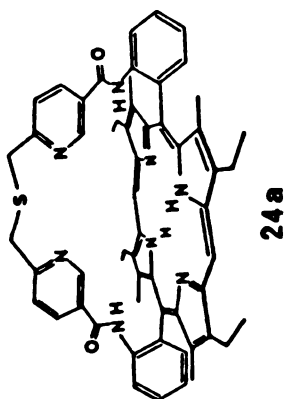


A10. 60 M Hz ^1H NMR spectrum of ethyl 5-(2-chloromethyl)pyridinecarboxylate (20), CDCl_3 .

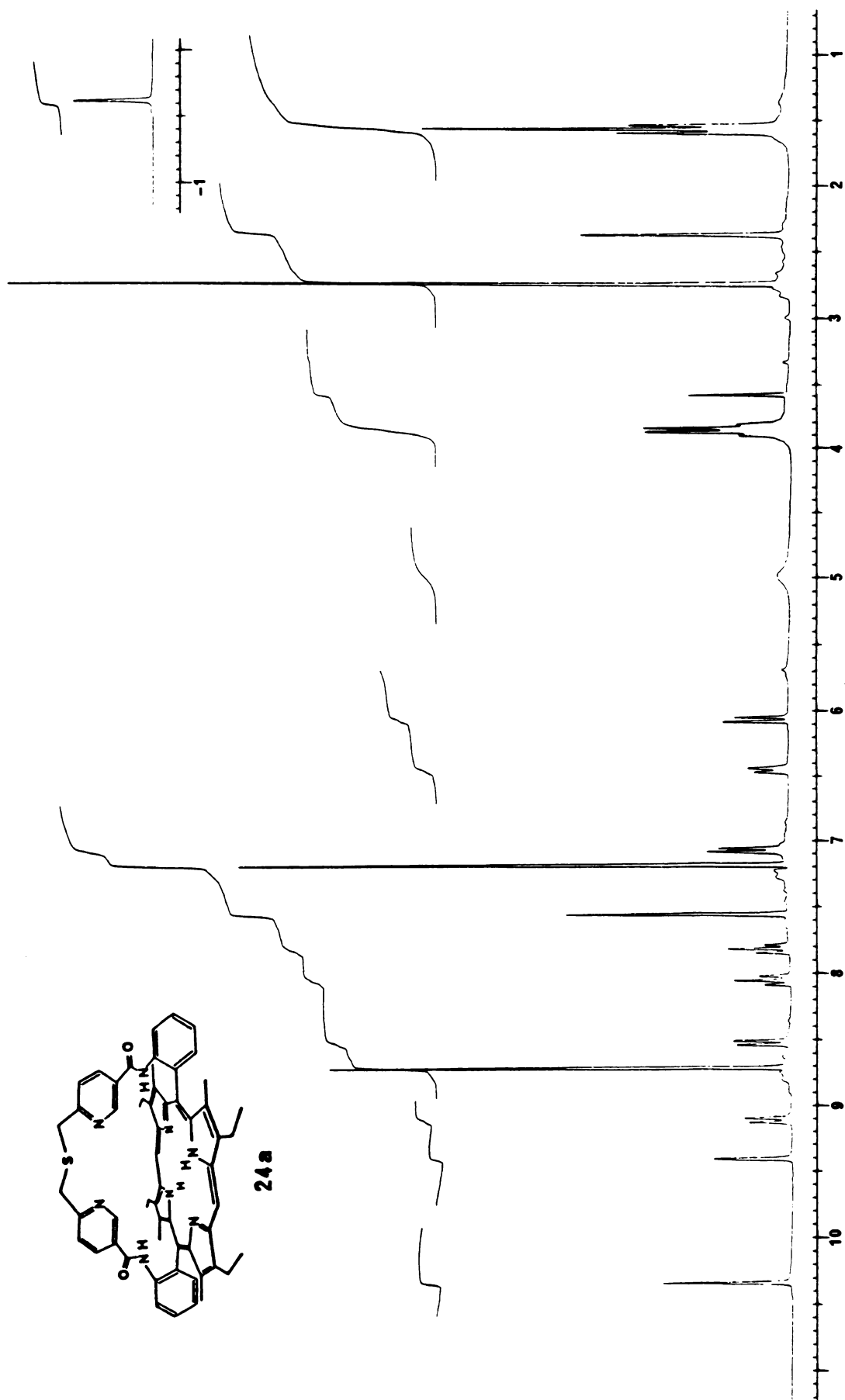




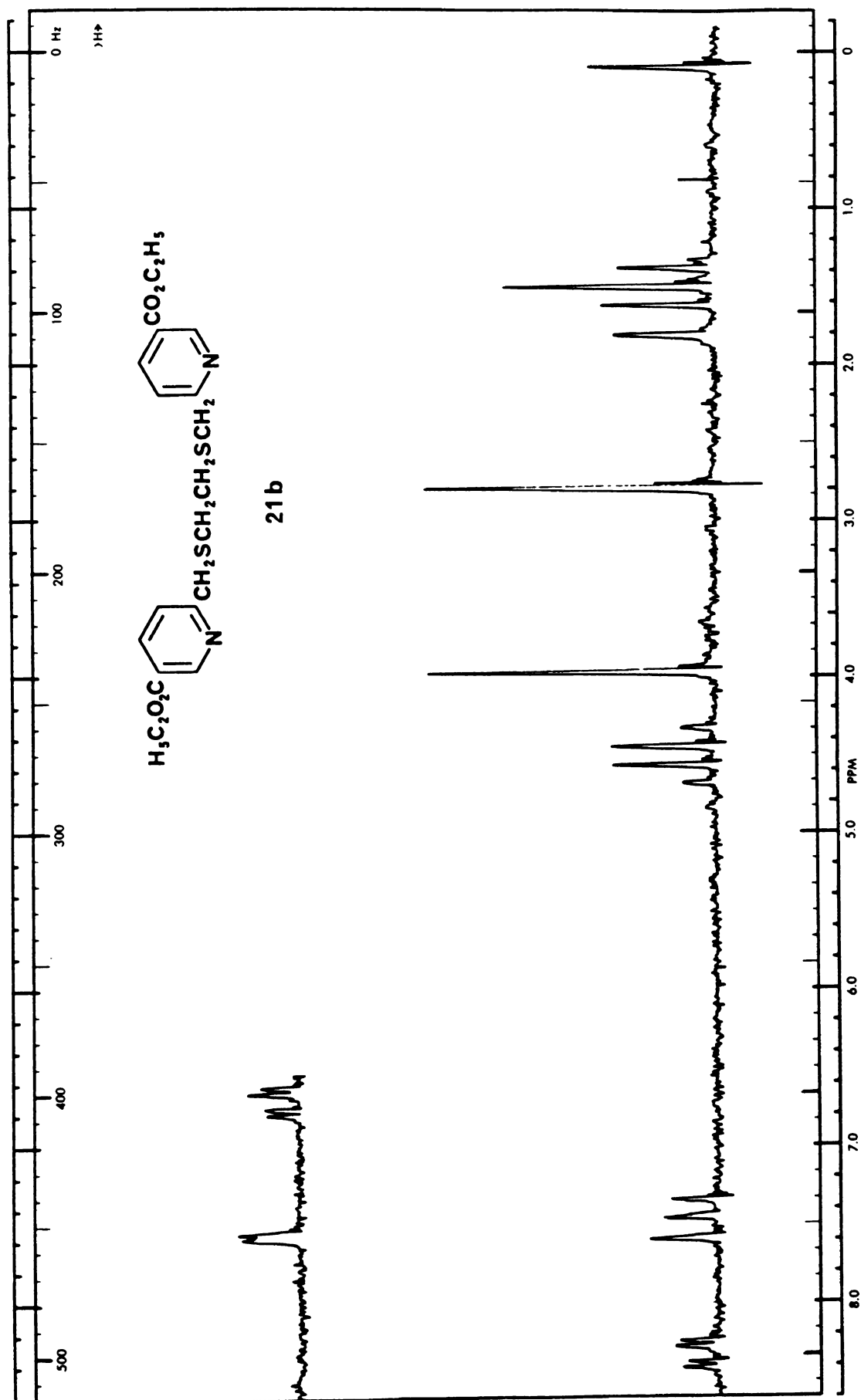
A11. 60 M Hz ^1H NMR spectrum of bis[2-(5-ethoxycarbonyl)picolyl] sulfide (21a), CDCl_3 .



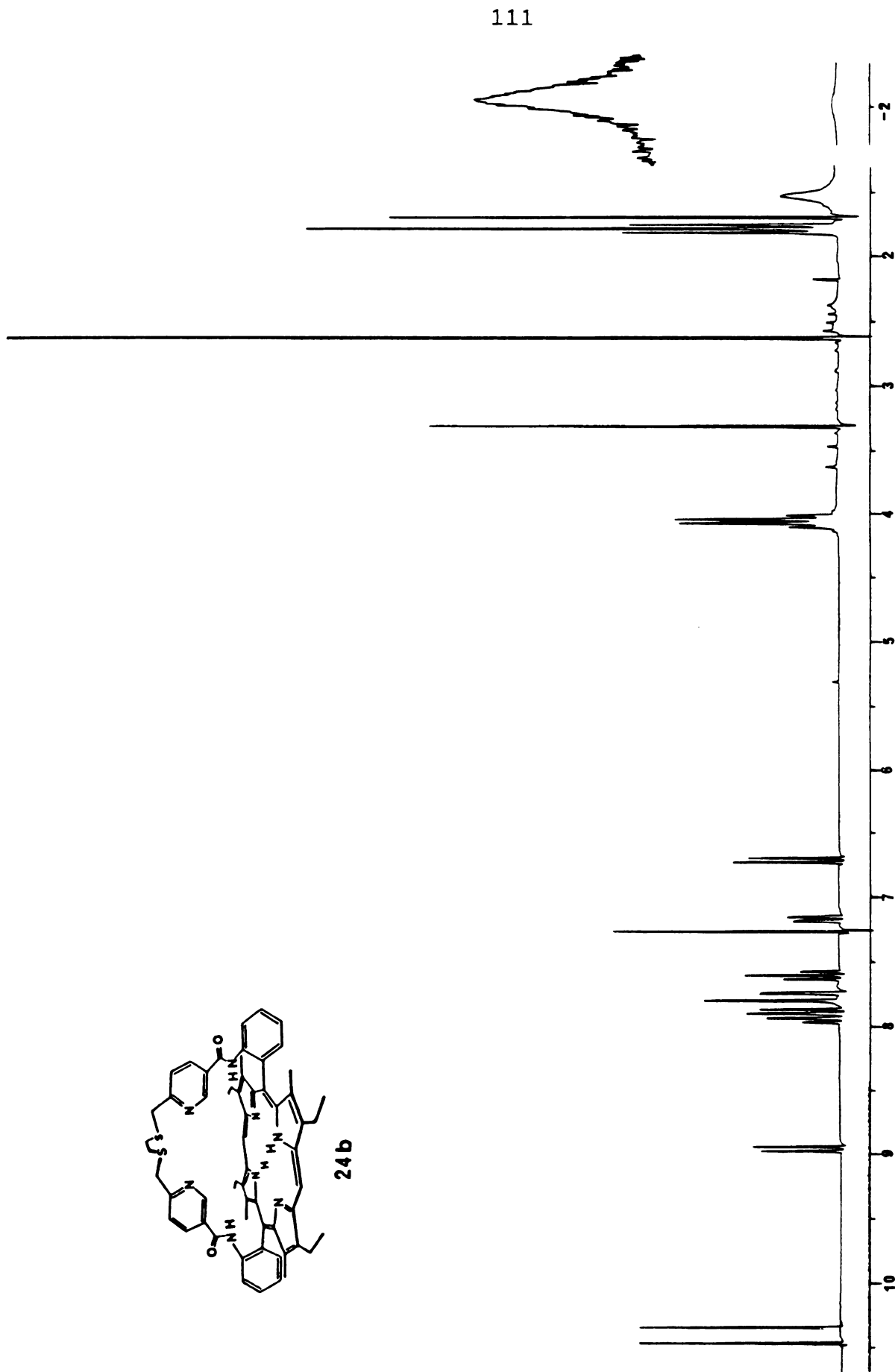
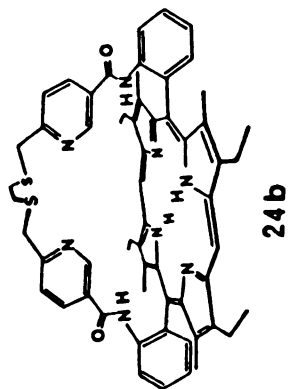
A12a. 250 M Hz ^1H NMR spectrum of 5,15-cis-[o,o']-[6,6']-(2-thiatriethylene)-dincotinamidodiphenyl]-2,8,12,18-tetraethyl-3,7,13,17-tetramethylporphyrin (24a), CDCl_3 .



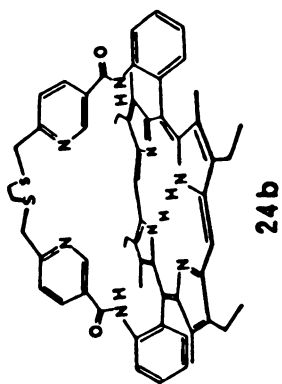
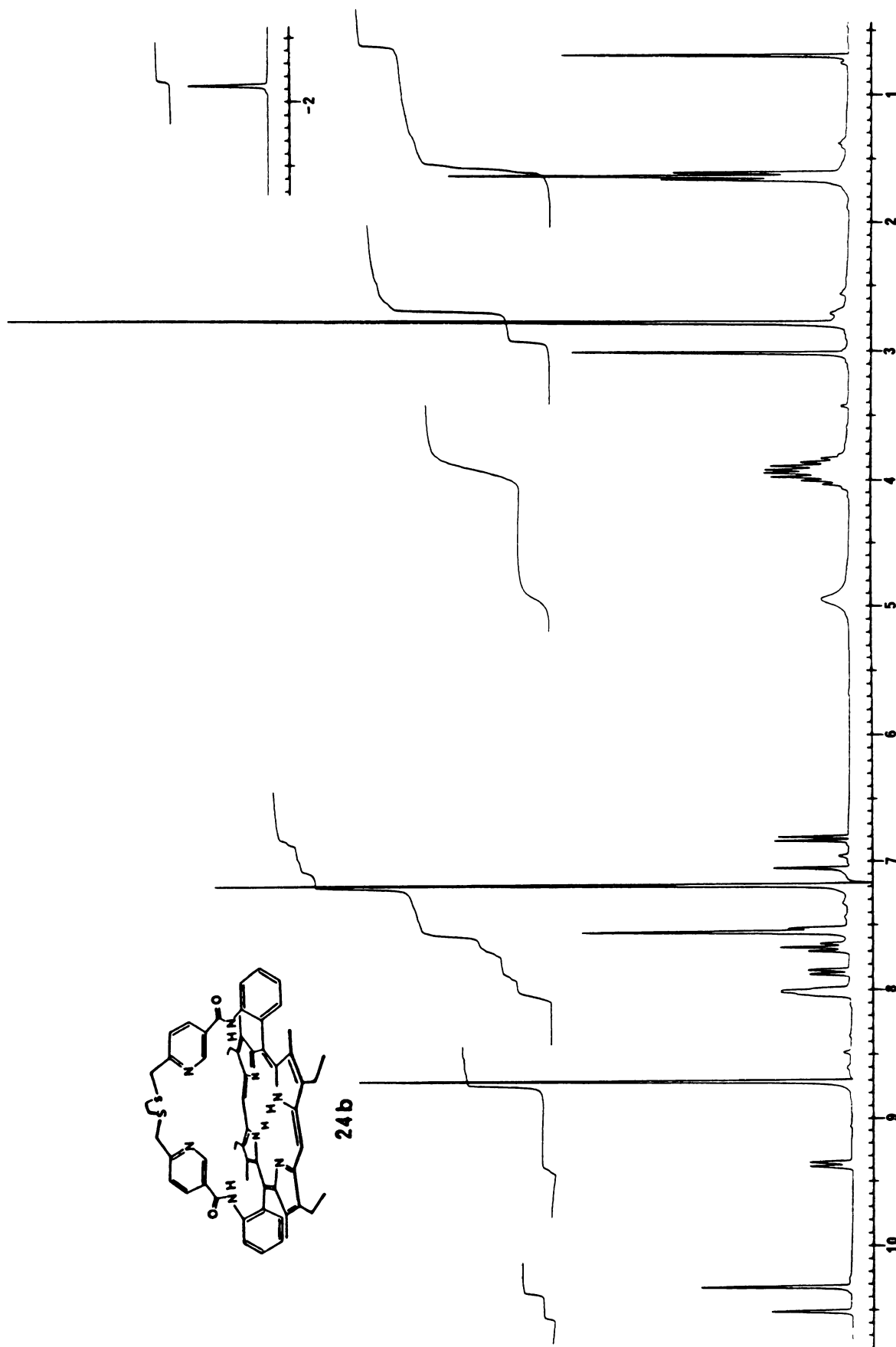
A12b. 250 M Hz ^1H NMR spectrum of 5,15-cis-{o,o'}-[6,6'-(2-thiatrimethylene)-dnicotinamidodiphenyl]-2,8,12,18-tetraethyl-3,7,13,17-tetramethylporphyrin (24a), Pyridine- d_5 .



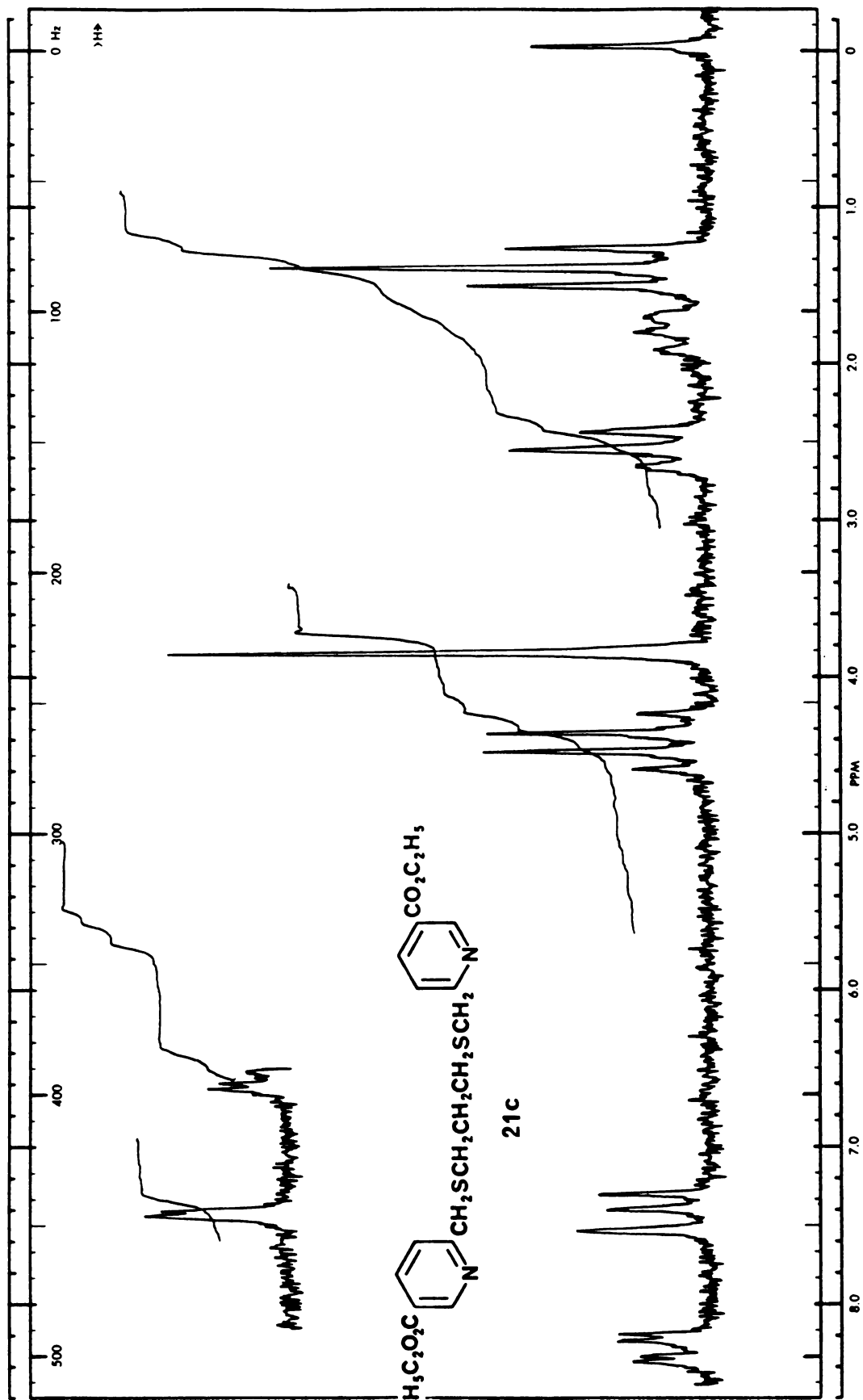
A13. 60 M Hz ^1H NMR spectrum of ethyl 5,5'-[2,2'-(2,5-dithiahexamethylene)]-dipyridinedicarboxylate (21b), CDCl_3 .



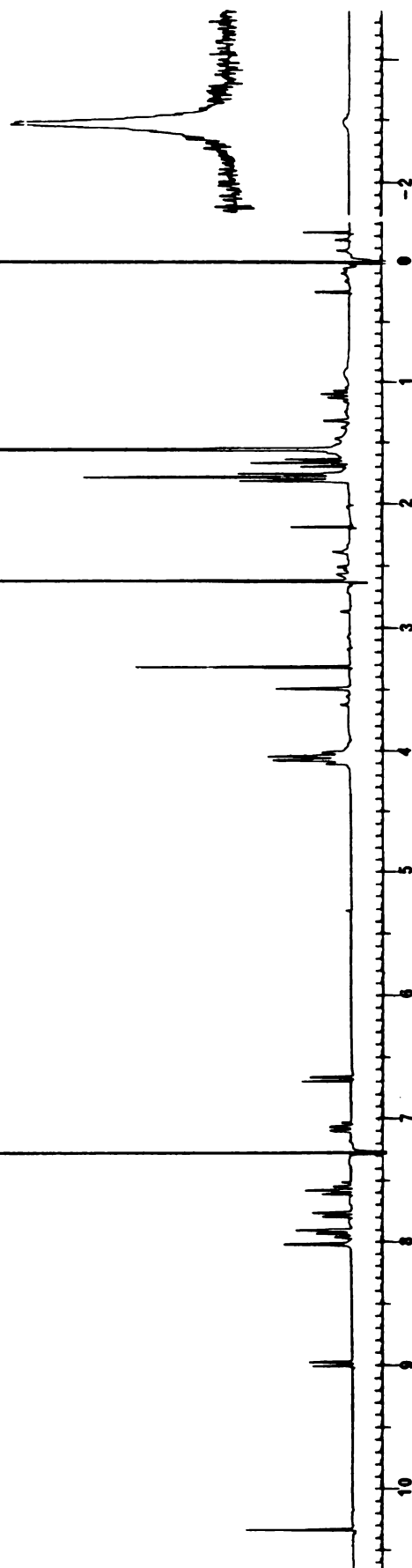
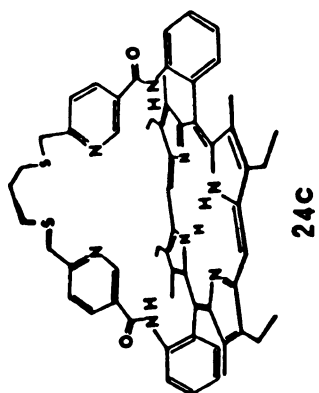
A14a. 250 M Hz ^1H NMR spectrum of 5,15-cis-{o,o'}-[6,6'-(2,5-dithiahexamethylene)-dnicotinamidodiphenyl]-3,7,13,17-tetraethyl-3,7,13,17-tetramethylporphyrin (**24b**), CDCl_3 .



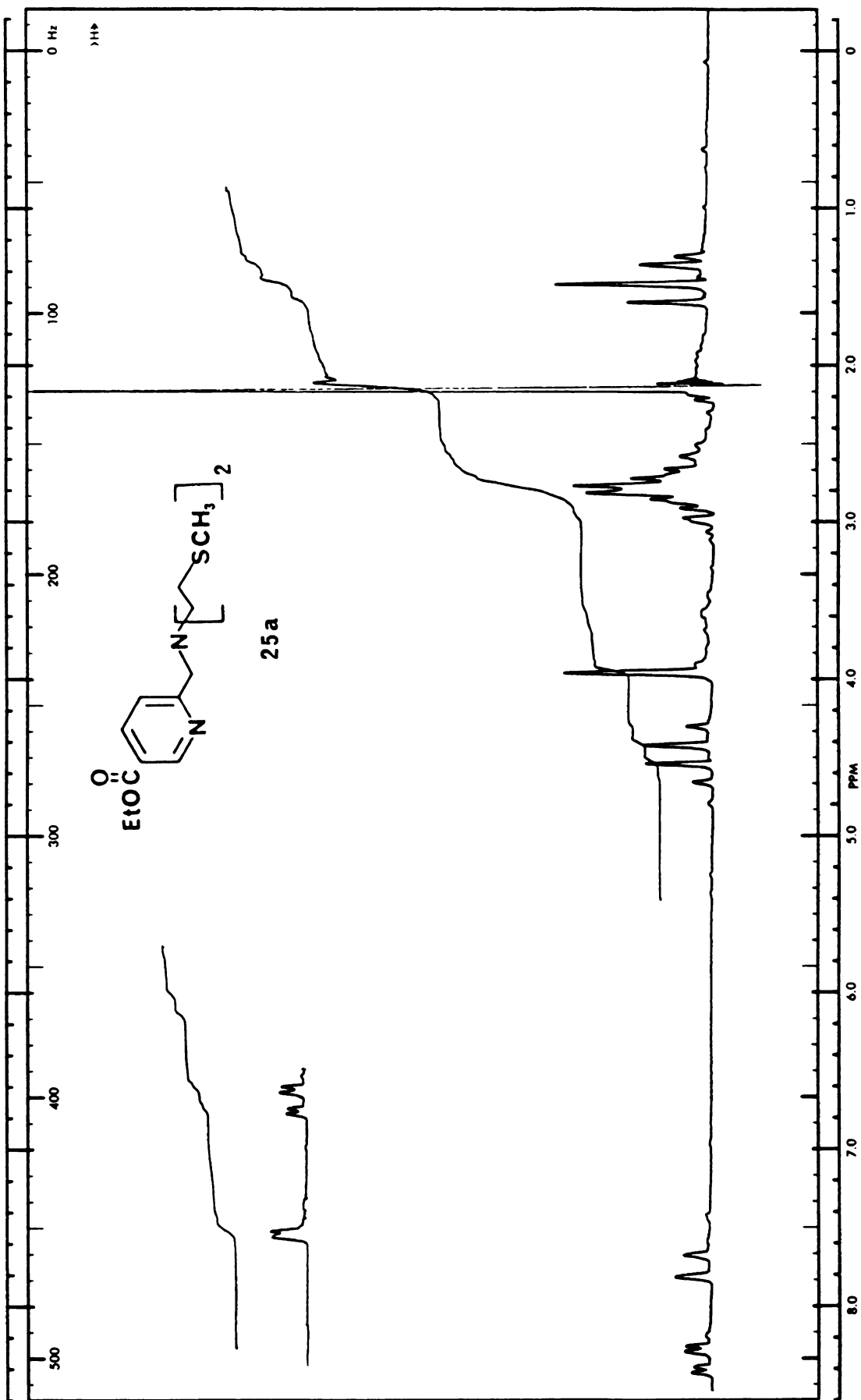
A14b. 250 M Hz ^1H NMR spectrum of 5,15-cis-{o,o'}-[6,6']-(2,5-dithiahexamethylene)-dinicotinamidodiphenyl]-2,8,12,18-tetraethyl-3,7,13,17-tetramethylporphyrin (24b), Pyridine- d_5 .



A15. 60 M Hz ^1H NMR spectrum of ethyl 5,5'-[2,2'-(2,6-dithiaheptamethylene)]-dipyridinedicarboxylate (21c), CDCl_3 .

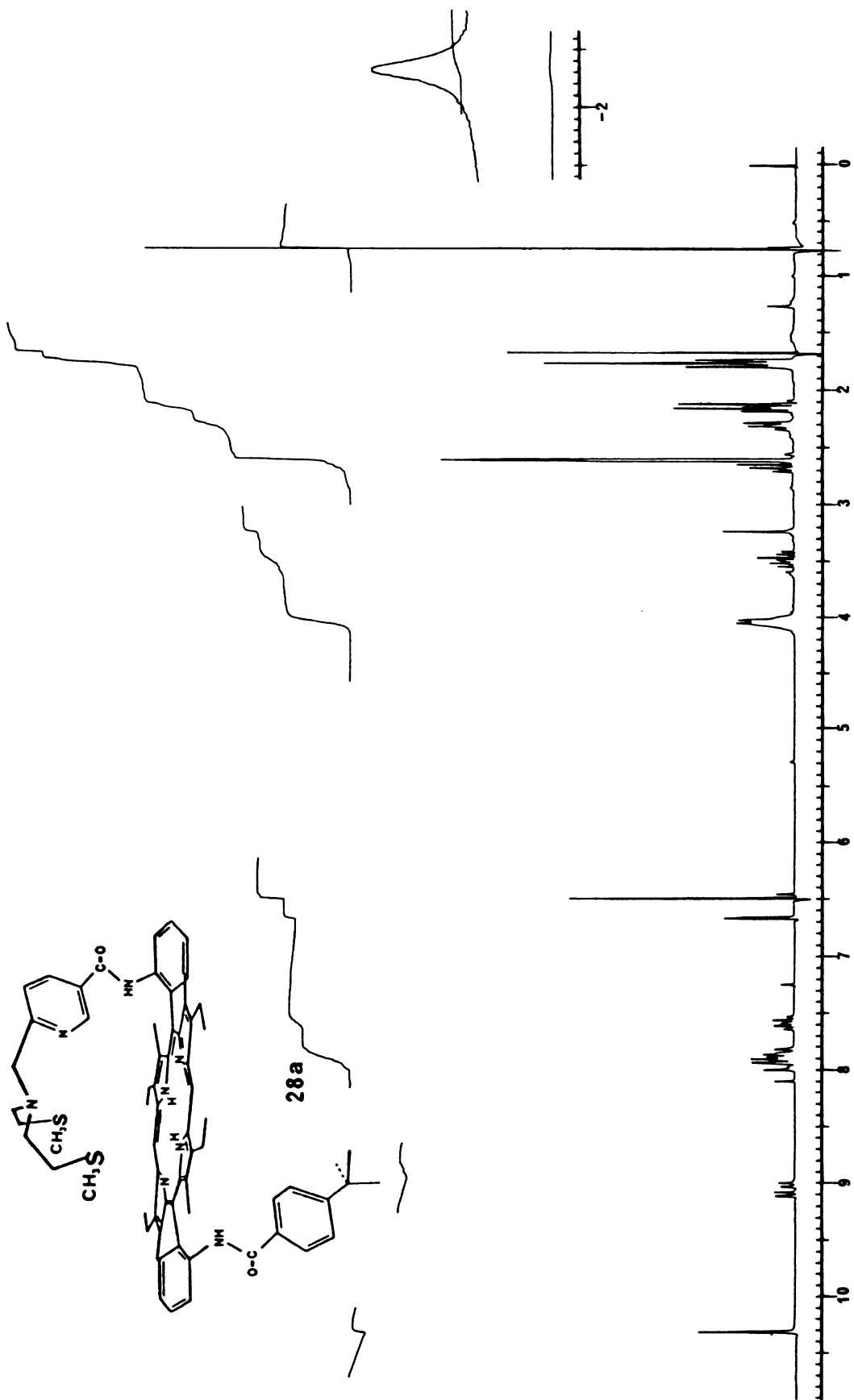


A16. 250 M Hz ^1H NMR spectrum of 5,15-cis-{o,o'}-{6,6'}-(2,6-dithiaheptamethylene)-dinicotinamido]diphenyl}-2,8,12,18-tetraethyl-3,7,13,17-tetramethylporphyrin (24c), CDCl_3 .

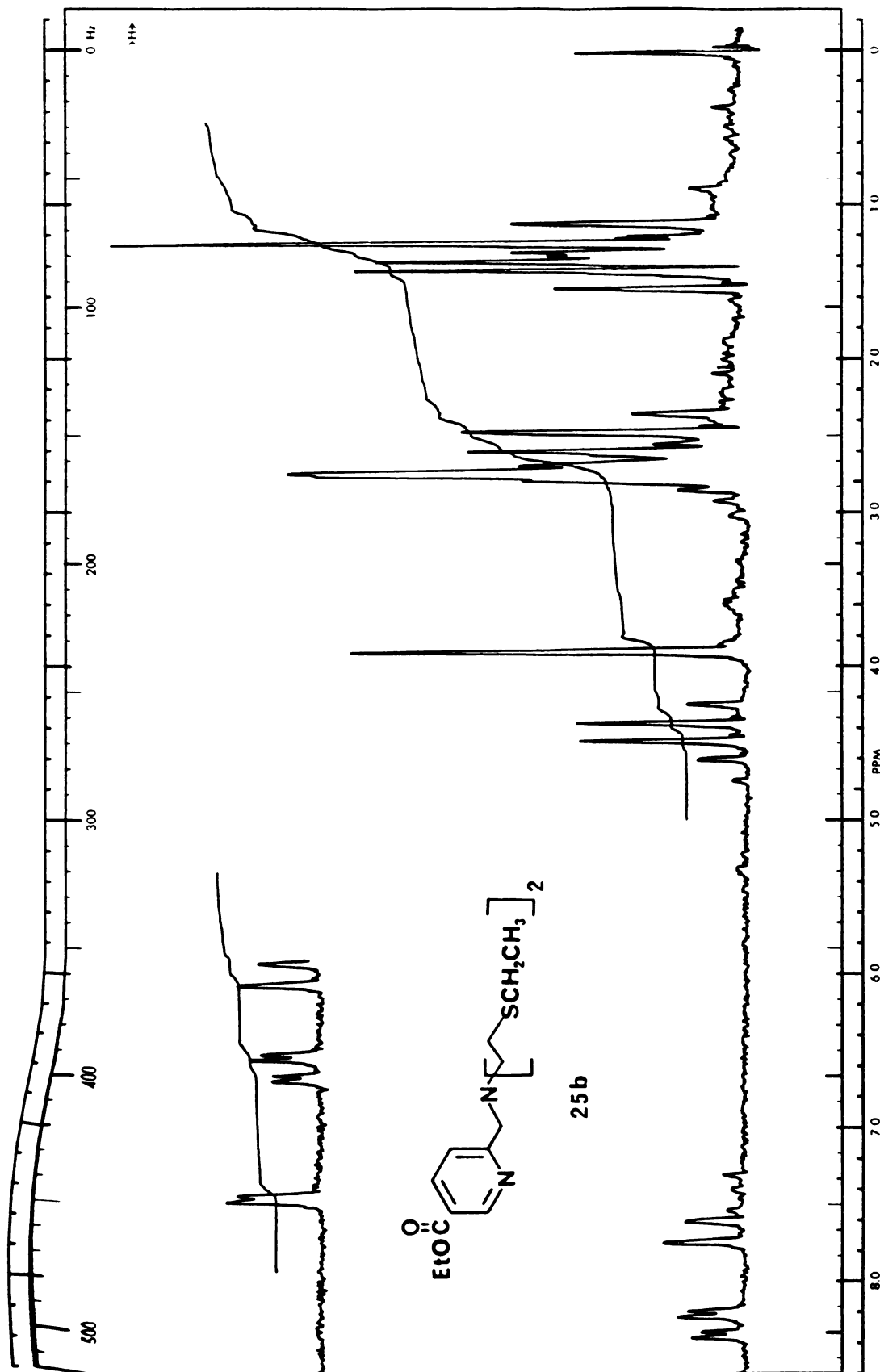


A17. 60 M Hz ^1H NMR spectrum of ethyl 6-[N,N-bis(3-thiabutyl)amino]methyl-nicotinate (25a), CDCl_3 .

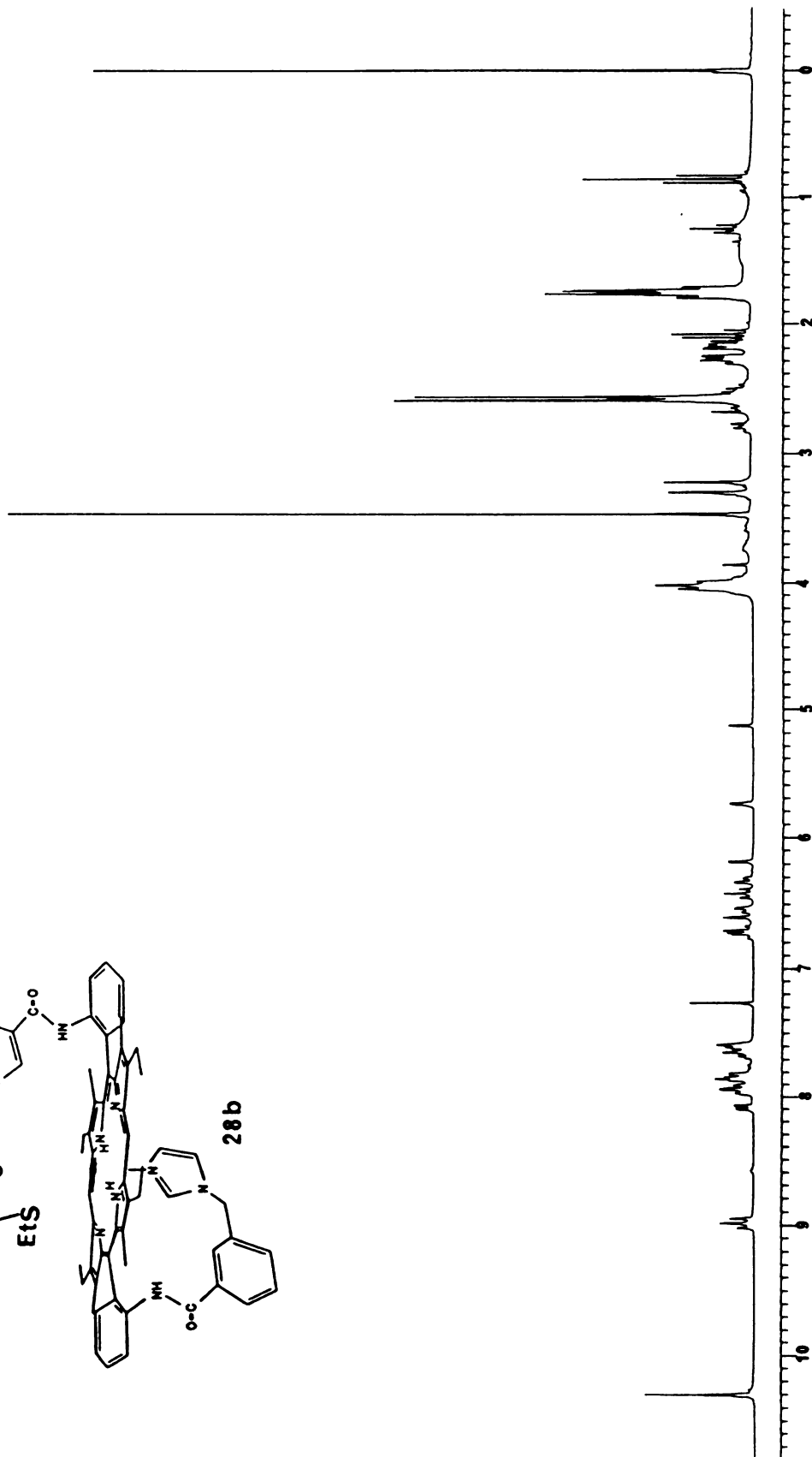
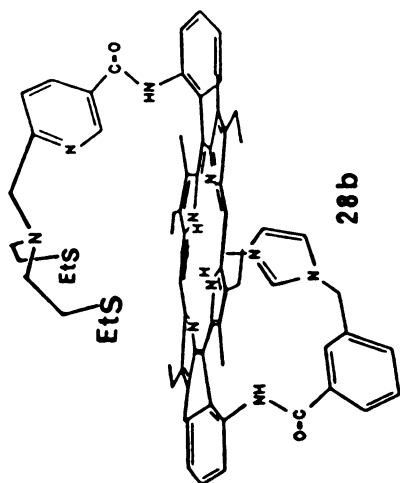




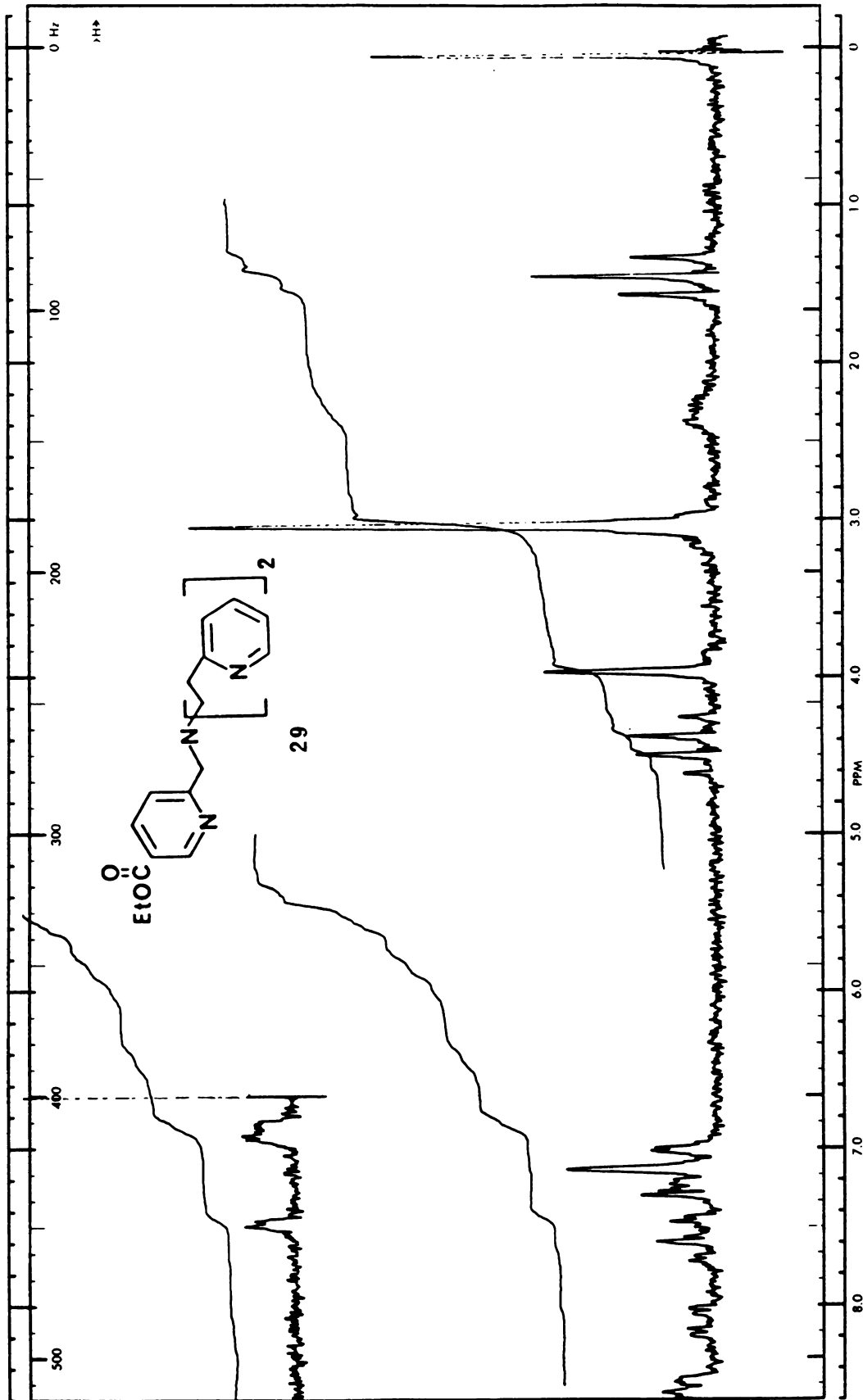
A18. 250 M Hz ^1H NMR spectrum of trans-5-[o-(p-tert-butylbenzamido)phenyl]-15-(o-[6-[N,N-bis(3-thiabutyl)amino]methylnicotinamido)phenyl]-2,8,12,18-tetraethyl-3,7,13,17-tetramethylporphyrin (28a), CDCl_3 .



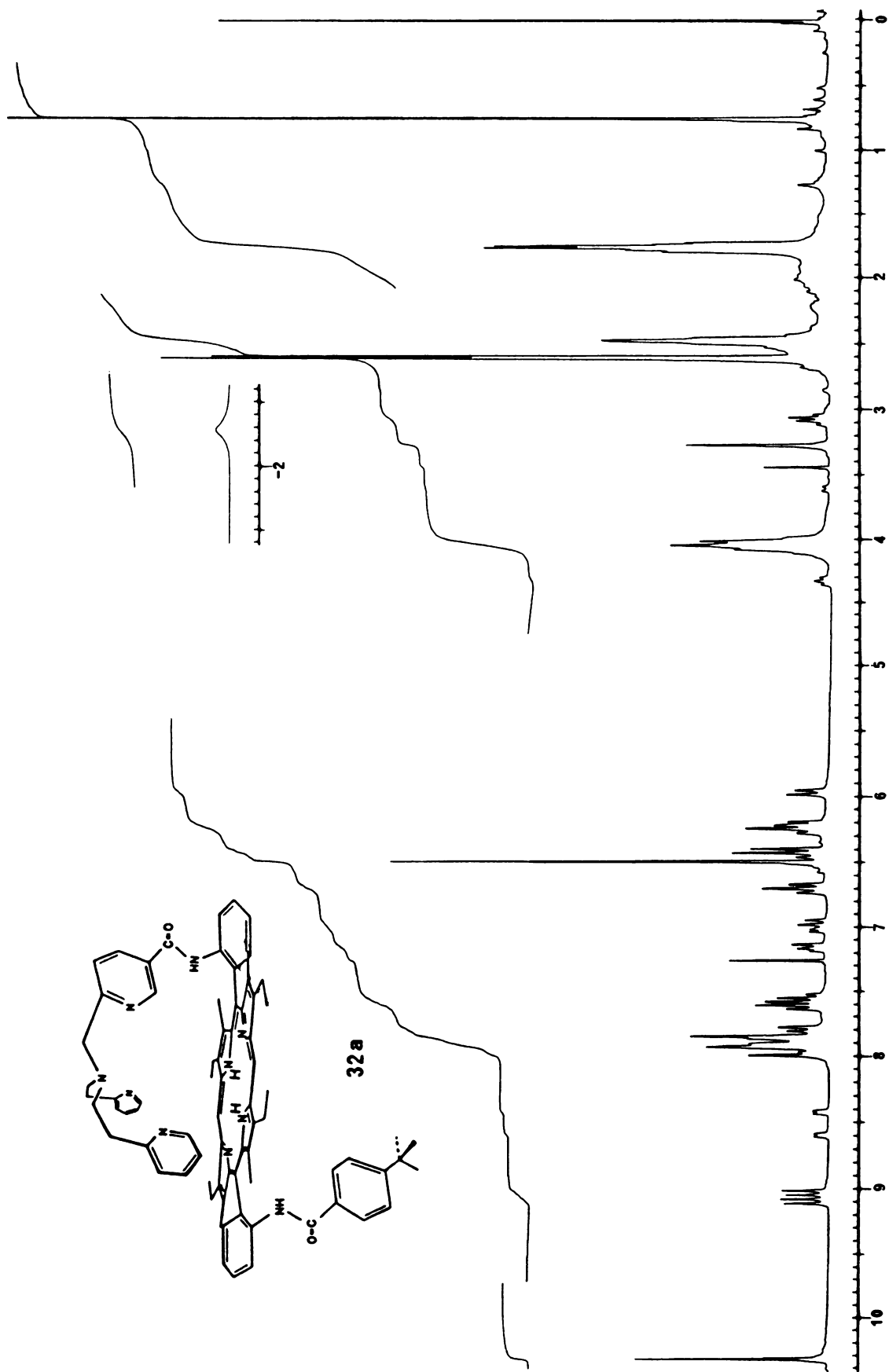
A19. 60 M Hz ^1H NMR spectrum of ethyl 6-[N,N-bis(3-thiapentyl)amino]methyl-nicotinate (25b), CDCl_3 .



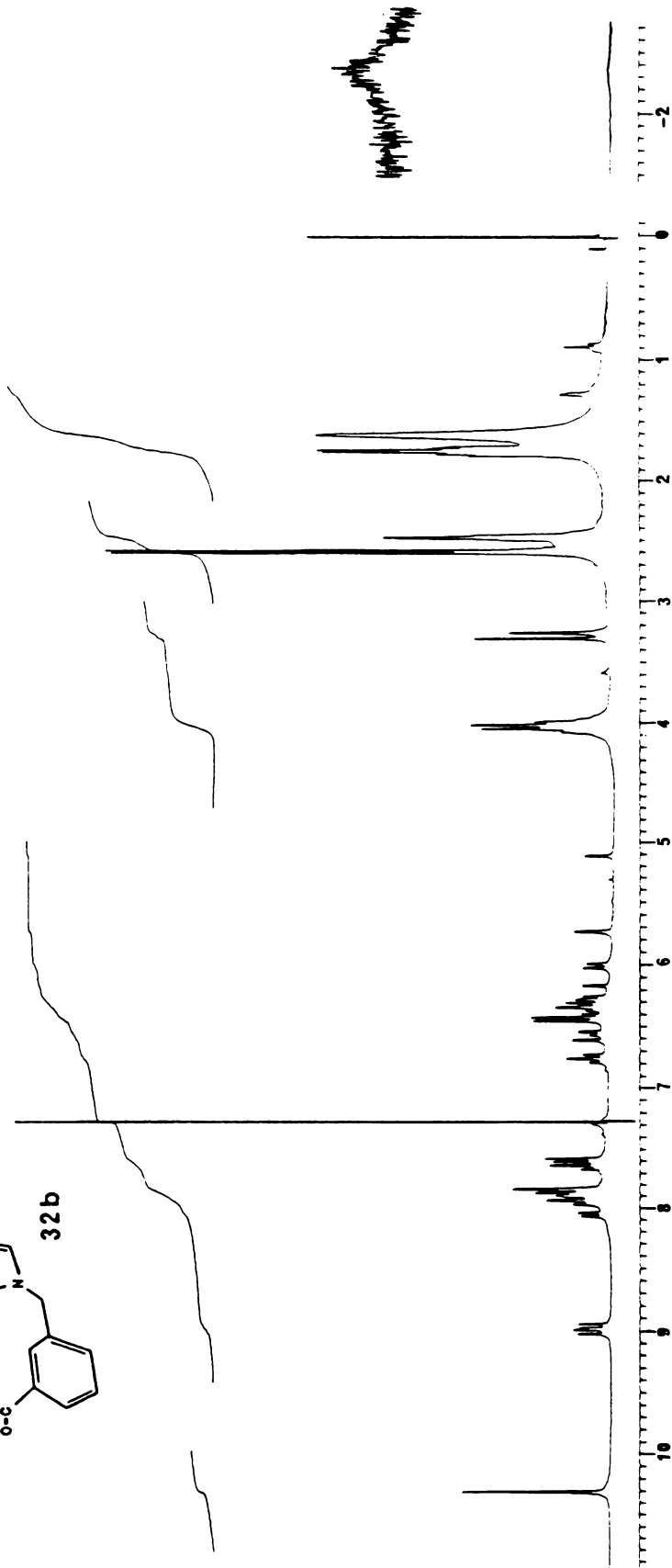
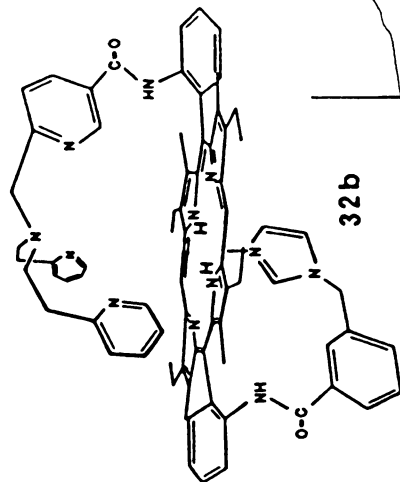
A20. 250 M Hz ^1H NMR spectrum of trans-5-{o-[m-(N-imidazolyl)toluamido]phenyl}-15-(o-[6-[N,N-bis(3-thiapentyl)amino]methylnicotinamido]phenyl)-2,8,12,18-tetraethyl-3,7,13,17-tetramethylporphyrin (28b), CDCl_3 .



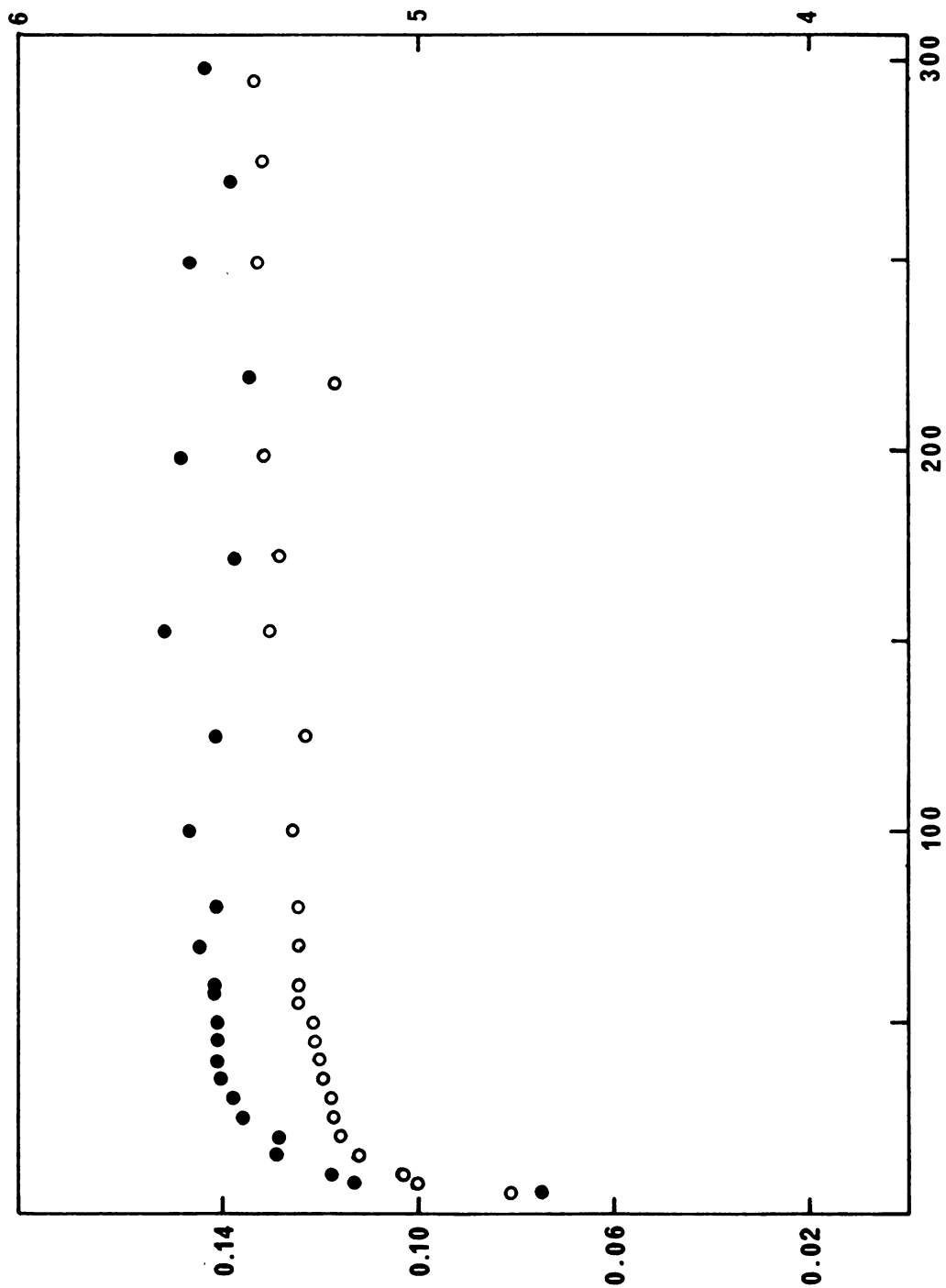
A21. 60 M Hz ^1H NMR spectrum of ethyl 6-[(2-pyridyl)ethyl]amino]methyl-nicotinate (29), CDCl_3 .



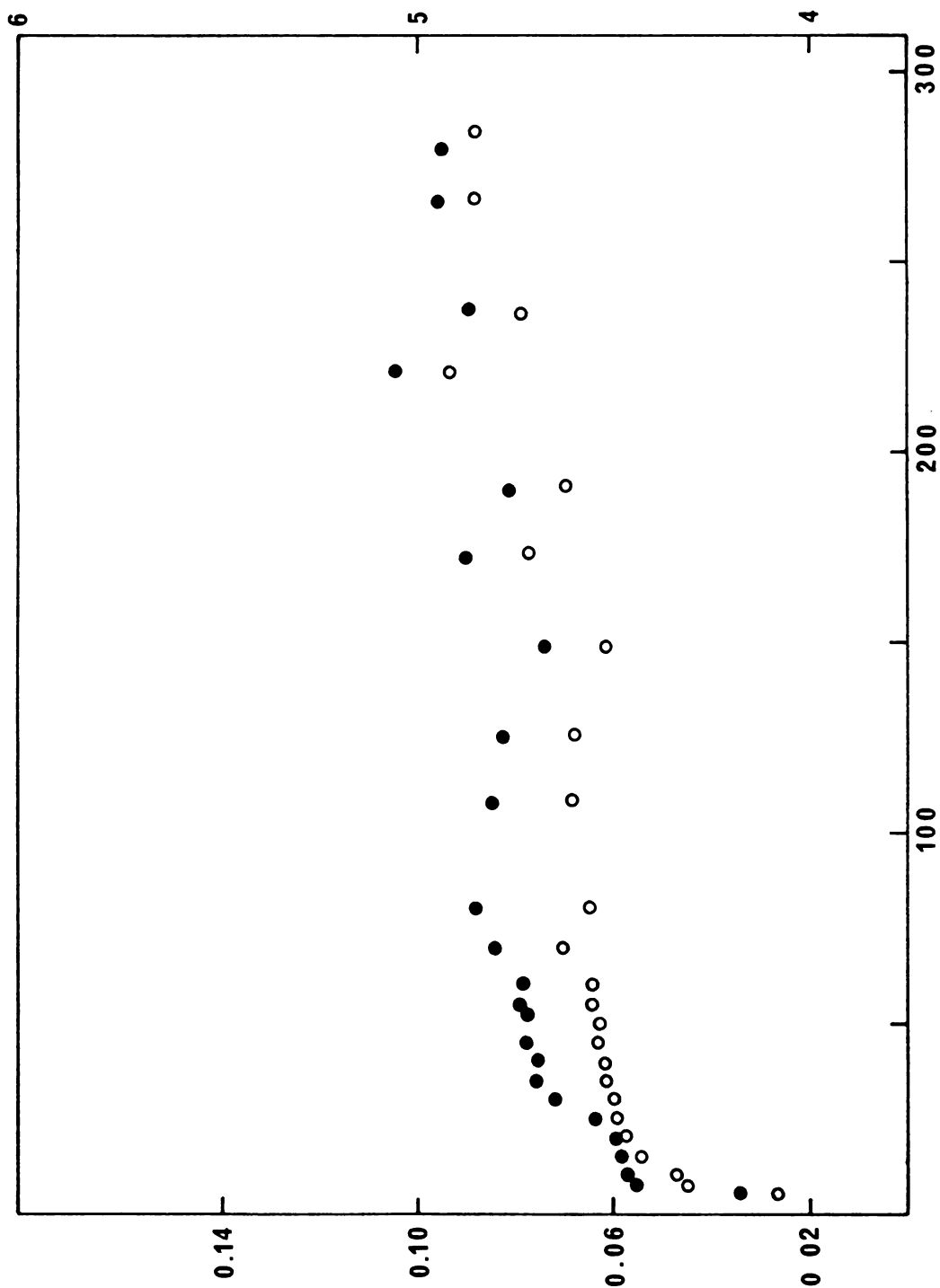
A22. 250 M Hz ^1H NMR spectrum of trans-5-[o-(p-tert-butylbenzamido)phenyl]-15-[o-{6-[N,N-bis[2-(2-pyridyl)ethyl]amino]methylnicotinamido}phenyl]-2,8,12,18-tetraethyl-3,7,13,17-tetramethylporphyrin (32a), CDCl_3 .



A23. 250 M Hz ^1H NMR spectrum of trans-5-{o-[m-(N-imidazolyl)toluamido]phenyl}-15-[o-(6-{N,N-bis[2-(2-pyridyl)ethyl]amino}methyl)nicotinamido]phenyl}-2,8,12,18-tetraethyl-3,7,13,17-tetramethylporphyrin (32b), CDCl_3 .



A24. Effective magnetic moment as a function of temperature for $[\text{Fe}(\text{P})\text{-OH}(\text{N}_4)]$ and $[\text{Fe}(\text{P})\text{-Cl}\text{Cu}(\text{N}_4)(\text{Cl})(\text{OH})]$, blocked with *t*-butylbenzene (32a-1 and 32a-2).



A25. Effective magnetic moment as a function of temperature for $[\text{Fe}(\text{P})\text{-OH}(\text{N}_4)]$ and $[\text{Fe}(\text{P})\text{-Cl Cu}(\text{N}_4)(\text{Cl})(\text{OH})]$, blocked with imidazole(32b-1 and 32b-2).

APPENDIX B

List of
Appendix Table

Table		Page
B1.	Molar magnetic susceptibility and effective magnetic moment as a function of temperature for the mononuclear Fe porphyrin blocked with imidazole (32b-1).	125
B2.	Molar magnetic susceptibility and effective magnetic moment as a function of temperature for the binuclear Fe & Cu porphyrin blocked with imidazole (32b-2).	126
B3.	Molar magnetic susceptibility and effective magnetic moment as a function of temperature for the μ -oxo-bridged Fe & Cu porphyrin blocked with imidazole (32b-3).	127
B4.	Molar magnetic susceptibility and effective magnetic moment as a function of temperature for the mononuclear Fe porphyrin blocked with t-butylbenzene (32a-1').	128
B5.	Molar magnetic susceptibility and effective magnetic moment as a function of temperature for the mononuclear Fe porphyrin blocked with t-butylbenzene without tripyridine appending ligand.	129
B6.	Molar magnetic susceptibility and effective magnetic moment as a function of temperature for the mononuclear Fe porphyrin blocked with bis(t-butylbenzene).	130

B1. Molar magnetic susceptibility and effective magnetic moment as a function of temperature for the mononuclear Fe porphyrin blocked with imidazole (32b-1).

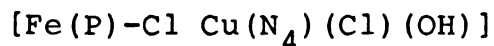
[Fe(P)-OH (N₄)]

C₇₆H₇₅FeN₁₂O₃, M.W. 1260.3541

Sample amount, 8.25 mg; 0.00825/1260.3541 = 0.006546 mmol

Temperature, °K	Mag Suscep x 10 ⁻⁶	Diamag Suscep x 10 ⁻⁶	After Correction x 10 ⁻⁶	per mole	B.M.
5.00	2.6826	-0.0403	2.7229	0.4160	4.08
7.496	1.9874	-0.0453	2.0327	0.3105	4.31
9.999	1.4945	-0.0465	1.5410	0.2354	4.34
14.996	1.0251	-0.0494	1.0745	0.1642	4.43
19.998	0.7662	-0.0509	0.8171	0.1248	4.47
24.994	0.6100	-0.0509	0.6609	0.1010	4.49
29.989	0.5007	-0.0510	0.5517	0.0843	4.50
34.966	0.4266	-0.0513	0.4779	0.0730	4.52
39.983	0.3672	-0.0516	0.4188	0.0640	4.52
45.014	0.3230	-0.0518	0.3748	0.0573	4.54
50.025	0.2847	-0.0521	0.3368	0.0515	4.54
54.941	0.2567	-0.0523	0.3090	0.0472	4.55
59.941	0.2302	-0.0525	0.2827	0.0432	4.55
70.519	0.1962	-0.0527	0.2489	0.0380	4.63
80.130	0.1591	-0.0527	0.2118	0.0324	4.56
107.820	0.1084	-0.0529	0.1613	0.0246	4.61
125.320	0.0851	-0.0530	0.1381	0.0211	4.60
148.640	0.0592	-0.0531	0.1123	0.0172	4.52
173.550	0.0528	-0.0532	0.1060	0.0162	4.74
190.790	0.0380	-0.0534	0.0914	0.0140	4.62
221.100	0.0365	-0.0535	0.0900	0.0137	4.92
235.920	0.0241	-0.0535	0.0776	0.0119	4.74
266.070	0.0192	-0.0535	0.0727	0.0111	4.86
284.280	0.0147	-0.0535	0.0682	0.0104	4.86

B2. Molar magnetic susceptibility and effective magnetic moment as a function of temperature for the binuclear Fe & Cu porphyrin blocked with imidazole (32b-2).

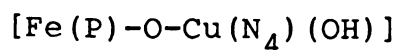


$\text{C}_{76}\text{H}_{75}\text{Cl}_2\text{CuFeN}_{12}\text{O}_3$, M.W. 1394.8061

Sample amount, 10.6 mg; $0.0106/1394.8061 = 0.007600$ mmol

Temperature, °K	Mag Suscep x 10 ⁻⁶	Diamag Suscep x 10 ⁻⁶	After Correction x 10 ⁻⁶	per mole	B.M.
4.998	3.2756	-0.0390	3.3146	0.4362	4.18
7.496	2.4574	-0.0417	2.4991	0.3288	4.44
9.999	1.8441	-0.0432	1.8873	0.2483	4.46
14.998	1.2873	-0.0462	1.3335	0.1755	4.59
19.999	0.9621	-0.0477	1.0098	0.1329	4.61
24.994	0.7758	-0.0487	0.8245	0.1085	4.66
29.989	0.6368	-0.0493	0.6861	0.0903	4.65
34.971	0.5497	-0.0497	0.5994	0.0789	4.70
39.979	0.4732	-0.0502	0.5234	0.0689	4.69
45.002	0.4212	-0.0504	0.4714	0.0620	4.72
50.017	0.3721	-0.0509	0.4230	0.0557	4.72
54.940	0.3378	-0.0510	0.3888	0.0512	4.74
59.940	0.3032	-0.0512	0.3544	0.0466	4.73
70.146	0.2601	-0.0513	0.3114	0.0410	4.80
80.130	0.2143	-0.0515	0.2658	0.0350	4.74
107.680	0.1528	-0.0517	0.2045	0.0269	4.81
125.220	0.1214	-0.0519	0.1733	0.0228	4.78
148.690	0.0880	-0.0522	0.1402	0.0184	4.68
172.430	0.0788	-0.0524	0.1312	0.0173	4.88
189.410	0.0614	-0.0527	0.1141	0.0150	4.77
220.840	0.0575	-0.0526	0.1101	0.0145	5.06
237.570	0.0421	-0.0526	0.0947	0.0125	4.87
266.450	0.0344	-0.0527	0.0871	0.0115	4.95
279.620	0.0299	-0.0527	0.0826	0.0109	4.94

B3. Molar magnetic susceptibility and effective magnetic moment as a function of temperature for the μ -oxo-bridged Fe & Cu porphyrin blocked with imidazole (32b-3).



$\text{C}_{76}\text{H}_{75}\text{CuFeN}_{12}\text{O}_4$, M.W. 1339.8995

Sample amount, 4.5 mg; $0.00450/1339.8985 = 0.003358$ mmol

Temperature, °K	Mag Suscep $\times 10^{-6}$	Diamag Suscep $\times 10^{-6}$	After Correction $\times 10^{-6}$	per mole	B.M.
5.000	1.2371	-0.0411	1.2782	0.3806	3.90
7.497	0.8884	-0.0451	0.9335	0.2780	4.08
9.995	0.6662	-0.0474	0.7136	0.2125	4.12
14.995	0.4487	-0.0492	0.4979	0.1483	4.22
19.999	0.3284	-0.0501	0.3785	0.1127	4.25
24.997	0.2572	-0.0507	0.3079	0.0917	4.28
29.984	0.2064	-0.0510	0.2574	0.0766	4.29
34.982	0.1731	-0.0512	0.2243	0.0668	4.32
39.979	0.1453	-0.0514	0.1967	0.0586	4.33
44.999	0.1257	-0.0516	0.1773	0.0528	4.36
49.993	0.1078	-0.0518	0.1596	0.0475	4.36
54.939	0.0955	-0.0520	0.1475	0.0439	4.39
59.945	0.0828	-0.0522	0.1350	0.0402	4.39
70.421	0.0675	-0.0523	0.1198	0.0357	4.48
80.120	0.0538	-0.0523	0.1061	0.0316	4.50
105.110	0.0305	-0.0525	0.0830	0.0247	4.56
125.080	0.0173	-0.0525	0.0698	0.0208	4.56
144.630	0.0100	-0.0526	0.0626	0.0186	4.64
168.410	0.0010	-0.0527	0.0537	0.0160	4.64
183.740	-0.0035	-0.0529	0.0494	0.0147	4.65
218.610	-0.0116	-0.0529	0.0413	0.0123	4.64
230.960	-0.0131	-0.0529	0.0398	0.0119	4.69
261.350	-0.0160	-0.0529	0.0369	0.0110	4.79
273.370	-0.0175	-0.0530	0.0355	0.0106	4.81

B4. Molar magnetic susceptibility and effective magnetic moment as a function of temperature for the mononuclear Fe porphyrin blocked with t-butylbenzene (32a-1').

[Fe(P)-Cl (N₄)], HCl gas treated.

C₇₆H₇₈ClFeN₁₀O₂, M.W. 1254.818

Sample amount, 6.7 mg; 0.0067/1254.818 = 0.005339 mmol

Temperature, °K	Mag Suscep x 10 ⁻⁶	Diamag Suscep x 10 ⁻⁶	After Correction x 10 ⁻⁶	per mole	B.M.
5.000	2.8632	-0.0415	2.9047	0.5440	4.68
9.999	1.6162	-0.0478	1.6640	0.3116	5.00
20.000	0.8425	-0.0502	0.8927	0.1672	5.17
30.001	0.5573	-0.0510	0.6083	0.1139	5.23
50.031	0.3258	-0.0519	0.3777	0.0707	5.32
74.916	0.2070	-0.0525	0.2595	0.0486	5.40
99.900	0.1456	-0.0527	0.1983	0.0371	5.44
149.910	0.0844	-0.0528	0.1372	0.0260	5.58
199.720	0.0550	-0.0532	0.1082	0.0203	5.69
248.610	0.0378	-0.0532	0.0910	0.0172	5.85
300.200	0.0259	-0.0533	0.0792	0.0148	5.96

B5. Molar magnetic susceptibility and effective magnetic moment as a function of temperature for the mononuclear Fe porphyrin blocked with t-butylbenzene without tripyridine appending ligand.

[Fe(P)-Cl]

$C_{55}H_{58}ClFeN_6O$, M.W. 910.4028

Sample amount, 4.7 mg; $0.0047/910.4028 = 0.005163$ mmol

Temperature, °K	Mag Suscep $\times 10^{-6}$	Diamag Suscep $\times 10^{-6}$	After Correction $\times 10^{-6}$	per mole	B.M.
5.628	3.4113	-0.0402	3.4515	0.6686	5.49
9.995	1.9646	-0.0446	2.0092	0.3892	5.58
19.998	0.9888	-0.0481	1.0369	0.2009	5.67
29.990	0.6477	-0.0493	0.6970	0.1350	5.69
49.980	0.3754	-0.0504	0.4258	0.0825	5.74
74.860	0.2361	-0.0508	0.2869	0.0556	5.77
100.860	0.1652	-0.0511	0.2163	0.0419	5.79
150.590	0.0922	-0.0515	0.1437	0.0278	5.79
201.580	0.0599	-0.0518	0.1117	0.0216	5.91
251.150	0.0392	-0.0517	0.0909	0.0176	5.95
299.800	0.0247	-0.0518	0.0765	0.0148	5.96



B6. Molar magnetic susceptibility and effective magnetic moment as a function of temperature for the mononuclear Fe porphyrin blocked with bis(*t*-butylbenzene).

[Fe(P)-OH]

$C_{66}H_{71}FeN_6O_3$, M.W. 1052.1723

Sample amount, 10.8 mg; $0.0108/1052.1723 = 0.010264$ mmol

Temperature, °K	Mag Suscep $\times 10^{-6}$	Diamag Suscep $\times 10^{-6}$	After Correction $\times 10^{-6}$	per mole	B.M.
4.999	6.1942	-0.0398	6.2340	0.6073	4.93
	Free base, 5 % correction ----->			0.6377	5.05
10.000	3.4907	-0.0458	3.5365	0.3445	5.25
				0.3617	5.38
20.001	1.8339	-0.0497	1.8836	0.1835	5.42
				0.1927	5.55
29.997	1.2270	-0.0510	1.2780	0.1245	5.47
				0.1307	5.60
50.029	0.7366	-0.0523	0.7889	0.0769	5.55
				0.0807	5.68
74.877	0.4845	-0.0529	0.5374	0.0524	5.60
				0.0550	5.73
99.970	0.3536	-0.0531	0.4067	0.0396	5.63
				0.0416	5.77
148.220	0.2268	-0.0533	0.2801	0.0273	5.69
				0.0287	5.83
196.380	0.1620	-0.0538	0.2158	0.0210	5.74
				0.0221	5.89
245.900	0.1213	-0.0538	0.1751	0.0171	5.80
				0.0180	5.94
300.330	0.0970	-0.0540	0.1510	0.0147	5.94
				0.0154	6.08



BIBLIOGRAPHY



BIBLIOGRAPHY

1. W. S. Caughey, W. J. Wallace, J. A. Volpe, and S. Yoshikawa, in "The Enzymes", ed. P. D. Boyer, 3rd Ed., Vol. XIII, pp. 299-344, Academic Press, New York (1976).
2. M. M. Briggs and R. A. Capaldi, *Biochemistry*, 16, 73 (1977).
3. D. C. Wharton, in "Inorganic Biochemistry", ed. G. H. Eichhorn, Elsevier, Amsterdam, Vol. 2, Chapter 27 (1975).
4. D. F. Wilson and M. Erecińska, in "The Porphyrins", ed. D. Dolphin, Academic Press, New York, Vol. VII, Chapter 1 (1979).
5. "Cytochrome Oxidase", T. E. King, Y. Oori, B. Chance and K. Okunuki, Eds., Elsevier, New York (1979).
6. B. G. Malström, "Metal Ion Actiation of Dioxygen", T. G. Spiro, Ed., Wiley, New York (1980).
7. D. Keilin, *Proc. Roy. Soc., London*, B98, 312 (1925).
8. M. Erecinska and D. F. Wilson, *Arch. Biochem. Biophys.* 188, 1 (1978).
9. H. Beinert, D. E. Griffiths, D. C. Wharton, and R. H. Sands, *J. Biol. Chem.*, 237, 2337 (1962).
10. Y. Fujihara, T. Kuwana, and C. R. Hartzell, *Biochem. Biophys. Res. Commun.*, 61, 538 (1974).
11. B. F. Van Gelder and H. Beinert, *Biochim. Biophys. Acta*, 189, 1 (1969).
12. G. Palmer, G. T. Babcock, and L. E. Vickery, *Proc. Natl. Acad. Sci. U.S.A.*, 73, 2206 (1976).
13. G. T. Babcock, L. E. Vickery, and G. Palmer, *J. Biol. Chem.*, 253, 2400 (1978).
14. B. G. Malström, *Adv. Chem. Ser.*, No. 162, 173 (1977).
15. M. F. Tweedle, L. J. Wilson, L. Garcia-Iniguez, G. T. Babcock, and G. Palmer, *J. Biol. Chem.*, 253, 8065 (1978).



16. T. H. Moss, E. Shapiro, T. E. King, H. Beinert, and C. Hartzell, *ibid.*, 253, 8072 (1978).
17. K. -E. Falk, T. Vännngård, and J. Ångström, *FEBS Lett.*, 75, 23 (1977).
18. G. T. Babcock, L. E. Vickery, and G. Palmer, *J. Biol. Chem.*, 251, 7907 (1976).
19. J. A. Fee and R. G. Briggs, *Biochim. Biophys. Acta*, 400, 439 (1975).
20. W. E. Blumberg and J. Peisach, in "Cytochrome Oxidase", Eds., T. E. King et al., P. 153, Elsevier, New York (1979).
21. C. A. Reed and J. T. Landrum, *FEBS Lett.*, 106, 265 (1979).
22. R. W. Shaw, J. E. Rife, M. H. O'Leary, and H. Beinert, *J. Biol. Chem.*, 256, 1105 (1980).
23. R. H. Petty, B. R. Welch, L. J. Wilson, L. A. Bottomley, and K. M. Kadish, *J. Am. Chem. Soc.*, 102, 611 (1980).
24. B. Chance and L. Powers, *Biophys. J.* 33, 95a (1981).
25. L. Powers, B. Chance, Y. Ching, and P. Angiolillo, *Biophys. J.*, 34, 465 (1981).
26. T. Prosperi and A. A. G. Tomlinson, *J. Chem. Soc., Chem. Commun.*, 196 (1979).
27. R. J. Saxton and L. J. Wilson, *J. Chem. Soc., Chem. Commun.*, 359 (1984).
28. V. Chunplang and L. J. Wilson, *J. Chem. Soc., Chem. Commun.*, 1761 (1985).
29. G. N. La Mar, J. S. de Ropp, L. Latos-Grazynski, A. L. Balch, R. B. Johnson, K. M. Smith, D. W. Parish, and R. -J. Cheng, *J. Am. Chem. Soc.*, 105, 782 (1983).
30. E. Bayer, D. Krauss, A. Roder, and D. Schretzmann, "Oxidases and related Redox Systems", Vol. I, T. E. King, H. S. Mason, and M. Morrison, Eds., University Park Press, Baltimore, Md., Chapter II (1973).
31. J. V. Bannister, Ed., "Structure and Function of Haemocyanin", Springer-Verlag, West Berlin (1977).
32. M. G. Simmons and L. J. Wilson, *J. Chem. Soc., Chem.*

- Commun., 634 (1978).
33. K. M. Kadish, G. Larson, D. Lexa, and M. Momenteau, J. Am. Chem. Soc., 97, 282 (1975).
 34. M. J. Gunter, L. N. Mander, K. S. Murray, and P. E. Clark, J. Am. Chem. Soc., 103, 6784 (1977).
 35. C. M. Elliott, J. Chem. Soc., Chem. Commun., 399 (1978).
 36. R. H. Petty and L. J. Wilson, J. Chem. Soc., Chem. Commun., 483 (1978).
 37. D. A. Buckingham, M. J. Gunter, and L. N. Mander, J. Am. Chem. Soc., 100, 2899 (1978).
 38. J. T. Landrum, C. A. Reed, K. Hatano, and W. R. Scheidt, J. Am. Chem. Soc., 100, 3232 (1978).
 39. C. K. Chang, in "Biological & Clinical Aspects of Oxygen", ed. W. S. Caughey, Academic Press, New York, p. 437 (1979).
 40. M. J. Gunter, L. N. Mander, G. M. McLaughlin, K. S. Murray, K. J. Berry, P. E. Clark, and D. A. Buckingham, J. Am. Chem. Soc., 102, 1470 (1980).
 41. C. M. Elliott and K. Akabori, J. Am. Chem. Soc., 104 2671 (1982).
 42. R. J. Saxton, L. W. Olson, and L. J. Wilson, J. Chem. Soc., Chem. Commun., 984 (1982).
 43. B. Lucas, J. R. Miller, J. Silver, and M. T. Wilson, J. Chem. Soc., Dalton Trans., 1035 (1982).
 44. S. E. Dessens, C. L. Merril, R. J. Saxton, R. L. Ilaria, Jr., J. W. Lindsey, and L. J. Wilson, J. Am. Chem. Soc., 104, 4357 (1982).
 45. C. K. Schauer, K. Akabori, C. M. Elliott, and O. P. Anderson, J. Am. Chem. Soc., 106, 1127 (1984).
 46. M. J. Gunter, K. J. Berry, and K. S. Murray, J. Am. Chem. Soc., 106, 4227 (1984).
 47. A. H. Alberts, R. Annunziata, and J. -M. Lehn., J. Am. Chem. Soc., 99, 8502 (1977).
 48. C. K. Chang, J. Am. Chem. Soc., 99, 2819 (1977).
 49. C. K. Chang, Unpublished results.

50. K. J. Berry, P. E. Clark, M. J. Gunter, and K. S. Murray, *Nouv. J. Chim.*, 4, 581 (1980).
51. A. P. Ginsberg, *Inorg. Chim. Acta Rev.*, 5, 45 (1971).
52. C. K. Chang, M. S. Koo, and B. Ward, *J. Chem. Soc., Chem. Commun.*, 716 (1982).
53. M. A. Augustin, J. K. Yandell, A. W. Addison, and K. D. Karlin, *Inorg. Chim. Acta*, 55, L35 (1981).
54. E. Uhlig, W. Hepp, Le My Ngu, and K. Schmiedeknecht, *Revue Roumaine de Chimie*, 22, 8, 1165 (1977).
55. S. E. Livingstone and J. D. Nolan, *Aust. J. Chem.*, 23, 1553 (1970).
56. D. E. Nikles, M. J. Powers, and F. L. Urbach, *Inorg. Chim. Acta*, 37, L499 (1979).
57. N. von Zweigbergk, *Berichte*, 45, 3337 (1912).
58. M. V. Mukhina and I. V. Postovskii, *Khim. Geterotsikl. Soedin., Akad. Nauk Latv. SSR*, 5, 792 (1965).
59. A. K. Bose, F. Greer, and C. C. Price, *J. Org. Chem.*, 23, 1335 (1958)
60. K. Balenović, N. Bregant, D. Cerar, and M. Tkalcic, *J. Org. Chem.*, 16, 1308 (1951).
61. K. Balenović and N. Bregant, *J. Org. Chem.*, 17, 1328 (1952).
62. R. G. Jones, E. C. Kornfeld, and K. C. McLaughlin, *J. Am. Chem. Soc.*, 72, 4526 (1950).
63. H. Fischer and K. Morgenroth, *Liebigs Ann. Chem.*, 466, 166 (1928).
64. C. B. Wang, Ph. D. Thesis, Michigan State University (1981).
65. I. Matsumoto and J. Yoshizawa, Japan, *Kokai* 73 29,783 (1973).
66. A. G. Anderson, Jr., N. E. T. Owen, F. J. Freenor, and D. Erickson, *Synthesis*, 398 (1976).
67. R. Young and C. K. Chang, *J. Am. Chem. Soc.*, 107, 898 (1985).
68. C. K. Chang, R. K. DiNello, and D. Dolphin, *Inorg.*

- Synth., 20, 147 (1980).
69. N. Sadasivan, H. I. Eberspaecher, W. H. Fuchsman, and W. S. Caughey, *Biochemistry*, 8, 534 (1969).
 70. J. H. Van Vleck, "Electric and Magnetic Susceptibilities", Oxford University Press, London (1932).
 71. A modified version of the original program described by J. L. Dye and V. A. Nicely, *J. Chem. Educ.*, 48, 443 (1971).
 72. J. Jaud, Y. Journaux, J. Galy, and O. Kahn, *Nouv. J. Chim.*, 4, 629 (1980).
 73. C. J. O'Connor, D. P. Freyberg, and E. Sinn, *Inorg. Chem.*, 18, 1077 (1979).
 74. N. D. Chasteen and R. L. Belford, *Inorg. Chem.*, 9, 169 (1970).
 75. M. J. Gunter and L. N. Mander, *J. Org. Chem.*, 46, 4792 (1981).
 76. E. Margoliash and A. Shejter, *Advan. Protein Chem.*, 21, 114 (1966).
 77. J. V. Dagdigian and C. A. Reed, *Inorg. Chem.*, 18, 2623 (1979).
 78. R. D. Bereman, M. R. Churchill, and G. Shields, *Inorg. Chem.*, 18, 3117 (1979).
 79. U. Sakaguchi and A. W. Addison, *J. Chem. Soc., Dalton Trans.*, 600 (1979).
 80. K. D. Karlin, P. L. Dahlstrom, M. L. Stanford, and J. Zubieta, *J. Chem. Soc., Chem. Commun.*, 465 (1979).
 81. K. D. Karlin, P. L. Dahlstrom, J. R. Hyde, and J. Zubieta, *J. Chem. Commun.*, 906 (1980).
 82. K. D. Karlin, J. R. Hyde, and J. Zubieta, *Inorg. Chim. Acta*, 66, L23 (1982).
 83. K. D. Karlin, J. C. Hayes, J. P. Hutchinson, J. R. Hyde, and J. Zubieta, *Inorg. Chim. Acta*, 64, L219 (1982).
 84. K. D. Karlin, J. C. Hayes, Shi Juen, J. P. Hutchinson, and J. Zubieta, *Inorg. Chem.*, 21, 4106 (1982).
 85. "Copper Coordination Chemistry: Biochemical & Inorganic Perspectives" Eds. by K. D. Karlin and J. Zubieta,

Adenine Press, New York (1983).

86. D. Razavi, Fr. 1,461,687 (1966).
87. D. J. Liston, B. J. Kennedy, K. S. Murray, and B. O. West, Inorg. Chem., 24, 1561 (1985).
88. C. A. Reed, T. Mashiko, S. P. Bentley, M. E. Kastner, W. R. Scheidt, K. Spartalian, and G. Lang, J. Am. Chem. Soc., 101, 2948 (1979).
89. M. M. Maltempo, T. H. Moss, and M. A. Cusanovich, Biochim. Biophys. Acta, 342, 290 (1974).
90. T. Kitagawa, M. Abe, and H. Ogoshi, J. Chem. Phys. 69, 4516 (1978).
91. M. Abe, T. Kitagawa, and Y. Kyogoku, J. Chem. Phys. 69, 4526 (1978).
92. G. Chottard, et al., Inorg. Chem., 20, 1718 (1981).
93. W. A. Oetling and A. Salehi, Unpublished results.
94. S. M. Nelson and J. Rodgers, Inorg. Chem., 6, 1390 (1967).







MICHIGAN STATE UNIVERSITY LIBRARIES



3 1293 03142 5366